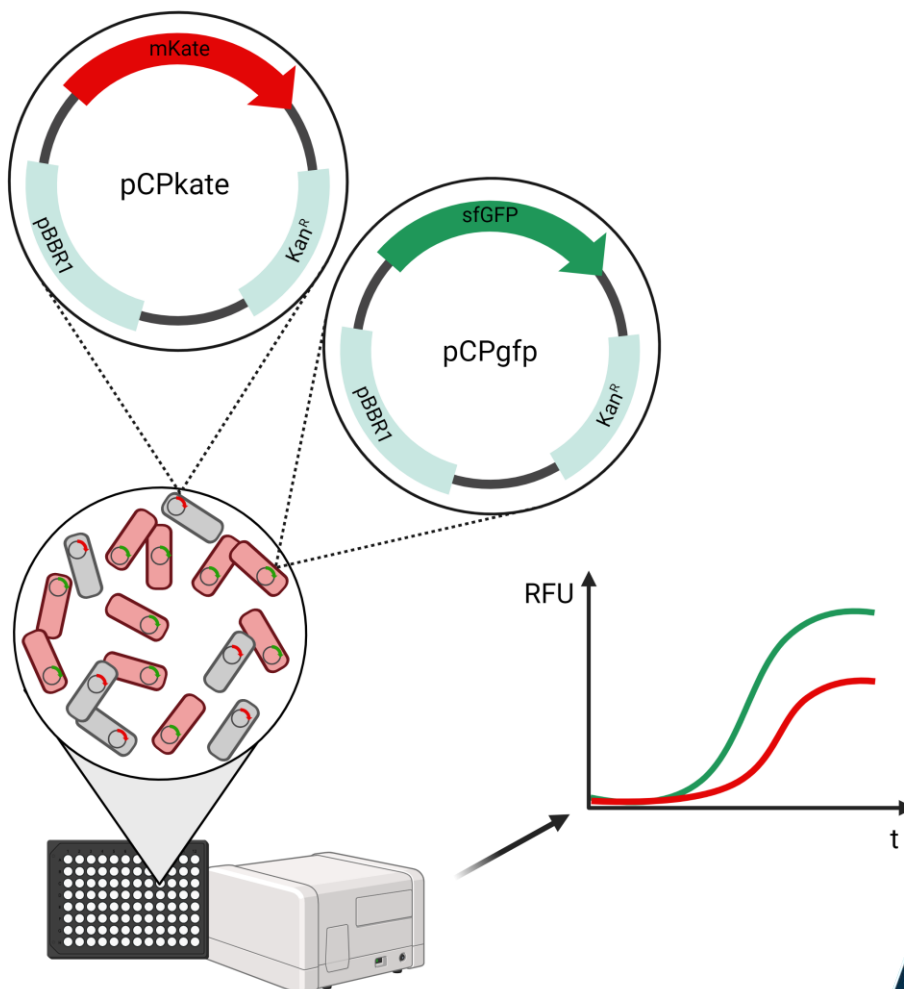


Faculty of Biosciences, Fisheries and Economics

Broad-Host-Range Genetic Tools for Observing Microbial Consortia

Luisa Deppe

Master's Thesis in Marine Biotechnology (BIO-3901), May 2023



Acknowledgements

The research for this master's thesis was conducted in the Microalgae & Microbiomes Research Group (M2RG) under the supervision of Professor Hans Christopher Bernstein and PhD candidate Dennis Tin Chat Chan at the Faculty of Biosciences, Fisheries and Economics at the UiT – The Arctic University of Norway. The thesis comprises 60 ECTS credits and was submitted to the UiT for the degree of Master of Science (M.Sc.) in Marine Biotechnology.

Now that I have completed my master's project, two exciting and unforgettable years of living and studying in Tromsø north of the Arctic Circle are coming to an end. I would therefore like to take this opportunity to thank the following people without whom I would not have been able to complete this project.

First and foremost, I would like to thank my main supervisor Hans Christopher Bernstein for giving me the opportunity to write this master's thesis under his supervision in the M2RG research group. Hans, thank you for your continuous support, your invaluable input and constructive feedback during the entire process.

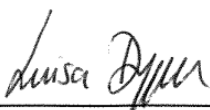
Furthermore, I would like to thank my second supervisor Dennis Tin Chat Chan for his guidance and willingness to answer any queries regarding the practical work in the laboratory and the analysis of my data in R. Thank you for being approachable at all times, for introducing me to the work with microorganisms and synthetic biology and for your insight and knowledge in R. I would also wish to thank Stina Krsmanovic and Johan Bjerg for providing lab training which laid the foundations for my research.

I am also thankful to the entire Microalgae & Microbiomes Research Group for welcoming me into a positive working environment. It was a pleasure to be part of your group. You have made this year very memorable for me.

Finally, I would like to thank my friends and family, especially my parents, for always being there for me and supporting me during this intense academic year. Jan, thank you for all your love, support, and motivation and for always having my back on this journey.

UiT, The Norwegian College of Fishery Science

Tromsø, May 2023



Luisa Deppe



Hans Christopher Bernstein

Abstract

Microbial communities are complex assemblages that are key to ecosystem stability and human health. Synthetic ecology aims to design and construct microbial consortia with reduced complexity that enable innovative applications beyond monocultures. However, their robust and performance-based design is constrained by limited knowledge of growth dynamics and derived binary interactions that are critical for community functioning. Decoupling population dynamics and inferring interspecies interactions from strain-specific fitness data remains a major challenge due to the difficulty of monitoring and quantifying species-specific growth in mixed microbial communities. Existing methods have the disadvantage that they are not suitable for fast, scalable, high throughput applications such as those needed at the interface between synthetic biology and microbial ecology, where the screening of large design spaces associated with the construction and observation of synthetic co-cultures is required. In this thesis, a standardized platform functioning as a tractable tool for the interrogation of population dynamics based on measurements of strain-specific fluorescence in microbial co-cultures was developed. This was accomplished by constructing a set of broad-host-range plasmids in the BASIC environment that constitutively express fluorescent reporter proteins and estimating the ecological fitness of species in terms of specific growth rate (μ) and carrying capacity (K) from static and time-course optical density and fluorescence measurements through regression analysis of bacterial growth models. Experimental investigation of model binary co-cultures constructed from six model and non-traditional bacterial hosts demonstrated successful decoupling of population dynamics and inference of interspecies interactions in 96-well plates based on fluorescence. Furthermore, the results emphasize the need for the right choice of genetic tools for a meaningful interrogation of co-culture dynamics and inference of interactions, consistent with the finding that the suitability of fluorescence as a surrogate for bacterial biomass depends on the combination of host species and fluorescent protein. It is anticipated that this toolkit can contribute to applications in synthetic microbial ecology and biotechnology by providing a flexible, scalable, and reproducible approach to decouple populations dynamics in synthetic co-cultures.

Keywords: co-cultures, ecological fitness, fluorescent proteins, interspecies interactions, population dynamics, synthetic biology

List of Abbreviations

BASIC	Biopart Assembly Standard for Idempotent Cloning
cPCR	Colony-PCR
DSMZ	German Collection of Microorganisms and Cell Cultures
F_{max}	Metric of carrying capacity from maximum fluorescence measured [RFU]
iP	BASIC Prefix sequence
iS	BASIC Suffix sequence
K	Metric of carrying capacity derived from logistic equation [OD600] or [RFU]
m_B	Metric of metabolic burden [%]
OD_{max}	Metric of carrying capacity from maximum optical density measured [OD600]
OD600	Optical density measured at 600 nm
qPCR	Quantitative PCR
RFU	Relative fluorescence units
SEVA	Standard European Vector Architecture
Taq	DNA Polymerase from <i>Thermus aquaticus</i>
μ	Specific growth rate [h^{-1}]
Ξ	Metric of fitness maintenance [%]

Table of Contents

Acknowledgements	I
Abstract	III
List of Abbreviations	IV
List of Figures	VIII
List of Tables	XI
1 Introduction	1
1.1 Main Objectives.....	2
2 Background	3
2.1 Synthetic Biology and Common Standards	3
2.1.1 The Synthetic Biology Open Language (SBOL).....	4
2.1.2 The Standard European Vector Architecture (SEVA).....	4
2.1.3 The Biopart Assembly Standard for Idempotent Cloning (BASIC).....	6
2.1.4 The Microbial Chassis and Chassis-Effect	7
2.1.5 Synthetic Ecology and Co-Cultures	9
2.2 Dynamics of Bacterial Growth.....	9
2.2.1 Assessing and Quantifying Bacterial Growth	10
2.2.2 Measures of Bacterial Fitness.....	12
2.2.3 Binary Growth Interactions	13
2.3 Inverse Modelling in Microbial Ecology	13
2.3.1 Nonlinear Regression	14
2.3.2 Linear Regression of Transformed Nonlinear Models.....	15
2.4 Bacterial Strains.....	15
2.4.1 <i>Escherichia coli</i>	15
2.4.2 <i>Pseudomonas</i> Genus	16
2.4.2.1 <i>Pseudomonas deceptionensis</i>	16
2.4.2.2 <i>Pseudomonas fluorescens</i>	17
2.4.2.3 <i>Pseudomonas putida</i>	17
2.4.3 <i>Halopseudomonas</i> Genus.....	18
2.4.3.1 <i>Halopseudomonas aestusnigri</i>	18
2.4.3.2 <i>Halopseudomonas oceani</i>	19
2.5 The Open Science Framework (OSF)	19
3 Materials and Methods	20
3.1 Bacterial Strains and Cultivation Conditions	20

3.2	BASIC DNA Assembly.....	20
3.2.1	BASIC Clip Reaction.....	21
3.2.2	BASIC Clip Purification.....	21
3.2.3	BASIC Clip Assembly.....	22
3.2.4	Heat-Shock Transformation of BASIC Constructs and Assembly Confirmation.....	22
3.3	Electroporation.....	23
3.4	Colony-PCR (cPCR).....	24
3.5	Agarose Gel Electrophoresis.....	25
3.6	Plasmid Preparation.....	25
3.7	Fluorometric Quantification of DNA.....	26
3.8	Growth Assays.....	26
3.9	Data Processing and Quantitative Analysis.....	28
3.9.1	Modelling Growth and Estimating Growth Parameters.....	28
3.9.1.1	Estimating Specific Growth Rates.....	28
3.9.1.2	Estimating Carrying Capacity.....	29
3.9.2	Calculating Metabolic Burden.....	30
3.9.3	Inferring Co-Culture Growth Dynamics and Binary Interactions.....	30
3.10	Conducting Open Science and Reproducible Research.....	31
4	Results.....	32
4.1	Broad-Host-Range Device Platform.....	32
4.1.1	Reporter Plasmids Integrated into the BASIC Standard.....	32
4.1.2	Bacterial Hosts for Fluorescent Reporter Plasmids.....	35
4.2	Characterization of the Genetic Device Platform.....	36
4.2.1	Observation of Batch Effects and Reproducibility.....	37
4.2.2	Growth Parameters from Monoculture Growth Data.....	37
4.2.2.1	Specific Growth Rate Estimates.....	38
4.2.2.1.1	<i>Escherichia coli</i>	39
4.2.2.1.2	<i>Pseudomonas putida</i>	41
4.2.2.1.3	<i>Halopseudomonas aestusnigri</i>	42
4.2.2.1.4	<i>Halopseudomonas oceani</i>	43
4.2.2.1.5	<i>Pseudomonas deceptionensis</i>	44
4.2.2.1.6	<i>Pseudomonas fluorescens</i>	45
4.2.2.2	Estimates of Carrying Capacity.....	46
4.2.3	Quantification of the Metabolic Burden.....	49
4.3	Inference of Combinatorial Growth Dynamics by Fluorescence.....	52
4.3.1	Selection of Suitable Binary Co-Cultures.....	52

4.3.2	Evaluation of Experimental Data from Combinatorial Growth Experiments.....	54
4.3.2.1	Estimates of Bacterial Fitness in Combinatorial Co-Cultures.....	55
4.3.2.2	Influence of Plasmid Bearing Strains on the Prediction of Growth Dynamics	59
4.3.2.3	Quantification of the Metabolic Burden.....	60
4.3.2.4	Growth Interactions Derived from Growth Parameter Estimates.....	62
5	Discussion	68
5.1	Synthetic Microbial Communities as a Platform for Biotechnology	69
5.2	Balancing Practicality and Uncertainty.....	71
5.3	Advancing Broad-Host-Range Synthetic Biology.....	75
5.4	Measures of Ecological Fitness.....	76
5.5	Standardized Model Systems	77
5.6	Future Directions.....	78
6	Conclusion	82
7	References	84
8	Appendix	93
8.1	Appendix A	93
8.2	Appendix B	96
8.3	Appendix C	97
8.4	Appendix D	99
8.5	Appendix E.....	102
8.6	Appendix F.....	104

List of Figures

Figure 1: Schematic of the pre-formatted structure of SEVA plasmids.	5
Figure 2: Alphanumerical schematic of the standardized nomenclature of SEVA plasmid vectors.	5
Figure 3: Schematic of the characteristic format of BASIC DNA assembly compositions and BASIC Linker structure.	8
Figure 4: Bacterial growth curve showing all four stages of growth. Exponential cell growth is mathematically expressed by an ordinary differential equation, whereas sigmoidal cell growth through lag-, log-, and stationary phase can be modelled with a logistic differential equation.	11
Figure 5: Standardized 96-well microplate layout for all monoculture and co-culture growth experiments.	27
Figure 6: BASIC DNA assembly workflow and schematic of linearized broad-host-range reporter plasmids.	34
Figure 7: Confirmation of successful integration of the BB23-backbone into the pCPcer plasmid.	35
Figure 8: Quantification of statistically significant batch effects for three wild-type strains based on the comparison of their specific growths rate from two experimental replicates.	38
Figure 9: The comparison of the specific growth rates estimated from OD600 and fluorescence reveals that the growth of <i>E. coli</i> DH5 α can be best assessed using the pCPcit plasmid. In addition, the measurement of background fluorescence for Ec pCPgfp and Ec pCPcit unveils a signal overlap of the sfGFP and mCitrine proteins.	40
Figure 10: The comparative analysis of the specific growth rates obtained from OD600 and fluorescence data for all strains shows that the growth of <i>P. putida</i> can be best approximated using the mCerulean fluorescent reporter protein.	41
Figure 11: The statistically non-significant difference between the specific growth rates determined from OD600 and Cerulean fluorescence for <i>Ha</i> pCPcer signifies a proportionality between fluorescence and biomass and thus implies that the pCPcer plasmid is the tool of choice to assess the growth of <i>H. aestusnigri</i>	42
Figure 12: The estimates of specific growth rate obtained from OD600 and fluorescence measurements for all plasmid bearing <i>H. oceani</i> strains show statistically significant differences in their values.	43
Figure 13: The growth of <i>P. deceptionensis</i> is best assessed by tracking of EYFP fluorescence as signified by the statistically non-significant difference between the specific growth rates obtained from OD600 and EYFP fluorescence for <i>Pd</i> pCPeyfp.	44
Figure 14: The comparison of specific growth rates obtained from growth curve and fluorescence curve data for <i>Pf</i> pCPgfp, <i>Pf</i> pCPeyfp and <i>Pf</i> pCPcit reveals statistically non-significant differences, indicating that GFP, EYFP and Citrine fluorescence are proportional to the population density of <i>P. fluorescens</i> making the pCPgfp, pCPeyfp and pCPcit plasmids good reporter tools to assess growth performance.	45

Figure 15: Two metrics of carrying capacity determined from optical density growth curve data reveal an overall reasonable model fit of the logistic equation used to estimate the ecological carrying capacity of strains despite some observed errors related to model fitting.....	47
Figure 16: The carrying capacity between host strains shows an effect of metabolic burden from different plasmids and a limited qualitative validity.....	48
Figure 17: The visual representation of metabolic burdens shows that the growth of <i>P. deceptionensis</i> and <i>P. fluorescens</i> is most strongly affected upon transformation with the reporter plasmids, signified by large differences in the m_B values.	50
Figure 18: Statistically significant relationships show the chassis-effects between species for each of the broad-host-range reporter plasmids.	51
Figure 19: Selection procedure to determine suitable pairs of plasmid bearing strains for combinatorial two-species co-cultures.....	53
Figure 20: Growth curves of co-cultivated species plotted from strain-specific fluorescence measurements show consistency between replicates, whereas the derived growth parameters μ_{fl} , K_{fl} and F_{max} indicate some inconsistencies between the two measures of carrying capacity.	58
Figure 21: The individual examination of the fluorescence curves shows that due to the different size ranges of the measured RFU values, the increase in fluorescence of <i>Pd</i> pCPeyfp cannot be clearly identified in the joint diagram.....	59
Figure 22: The comparison of the fluorescence curves and growth parameters μ and K for the “good” and “bad” strain combinations of the same binary co-cultures reveals that the prediction of fitness competition depends on the choice of plasmid bearing strains for each species.	60
Figure 23: The metabolic burdens of the “bad” combinations show the greatest variance, yet no correlation can be inferred between the metabolic load and combinations where the outcome of competitive growth between species depended on the choice of plasmid bearing strains.	61
Figure 24: Confirmation of the presence of the promoter-reporter cassettes in the newly assembled broad-host-range reporter plasmids by cPCR.	93
Figure 25: Confirmation of successful integration of the BB23-backbone into the pCPgfp, pCPrfp, and pCPkate plasmid.....	94
Figure 26: Confirmation of successful integration of the BB23-backbone into the pCPgfp, pCPrfp, and pCPkate plasmid.....	95
Figure 27: Confirmation of the successful transformation of <i>P. putida</i> with the plasmids pCPgfp, pCPrfp and pCPkate by verifying the presence of the respective promoter-reporter cassettes.....	96
Figure 28: Confirmation of the successful transformation of <i>P. putida</i> with the plasmids pCPeyfp, pCPcit and pCPcer by verifying the presence of the respective promoter-reporter cassettes.	96
Figure 29: Confirmation of the successful transformation of <i>H. aestusnigri</i> with the plasmids pCPgfp, pCPrfp, pCPkate, pCPcit and pCPcer by verifying the presence of the respective promoter-reporter cassettes.	97
Figure 30: Confirmation of the successful transformation of <i>H. aestusnigri</i> with the plasmid pCPeyfp by verifying the presence of the respective promoter-reporter cassette.	98

Figure 31: Confirmation of the successful transformation of <i>H. oceanii</i> with the plasmid pCPgfp by verifying the presence of the respective promoter-reporter cassette.	99
Figure 32: Confirmation of the successful transformation of <i>H. oceanii</i> with the plasmid pCPrfp by verifying the presence of the respective promoter-reporter cassette.	99
Figure 33: Confirmation of the successful transformation of <i>H. oceanii</i> with the plasmid pCPkate by verifying the presence of the respective promoter-reporter cassette.	100
Figure 34: Confirmation of the successful transformation of <i>H. oceanii</i> with the plasmid pCPeyfp by verifying the presence of the respective promoter-reporter cassette.	100
Figure 35: Confirmation of the successful transformation of <i>H. oceanii</i> with the plasmid pCPcit by verifying the presence of the respective promoter-reporter cassette.	101
Figure 36: Confirmation of the successful transformation of <i>H. oceanii</i> with the plasmid pCPcer by verifying the presence of the respective promoter-reporter cassette.	101
Figure 37: Confirmation of the successful transformation of <i>P. deceptionensis</i> with the plasmids pCPgfp and pCPrfp by verifying the presence of the respective promoter-reporter cassettes.	102
Figure 38: Confirmation of the successful transformation of <i>P. deceptionensis</i> with the plasmids pCPkate and pCPeyfp by verifying the presence of the respective promoter-reporter cassettes.	102
Figure 39: Confirmation of the successful transformation of <i>P. deceptionensis</i> with the plasmids pCPcit and pCPcer by verifying the presence of the respective promoter-reporter cassettes.	103
Figure 40: Confirmation of the successful transformation of <i>P. fluorescens</i> with the plasmids pCPgfp and pCPrfp by verifying the presence of the respective promoter-reporter cassettes.	104
Figure 41: Confirmation of the successful transformation of <i>P. fluorescens</i> with the plasmids pCPkate and pCPeyfp by verifying the presence of the respective promoter-reporter cassettes.	104
Figure 42: Confirmation of the successful transformation of <i>P. fluorescens</i> with the plasmids pCPcit and pCPcer by verifying the presence of the respective promoter-reporter cassettes.	105

List of Tables

Table 1: Overview of constructed broad-host-range reporter plasmids.	33
Table 2: Overview of plasmid bearing strains and their IDs used hereinafter.	36
Table 3: Overview of plasmid bearing strains with statistically non-significant differences between the specific growth rates determined from OD600 and strain fluorescence, indicating a proportionality between fluorescence and biomass that makes them highly suitable strains for approximating the growth performance of the corresponding species.	39
Table 4: Final choices of strain-strain combinations for binary co-cultures.	54
Table 5: Interrogation of population dynamics in terms of specific growth rate estimated from strain-specific fluorescence measurements shows that <i>P. putida</i> has the highest fitness among all species and that most bidirectional interactions between the species are antagonistic in nature.	65
Table 6: Decoupling and inferring growth dynamics in terms of carrying capacity, interpreted by the parameter K of a logistic growth model, shows that most interactions between species are antagonistic. The results suggest that <i>H. oceanii</i> achieves the higher carrying capacity in co-culture with four of the five other species. However, this is questionable because of the very high Ξ_K values, which are more indicative of uncertainties in the model fitting.	66
Table 7: Decoupling and inferring of growth dynamics in terms of carrying capacity, interpreted as the maximum fluorescence measured during cultivation, indicates that most interactions between species are antagonistic. Furthermore, it shows that the decoupling of growth dynamics is biased depending on the approach used to interpret the ecological carrying capacity.	67

1 Introduction

Microorganisms are ubiquitous in virtually all known ecosystems on Earth and of substantial importance for ecosystem functioning (De Roy et al., 2014). They drive global biogeochemical cycles thereby influencing nutrient fluxes and mediating important processes such as primary production and decomposition, making them essential to life on Earth (De Roy et al., 2014; Lawson et al., 2019). Microorganisms account for the majority of the existing genetic and physiological versatility and thus harbour a huge metabolic potential, some of which is still undiscovered and unexploited to date (Lawson et al., 2019). In nature, most microorganisms live in inherently complex multispecies assemblages in which members thrive together in a cohesive environment and interact and communicate with one another (Bernstein, 2019). So-called microbial communities or consortia are characterized by complex and mostly undefined community members, functional heterogeneity, and dynamic interactions, which severely limits the study of community activities as well as the biological and ecological principles that govern their functioning (Zengler et al., 2019).

Continuous advances in microbial biodesign and bioengineering have led to an enormous variety of industrial, commercial and environmental biotechnological applications, many of which have proven indispensable to modern society (Cameron et al., 2014; Liao et al., 2016). Despite technological advances, the engineering of microorganisms in monocultures is increasingly reaching its limits (Lindemann et al., 2016), sparking interest in microbial communities as bioprocess platforms capable of performing functions beyond the metabolic limits of conventional monocultures (Bernstein & Carlson, 2012; Lindemann et al., 2016; Tsoi et al., 2019). However, limited understanding of complex community dynamics currently constrains the outputs of (engineered) microbial communities and the efficient use of their potential to address modern challenges (Lawson et al., 2019; Lindemann et al., 2016).

Artificial and synthetic microbial communities, due to their lower complexity and higher controllability, are a valuable tool to study temporal and spatial dynamics (De Roy et al., 2014) and to develop innovative and efficient biotechnological processes (Ibrahim et al., 2021). A better understanding of the biology of microbial consortia and interspecies interactions has led to the development of new design strategies and will further facilitate the construction of stable and productive synthetic co-cultures with desired functions and controllable outputs (De Roy et al., 2014; Fredrickson, 2015). A key factor influencing dynamics, functioning, and stability of communities are interspecies interactions (Lindemann et al., 2016). Yet, the study of microbial interactions is not straightforward. Methods used to infer binary interactions include transcriptome (Beliaev et al., 2014; McClure et al., 2018) and metabolome (Medlock et al., 2018; Phalak et al., 2022; Venturelli et al., 2018) based approaches, as well as measuring fitness-based growth dynamics (Carrara et al., 2015; Khan et al., 2018; Nestor et al., 2023; H.-S. Song et al., 2019), which allow the investigation of changes in indicative variables that are likely to occur as a result of interspecies interactions. While the growth performance of individual

populations in planktonic liquid cultures can be easily tracked in high throughput by measures of optical density, observing growth dynamics in microbial co-cultures requires alternative methods to monitor species-specific biomass (Schlechter et al., 2021). Currently used methods for decoupling populations dynamics in co-cultures, such as quantitative PCR (Junicke et al., 2014) and flow cytometry (Ogundero et al., 2022), do not lend themselves to simple and automated time-course measurements, representing a major limitation for inferring binary interactions from measures of species-specific fitness in microbial communities. Overcoming this limitation by developing new methods compatible with the high throughput observation and interrogation of microbial growth dynamics in co-cultures will provide more investigative opportunities for exploring larger design spaces in conjunction with the enormous potential of various life science applications attributed to synthetic co-cultures (Goers et al., 2014; Kehe et al., 2019).

1.1 Main Objectives

The interrogation of population dynamics and inference of interspecies interactions from strain-specific fitness data is challenging due to the lack of methods for the convenient and high throughput observation and quantification of individual species biomass in co-cultures. Therefore, the aim of this thesis was to develop and test a synthetic biology toolkit based on practical genetic tools for decoupling populations dynamics in microbial co-cultures, using scalable fluorescence measurements as proxy for species-specific biomass. This was achieved by reaching the following objectives:

- Construct a genetic device platform by building a set of broad-host-range fluorescent reporter plasmids in the BASIC environment and transforming these tools across a set of six well-established and non-traditional bacterial hosts.
- Characterize the genetic device platform by growing all wild-type and plasmid bearing strains in monoculture and estimating measures of bacterial fitness from OD600 and fluorescence data.
- Evaluate whether fluorescence can be used as a tool to assess ecologically important growth parameters by comparing growth parameter estimates obtained from fluorescence and optical density measurements.
- Demonstrate the functionality of the established tools by decoupling population dynamics in model co-cultures and inferring the presence and nature of binary interactions by comparing the fitness of individual strains grown in monoculture to their fitness when grown in co-culture with other strains.

2 Background

2.1 Synthetic Biology and Common Standards

Synthetic biology is an interdisciplinary, quantitative, and design-orientated scientific discipline that applies engineering principles and molecular biology tools to biological systems. It uses interchangeable modular parts such as promoters, protein coding sequences, and transcriptional terminators, to design, build, and test novel genetic networks and pathways within cells, and to redesign existing natural biological systems to perform tailored biological functions. (Adams, 2016; Benner & Sismour, 2005)

The foundation for the emergence of synthetic biology as a scientific discipline was laid in the 1960s with the discovery of cell regulation through molecular networks by Monod and Jacob (Monod & Jacob, 1961). From then on, many important scientific and technological advances were required until, at the beginning of the 21st century, in January 2000, the first research results on regulatory circuits – the toggle switch and the repressilator – were published. These included the development of molecular cloning techniques, the establishment of *in vitro* DNA amplification by PCR, the rise of ‘omics’ sciences, the transition to automated DNA sequencing, and development of computer-assisted tools and high throughput techniques. An important milestone in the progression of synthetic biology was the first international conference, SB1.0, held in 2004 at the Massachusetts Institute of Technology (MIT) in the USA, which united scientists from different disciplines to advance their collaborative effort in the design, construction and programming of cellular behavior. (Cameron et al., 2014)

The interdisciplinary nature of synthetic biology underlines the importance of collaboration and sharing at the different levels of the design, build and test phases between researchers and institutions. Despite the community's unanimity on the need to implement universal standards, the field of synthetic biology still faces challenges such as long development times, poor reproducibility and high failure rates, which can be attributed to the lack of a uniform set of standards widely accepted and used by synthetic biologists (Madsen et al., 2019; Müller & Arndt, 2012). The first repository of modular genetic parts with a common storage standard was the Registry of Standard Biological Parts (RSBP). The main intention of this registry was to reduce ambiguity and to promote sharing of parts between researchers (Cameron et al., 2014). The use of common standards can facilitate collaboration, communication of results, interchangeability of parts, reproducibility and innovation, while standardization of protocols will promote the use of robotics and the transition to automation in synthetic biology (Müller & Arndt, 2012; Tas et al., 2020). Many standards have already been developed, but most of them are only used by a small part of the community (Tas et al., 2020). Three promising standards for synthetic biologists are presented below in Chapters 2.1.1 - 2.1.3, including an

in silico tool for describing synthetic parts and designs, a vector repository, and a method for *in vitro* assembly of modular parts and part storage.

2.1.1 The Synthetic Biology Open Language (SBOL)

The Synthetic Biology Open Language (SBOL) is a standard for the schematic representation of synthetic parts and circuits with the objective of facilitating collaborate engineering and the sharing of biological designs and design information between research groups, commercial service providers and software tools (Galdzicki et al., 2014). It has become a widely accepted standard in the synthetic biology community, effectively reducing ambiguity in communication regarding the structure and function of synthetic designs (Cox et al., 2018).

2.1.2 The Standard European Vector Architecture (SEVA)

Plasmid vectors constitute an essential tool in synthetic biology, serving as a scaffold for the construction of genetic devices and circuits and their subsequent transfer into host organisms. Decades without any efforts to standardize cloning vectors led to a high degree of diversification and the resulting consequences, such as the impairment of data comparison, sharing and reproducibility (Martínez-García et al., 2022). Recent standardization attempts aimed at advancing synthetic biology led to the introduction of a standard for plasmid vector architecture and nomenclature in 2013 – the Standard European Vector Architecture (SEVA) (Silva-Rocha et al., 2013).

SEVA plasmid vectors are composed of three interchangeable DNA modules – an antibiotic selection marker, an origin of replication and a cargo module – which can be combined in various ways for customization (Figure 1). The antibiotic selection marker constitutes one of several antibiotic resistance genes (Ab^R) and its native promoter. The origins of replication available for selection are broad-host-range *oris* that determine the plasmid copy number. The cargo module can be a functional DNA sequence that determines the function of the plasmid, *e.g.*, heterologous gene expression. The default SEVA cargo contains a multiple cloning site (pUC18 polylinker) with additional restriction recognition sites outside of the polylinker. This way, synthetic devices or circuits can be assembled into SEVA plasmids. (Silva-Rocha et al., 2013)

The nomenclature of SEVA plasmids follows an alphanumerical scheme that assigns a unique code to each plasmid. The individual name of each plasmid begins with “pSEVA”, followed by a multiple-digit cipher consisting of four positions (Figure 2). The first position indicates the antibiotic resistance marker (AB^R) (Silva-Rocha et al., 2013). The second position identifies the origin of replication, *e.g.*, pBBR1 is assigned the number “3” (Silva-Rocha et al., 2013). While SEVA plasmids have long been suitable only for the engineering of Gram-negative bacteria, the collection was expanded in 2020 to

include a group of plasmid vectors suitable for the transformation of Gram-positive bacteria and yeasts. These are characterized by the presence of a double origin of replication (Martínez-García et al., 2020, 2022). The third position represents the cargo module, which can be either mono- or multifunctional, and the fourth position is for the gadgets (Martínez-García et al., 2022).

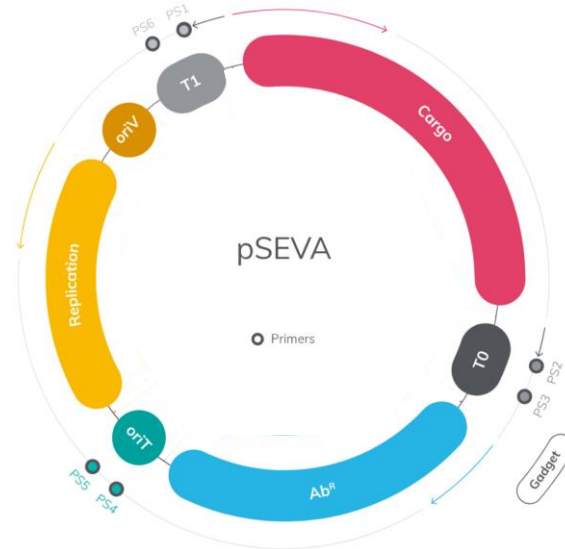


Figure 1: Schematic of the pre-formatted structure of SEVA plasmids.

All SEVA plasmid vectors are composed of three basic modules: an antibiotic resistance marker (Ab^R), a replication origin and a cargo, *e.g.*, multiple cloning site. T1 and T0 indicate transcriptional terminators that function to prevent transcriptional read-through. The colored arrows above the individual modules indicate the direction of transcription. (Modified from Martínez-García et al., 2020.)

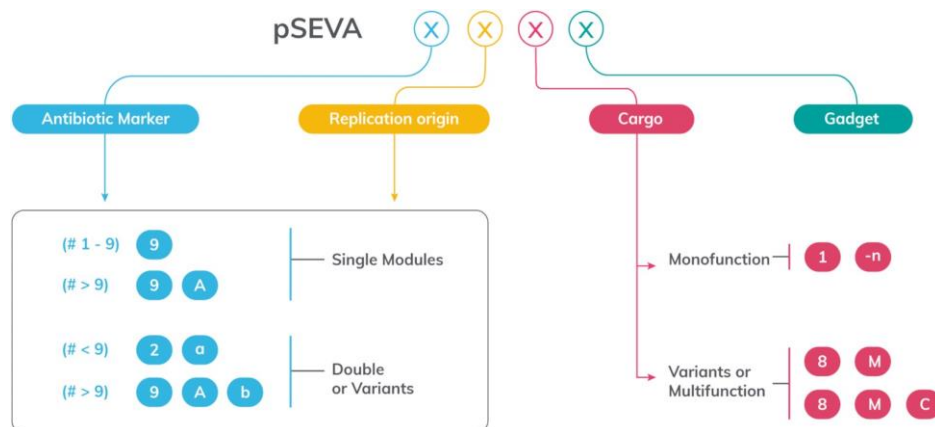


Figure 2: Alphanumerical schematic of the standardized nomenclature of SEVA plasmid vectors.

The figure shows the up-to-date rules for the naming of the four positions that constitute a SEVA plasmid. The first position is attributed to the antibiotic resistance marker and the second position to the origin of replication. Both follow a numeric code that uses the number 1-9 before adding capital letters. Variant or double resistance markers as well as replication origins are coded by the addition of a lowercase letter. As an example, kanamycin resistance is designated by the number “2” and the default gene for resistance comes from the pBAM1 plasmid. Chloramphenicol resistance is encoded by the *cat* gene from the pCC1FOS plasmid and is ascertained by the number “3”. The third position is the cargo that can be either mono-functional (number starting with 1) or multi-functional (number with capital letter). The default cargo designated by “1” is a polylinker. The gadgets, which are represented by the fourth position, are given lowercase Greek letters (α to ω). Hence, the plasmid pSEVA231 has a kanamycin resistance marker, a pBBR1 origin of replication, and the default multiple cloning site as cargo module. (Martínez-García et al., 2022)

2.1.3 The Biopart Assembly Standard for Idempotent Cloning (BASIC)

In addition to plasmid vectors, rapid and accurate assembly of DNA constructs constitutes an essential tool in synthetic biology, required for building genetic devices and circuits and iterating through the design-build-test cycle (Ellis et al., 2011; Haines et al., 2022). To date, a variety of DNA assembly methods with distinct advantages and disadvantages are available to synthetic biologists, some of which have already been summarized in detail (Casini et al., 2015; Ellis et al., 2011). Methods that allow the modular assembly of standardized genetic parts are best suited for high throughput and hierarchical assemblies and enable the reuse of integrated bioparts (Haines et al., 2022).

The **B**iopart **A**ssembly **S**tandard for **I**dempotent **C**loning (BASIC) is an orthogonal linker-guided method for the efficient and reliable multi-part assembly of DNA that was developed by Storch et al. in 2015 and additionally comprises a universal standard for single-part storage of DNA-bioparts and library construction (Storch et al., 2015). BASIC is characterized by the combinatorial and parallel assembly of bioparts, which is directed by the choice of linkers, and achieves assembly accuracies of over 90 % (Storch et al., 2015). The BASIC linkers are partially double stranded oligonucleotides and physically split into two half-linkers (Figure 3B). During DNA assembly, BASIC integrated bioparts are flanked by Suffix and Prefix half-linkers that anneal to their counterparts, thereby determining the order of assembly and leading to the formation of a part-linker-part-linker structure (Figure 3A) (Storch et al., 2020).

To integrate a biopart into the BASIC standard, it must be flanked with the BASIC Prefix (*iP*, 5'-TCTGGTGGGTCTCTGTCC 3') and BASIC Suffix (*iS*, 5'-GGCTCGGGAGACCTATCG-3') sequences (Storch et al., 2017). The *iP* and *iS* sequences have inward facing *Bsa*I recognition sites. Upon digestion with *Bsa*I, different 4 bp overhangs are generated at the Prefix and Suffix ends, to which the part annealing region of the BASIC Prefix and Suffix half-linkers anneals by end-specific ligation (Storch et al., 2015). After linker ligation, free linkers are removed by a purification step. The incubation of linker-adapted bioparts results in the annealing of the complementary single stranded regions of orthogonal linker pairs and thus DNA assembly (Storch et al., 2015).

In total, there are four different types of BASIC linkers with different functionalities that increase the genetic design space. While all linker types execute the same basic task of linking together DNA bioparts, some have additional properties. Neutral linkers are the simplest linkers, only allowing the assembly of DNA. Fusion linkers have a complete coding sequence read through and are therefore used to fuse proteins. RBS linkers encode a ribosome binding site (RBS) sequence with one of three translational strengths in their adapter region, which allows tuning of protein translation, *e.g.*, fluorescent reporter output. The last type are the methylated linkers, which encode the BASIC Prefix and Suffix sequences and restore the BASIC format in the new construct, allowing hierarchical assembly. A methylated cytosine protects the *Bsa*I sites from cleavage and thus destruction of the linkers during *Bsa*I digestion. Bioparts or composite parts flanked by methylated linkers can thus be

easily released from the construct into which they have been assembled and subsequently reused in further assemblies. This principle is also applied to the storage of BASIC integrated bioparts. The parts are therefore flanked with methylated linkers and then built into a storage vector, thereby restoring the BASIC format. In this way, parts can be stored in libraries in a common format, enabling the reuse and sharing of parts among researchers. (Storch et al., 2015, 2017)

In 2020, an OpenTrons DNA-BOT platform was launched for automated, low-cost assembly of DNA constructs using the BASIC methodology, taking genetic device and circuit construction to a new level and enabling the use of larger design spaces (Storch et al., 2020). Additionally, BASIC and its use of Bsal restriction enzymes is highly compatible with the SEVA plasmid collection, aligning two standards that are becoming increasingly popular in the field of synthetic biology, a notion further promoted by the introduction of the BASIC SEVA vector collection (Haines et al., 2022). SEVA plasmid vectors can be integrated into the BASIC format using functional primers that add the BASIC *iP* and *iS* sequences to the upstream and downstream ends of the amplified target vector part, *e.g.*, SEVA vector without cargo module (Chan et al., 2023). To circularize the BASIC integrated SEVA plasmid and store it as a biopart for BASIC assembly, it can be assembled with a cargo module, *e.g.*, fluorescent mScarlet counter-selection cassette (Storch et al., 2020), using methylated linkers.

2.1.4 The Microbial Chassis and Chassis-Effect

In synthetic biology, the cellular host that serves as a recipient for an engineered circuit is called a “chassis”. While the primary function of a chassis is to support and carry out programmed biological functions through the propagation of exogenous genetic information and the expression of encoded proteins, it is rarely considered itself as a design space for improving and tuning the function of genetic circuits (Kim et al., 2016). In this context, it is known that the host environment, the chassis, in which a genetic circuit operates has an influence on its behavior. This influence of the host physiology on the performance of the genetic circuit is termed the “chassis-effect”. The degree of uncertainty caused by the chassis-effect is difficult to predict and manifests itself from variations in performance across different hosts to complete circuit inoperability. This makes it challenging to expand programmed genetic devices into new, non-traditional chassis that may be more suitable for an intended application than the model hosts of synthetic biology, *e.g.*, *Escherichia coli*, *Bacillus subtilis*, *Saccharomyces cerevisiae* and *Pseudomonas Putida* (Chan et al., 2023).

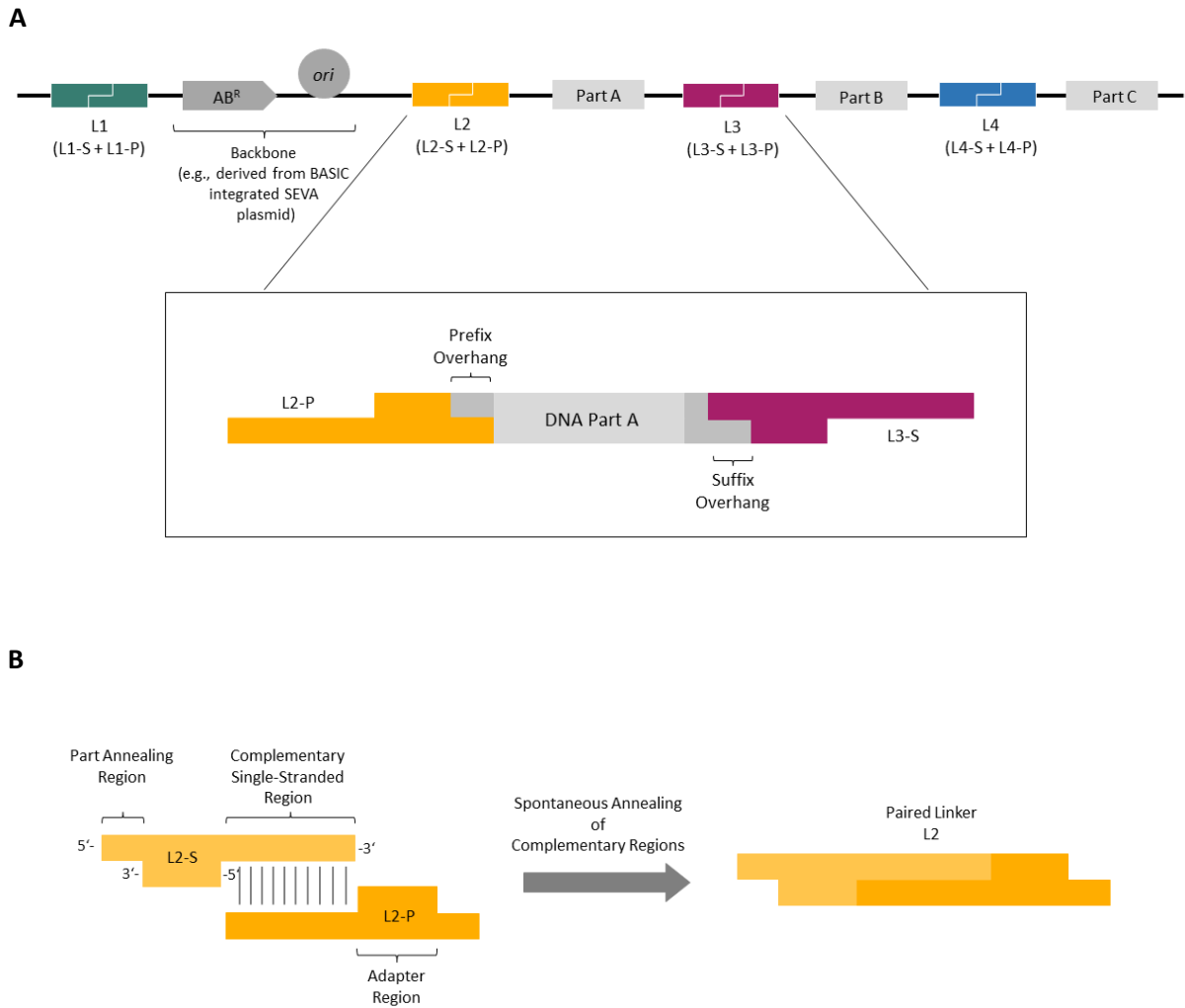


Figure 3: Schematic of the characteristic format of BASIC DNA assembly compositions and BASIC Linker structure.

A: The order of bioparts in BASIC DNA assembly is determined by the linkers and follows a part-linker-part-linker structure. Each biopart is flanked by a Prefix and Suffix half-linker, which anneal to the respective Prefix and Suffix overhangs of the biopart. One biopart in the assembly construct always constitutes the backbone consisting of an origin of replication (*ori*) and an antibiotic selection marker (*AB^R*) that is essential for the replication of the plasmids inside the host and for selection of positive transformants. The backbone used may originate from a BASIC integrated SEVA plasmid.

B: The Suffix and Prefix half-linkers LX-S and LX-P (X: 1-7) each feature a long single oligonucleotide strand, the complementary single stranded region, which anneal to form a BASIC linker pair. Unique complementary single stranded regions ensure that only the Suffix and Prefix half-linkers of the same linker pair anneal. The short single oligonucleotide strand of half-linkers constitutes the part annealing region where the half-linkers anneal to the BASIC characteristic 4 bp Suffix and Prefix overhangs of BASIC integrated and BsaI digested bioparts. The part annealing regions are identical for all linkers.

2.1.5 Synthetic Ecology and Co-Cultures

Synthetic microbial ecology is an emerging field in synthetic biology that aims to engineer microbial communities to fulfil desirable traits and tailored functions (Fredrickson, 2015). In contrast to synthetic biology, which seeks to design, build, and predict the dynamic behavior of genetic circuits in single cells, synthetic ecology aims to design, build, and predict the dynamic behavior, function, and interactions of multicellular systems such as microbial consortia (Dolinšek et al., 2016). The inherent complexity of natural microbial communities, characterized by largely undefined heterogeneity in composition, functionality and dynamic interactions, severely limits the (reproducible) interrogation of community activities, ecological principles and theories, as well as our ability to engineer them for controllable outputs (De Roy et al., 2014; Dolinšek et al., 2016; Zengler et al., 2019).

Synthetic microbial consortia are defined artificial systems with reduced complexity based on the co-cultivation of two or more selected and engineered microorganisms in a controlled environment (Bernstein & Carlson, 2012; De Roy et al., 2014; Liang et al., 2022). Synthetic co-cultures thus facilitate the study of the temporal and spatial dynamics that shape microbial community stability and functions, which has led to an increasing importance and interest in the field of synthetic ecology (De Roy et al., 2014). Emphasis is being placed on investigating and understanding the nature of binary interactions and how these principles can be used to engineer artificial interactions in synthetic microbial consortia with enhanced properties such as increased productivity and robustness (De Roy et al., 2014; Fredrickson, 2015). For example, a common design strategy for synthetic co-cultures is based on the principle of metabolic division of labor between two or more specialists (Lindemann et al., 2016), such as engineered syntrophy, or cross-feeding, where system performance benefits from metabolite exchange (Bernstein et al., 2012). The goal of synthetic ecology is therefore to design and construct robust and stable synthetic microbial communities with innovative applications beyond traditional monocultures (De Roy et al., 2014). Application fields include: Bioremediation and restoration ecology (Liang et al., 2022; Pawelczyk et al., 2008), construction of functional biomaterials (McCarty & Ledesma-Amaro, 2019), and medicine, *e.g.*, as an alternative to human faecal transplants in the treatment of *Clostridium difficile* infections, with the potential to replace antibiotics (Petrof et al., 2013; Shahinas et al., 2012).

2.2 Dynamics of Bacterial Growth

The measurement and study of bacterial growth dynamics, *i.e.*, the temporal changes in bacterial population density under defined growth conditions, is a key paradigm for microbiology (Schlechter et al., 2021) and of great importance for both fundamental and applied research in many adjacent scientific fields including synthetic biology (Chan et al., 2023; Lindemann et al., 2016) and biotechnology (Panikov, 2019; Sbarciog et al., 2011). Among other things, it provides the ability to

optimize bacterial growth for biotechnological processes (Jiru et al., 2017; Sbarciog et al., 2011); to study fitness cost of antibiotic resistance (A. R. Hall et al., 2011; Paulander et al., 2009); to gain insight into the evolutionary adaptation of microorganisms (Elena & Lenski, 2003; Shoemaker et al., 2021), and to infer interactions in mixed cultures (Nestor et al., 2023). The dynamics of bacterial growth can be visualized as growth curves by plotting measures of population density over time. In pure, planktonic batch cultures under controlled conditions, bacteria traverse through four distinct stages of cell growth, which can be observed within a growth curve (Figure 4).

2.2.1 Assessing and Quantifying Bacterial Growth

A variety of direct and indirect measures of population density can be used to quantify bacterial cells in planktonic culture. Determining the total number of cells by direct measures such as plate and microscopic cell counts or flow cytometry is often time and material consuming, less precise and not always compatible with high throughput methods (Panikov, 2019; Wilson et al., 2018). Thus, indirect methods of measuring population density are often preferred because they are usually simple, quick and can be used to screen large numbers of samples with little effort. Depending on the method used, a quantifiable cell property, *e.g.*, a change in overall mass or cellular component that increases as a result of bacterial growth, is measured (Panikov, 2019). The most commonly used indirect method for determining biomass concentration is optical density (OD) – where the turbidity, based on light scattering, of a planktonic bacterial culture is measured with a (microplate) spectrophotometer usually at a wavelength of 600 nm (OD600) (Schlechter et al., 2021). It is a simple, fast, and cost-effective proxy measurement that is readily suitable for high throughput applications in plate readers and automation (Beal et al., 2020). Although the measurement of optical density is a standard method for assessing bacterial growth, its application has limitations. This applies in particular to the observation of species-specific growth in (synthetic) microbial co-cultures and higher order consortia, as it is not possible to determine the OD of more than one bacterial strain or species in the same culture separately (Schlechter et al., 2021).

One way to overcome this limitation is fluorescence spectroscopy, where the fluorescence emission intensity serves as a proxy of bacterial population density (Schlechter et al., 2021; Wilson et al., 2018). Therefore, bacteria are genetically modified to constitutively express fluorescent reporter proteins with differential emission spectra enabling the monitoring and quantification of single species growth in mixed planktonic cultures. Similar to OD measurements, this method is compatible with high throughput assays and automation (Schlechter et al., 2021).

Relevant parameters characterizing bacterial growth are the specific growth rate μ and the maximum population density K (Figure 4). However, these cannot be derived directly from experimental measurements used to plot growth curves. To quantify these parameters, bacterial growth is modelled as a function of time, by fitting mathematical models with microbiologically relevant parameters to

growth curve data (Baty & Delignette-Muller, 2004; Worthan et al., 2023) – a process known as inverse modelling, which is explained in more detail in Chapter 2.3. The specific growth rate μ is a rate constant that describes the first order change in the number of cells per unit time under defined growth conditions during the log phase and is conventionally estimated from the exponential part of a growth curve. Exponential cell growth can be expressed by an ordinary differential equation that represents cell growth as a linear response (Figure 4) where the rate of change, *i.e.*, growth, is proportional to a dependent variable, *e.g.*, population density, OD600 or fluorescence emission intensity. This growth model can be solved as the basic equation of a line (Figure 4) and fitted to logarithmically transformed growth curve data, where the specific growth rate is the slope and N_0 represents the initial number of cells at time zero, corresponding to the initial conditions used for the solution (B. G. Hall et al., 2014). Alternatively, the specific growth rate can also be determined by regression analysis of parameterized growth models with a parameter accountable for the specific growth rate (Perni et al., 2005).

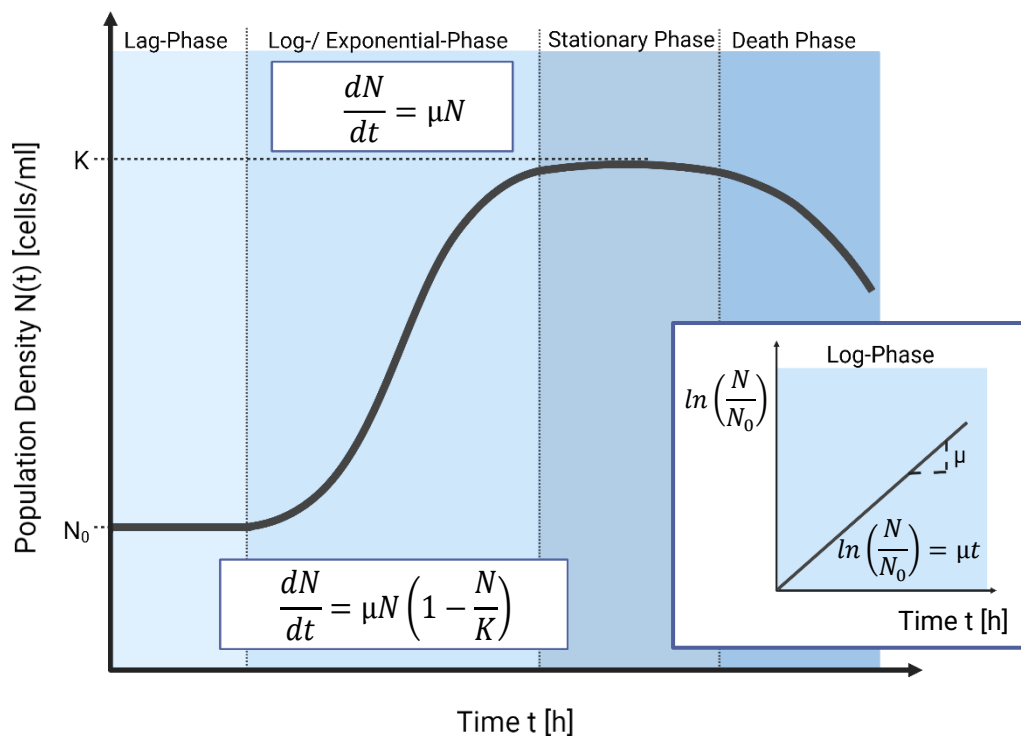


Figure 4: Bacterial growth curve showing all four stages of growth. Exponential cell growth is mathematically expressed by an ordinary differential equation, whereas sigmoidal cell growth through lag-, log-, and stationary phase can be modelled with a logistic differential equation.

Bacteria traverse through four distinct phases of cell growth: lag-phase, log-phase, stationary phase, and death phase. Common growth parameters derived from growth curve data are the specific growth rate μ [h^{-1}] and the maximum population density K [cells/ml]. The specific growth rate can be interpreted and determined as the slope of the straight line representing the linear relationship between the logarithm of the population density and time, which corresponds to the solution of the ordinary differential equation describing exponential cell growth.

N : population density [cells/ml]; N_0 : initial population density [cells/ml] at $t = 0$, corresponding to initial conditions.

(Created with BioRender.com)

To model the standard growth trajectory of a bacterial population, including the lag and stationary phase, and to estimate their respective growth parameters, alternative growth models must be used. A famous and widely used mathematical model based on an ordinary differential equation (ODE) to describe population dynamics was provided by Alfred J. Lotka (Lotka, 1925, 1956). This logistic differential equation describes the growth of a population that is limited by environmental factors, such as the availability of resources, space, or interactions with other populations. It therefore considers the saturation of population growth at a maximum population density K that the environment can sustain, also known as the carrying capacity (Figure 4). Logistic growth differs from exponential growth in that the growth rate, and thus the slope of the curve, slows down at a certain time t until it finally reaches an asymptote – the stationary phase. This population density N , at which the rate of change equals zero, is referred to as the maximum population density K . In the range of low population densities, N is very small compared to K and the logistic growth curve follows an approximately exponential trajectory. As the population density N increases, the growth curve flattens until it reaches the asymptote (Zwietering et al., 1990). Besides the standard logistic model provided by Alfred J. Lotka, there are numerous other mathematical models that can be used to describe bacterial growth dynamics (Baranyi et al., 1993; Baty & Delignette-Muller, 2004; Zwietering et al., 1990).

2.2.2 Measures of Bacterial Fitness

The study of population dynamics is one key to inferring bacterial interactions (Carrara et al., 2015; H.-S. Song et al., 2019). One way to study population dynamics is to examine the ecological fitness of a bacterial population, *i.e.*, its ability to survive and reproduce in a competitive and defined ecological context, including potential interactions with the environment and other species (Andrews & Harris, 1986). It is therefore a crucial parameter in the study of microbial communities, both from an ecological and synthetic biology point of view, as it affects the performance of microbial communities (Kehe et al., 2021) and genetic constructs operating inside bacterial hosts (Cardinale & Arkin, 2012).

From an ecological perspective, both the specific growth rate and the maximum population density are important measures of fitness and can be readily determined from experimental growth curve data by observing the changes in population density over time – as described in Chapter 2.2.1. In this thesis work, bacterial population growth dynamics were interrogated in terms of two measures. Firstly, with respect to fitness, *i.e.*, the specific growth rate, which in ecological terms indicates the number of progeny produced per unit time (Roller & Schmidt, 2015). High growth rates grant bacterial species competitive advantage over slow growing species, allowing them to outgrow slow growing species using the same resources (Bosdriesz et al., 2015). Secondly, population dynamics were interrogated with respect to the ecological carrying capacity, that is the maximum population density or amount of biomass that can be sustained by the environment. The ability of bacteria to dominate and outcompete initially fast-growing populations, *e.g.*, due to high substrate affinity or substrate

utilization efficiency, is an alternative strategy to secure the long-term survival of a bacterial population (Andrews & Harris, 1986; Yin et al., 2022).

2.2.3 Binary Growth Interactions

In nature, bacteria usually exist in close association with other microbes in communities of single or mixed species. Microbial communities are defined and shaped by complex microbial interaction networks, which at their most minimal level are based on the interactions between two species. These interspecies interactions are important for understanding the function, stability, productivity and structure of microbial communities and can have a positive, a negative or a neutral impact on the growth of each partner involved (Kehe et al., 2021; Nestor et al., 2023). Based on these one-way effects on the growth or fitness of a species, which represent a measure of the benefit or harm that each partner experiences from the association, the underlying type of the interaction can be inferred (Faust & Raes, 2012), which is referred to in this thesis as bidirectional interaction. Many different types of interactions and mechanisms mediating these interactions have been classified and have been discussed and summarized by other authors (Beck et al., 2016; Faust & Raes, 2012; García-Jiménez et al., 2021; Mougi, 2016; Tshikantwa et al., 2018).

In a highly simplified ecological framework, the numerous types of binary interaction modes described to this date can be grouped into three main categories – mutualism, commensalism, and antagonism – which for the purpose of this thesis work are defined as follows: Mutualism describes relationships in which both interacting partners benefit from the association, which means that both partners experience growth benefits. Commensalism is defined as a relationship in which one or neither of the species benefit from the association and neither of them is harmed. Relationships in which one or both partners are harmed and inhibited in their growth as a result of their interaction are defined as antagonistic. Characterizing the interactions between species and their underlying molecular mechanisms is crucial to understanding how microbial communities function and to optimize, engineer, and design the performance of communities to harness their potential for biotechnological applications (García-Jiménez et al., 2021).

2.3 Inverse Modelling in Microbial Ecology

Quantitative microbial ecology involves the estimation of parameters in mathematical functions that best represent the response variable of the process studied, *e.g.*, bacterial growth. Usually, these parameters are unknown quantities of biological importance that cannot be derived directly from experimental measurements or experimental observations (Robinson, 1985). The procedure during which the parameters that best approximate the given data are estimated by fitting a mathematical

model to experimental datasets is known as inverse modelling, a form of statistical regression analysis. Inverse modelling requires that both the response and predictor variables are known (Soetaert & Petzoldt, 2010).

2.3.1 Nonlinear Regression

Often, biological behavior is best modelled by mathematical equations that are nonlinear in their parameters and relate a response (\triangleq dependent variable) to a vector of predictor variables (\triangleq independent variables, covariates). These regression models of nonlinear functions can generally be written as follows:

$$Y_i = f(x_i, \hat{\theta}) + \varepsilon_i \quad , i = 1, 2, \dots, n \quad , n \in \mathbb{N}^+ \quad (1)$$

where Y_i designates the response, $f(x_i, \hat{\theta})$ is a known function of the covariate vector $x_i = (x_{i1}, \dots, x_{ik})^T$ and the parameter vector $\hat{\theta} = (\hat{\theta}_1, \dots, \hat{\theta}_p)^T$ with $k, p \in \mathbb{N}^+$ and ε_i represents random errors with assumed independence, mean zero, constant variance and normal distribution. (Smyth, 2002; L. Wu & Qiu, 2021)

The parameters $\hat{\theta}$ in the general, nonlinear regression model (Equation 1) can be estimated by fitting the function f to the experimental data of the response and predictor variables. This includes the identification of an optimal parameter set that minimizes the output of a chosen function representing a measure of goodness of fit with respect to the nonlinear parameters, *e.g.*, the residual sum of squares function (RSS, Equation 2), a procedure also known as least squares regression. (Smyth, 2002; Soetaert & Petzoldt, 2010)

$$RSS(\theta) = \sum_{i=1}^n (y_i - f(x_i, \theta))^2 \quad , n \in \mathbb{N}^+ \quad (2)$$

The optimal parameter set is determined by iteration, during which an initial set of parameter estimates is improved until the difference between the observed and fitted values of the response are minimized. This is done using optimization methods that aim to minimize a selected criterion function (Smyth, 2002). The initial set of parameters is used to calculate the corresponding response values at the same points x_i of the experimental observations, thus $f(x_i, \theta)$ represents the predicted response values. These predicted values are subtracted from the observed response values y_i to determine the residuals and calculate the residual sum of squares. Then the next set of parameter estimates is determined, and the RSS compared to the RSS of the initial set of parameters. This iteration process continues until the parameter estimates that best fit the dataset based on the least squares regression are determined (Robinson, 1985). The lower the RSS, the more accurate is the fit of the nonlinear

regression model. Depending on the mathematical model used, there can be more than one theoretical parameter combination for which the criterion function is minimized. Therefore, the choice of initial parameters is important and final parameter estimates should be examined for their biological meaningfulness (Robinson, 1985; Soetaert & Petzoldt, 2010).

2.3.2 Linear Regression of Transformed Nonlinear Models

Sometimes, it is possible to algebraically transform mathematical models that are nonlinear in their parameters into a linearized form in which the parameters become linear (Smyth, 2002; Xiao et al., 2011). This allows the transformed nonlinear model to be fitted to transformed data and parameter estimates to be determined by linear regression analysis (Robinson, 1985). Thus, in linear regression models, the response and predictor variables are assumed to have a linear relationship. The generalized linear regression model is given in Equation 3, where Y_i represents the observed response, θ_k indicates the unknown parameters that are to be estimated, x_{ip} are the covariates and ε_i is the random error (L. Wu & Qiu, 2021).

$$Y_i = \theta_0 + \theta_1 x_{i1} + \dots + \theta_k x_{ik} + \varepsilon_i \quad , i = 1, 2, \dots, n \quad , k, n \in \mathbb{N}^+ \quad (3)$$

A common statistical measure of goodness of fit used to specify how well the experimental data fits the linear regression model is the coefficient of determination, which is denoted by R^2 . Typically, the coefficient of determination takes values between 0 and 1, with higher values indicating higher model accuracy. Although R^2 values provide a simple indication of model fit, over-interpretation of this statistical measure should be avoided, as it only predicts the correlation between the variables, not their causality (Cornell & Berger, 1987; Kvålseth, 1985, p. 2; Ratkowsky, 1993). The regression analysis of linear models is often preferred because their parameter estimators are relatively unbiased, have minimum variance and are normally distributed compared to those of nonlinear regression models (Ratkowsky, 1993).

2.4 Bacterial Strains

2.4.1 *Escherichia coli*

Escherichia coli is a Gram-negative, asporogenous, facultative anaerobic and rod-shaped bacterium that belongs to the genus *Escherichia* of the family *Enterobacteriaceae*. The bacterium was described by Theodor Escherich in 1884, belongs to the best-characterized microbes and is recognized as an esteemed model organism. In nature, the bacterium inhabits non-host environments such as soil or

water habitats but also the gastrointestinal tracts of warm-blooded animals and humans (Yu et al., 2021). Despite its predominantly commensal relationship with its host, there are pathogenic strains in animals and humans that cause intestinal and extra-intestinal infections and diseases such as septicemia, meningitis and enteritis (Allocati et al., 2013; Yu et al., 2021). Multidrug-resistant *Escherichia coli* strains are spreading indefatigably and pose an immense risk to animal and human health (Allocati et al., 2013). *Escherichia coli* is an important model microbial species in synthetic biology that has contributed significantly to the beginnings of research and development in this field (Cameron et al., 2014).

Escherichia coli strain DH5 α is a widely used engineering lab strain derived from the K-12 strain, that has an endA1 mutation that causes inactivation of an intracellular nonspecific endonuclease I that degrades plasmid DNA (Anton & Raleigh, 2016). Its tolerance towards components of common transformation buffers, its ability to efficiently express foreign plasmids and maintain plasmid stability, and the fact that it can be efficiently transformed make the DH5 α strain an important host platform for cloning and synthetic biology applications (Anton & Raleigh, 2016; Y. Song et al., 2015).

2.4.2 *Pseudomonas* Genus

The *Pseudomonas* genus was first characterized by Migula in the late 19th century (Migula, 1894) and comprises a group of ubiquitous, metabolic and genetic diverse Gammaproteobacteria. Members are Gram-negative, aerobic and motile rods isolated from diverse terrestrial and aquatic ecosystems, including plants, soil, air, seawater and marine sediments (M. Wang & Sun, 2016). Some species thrive in extreme environments such as Antarctic and desert regions, hot springs and contaminated water and soil sources (Peix et al., 2018). More than 240 species, including plant, animal and human pathogens, have been validly published and the number is likely to further increase in future, making *Pseudomonas* the largest genus within the family of *Pseudomonadaceae* (Rudra & Gupta, 2021). Members of the genus *Pseudomonas* are used in numerous biotechnological applications and as microbial platforms in synthetic biology (Nikel et al., 2014).

2.4.2.1 *Pseudomonas deceptionensis*

Pseudomonas deceptionensis M1 is a strictly aerobic, Gram-negative bacterium isolated from marine sediments in the Antarctic Sea in 2011 (Carrión et al., 2011). The bacterial cells are rod-shaped (0.8 x 1.5-2.0 μm), catalase- and oxidase-positive, non-spore forming and motile (one single polar flagellum). *P. deceptionensis* M1 is psychrotolerant and grows in temperature ranges between -4 °C and 34 °C. The cells tolerate pH values between pH 5 and pH 10 and NaCl concentrations up to 6 % (w/v) on nutrient agar. Cultivation in King B medium has also shown no production of fluorescent pigments. *P. deceptionensis* M1 is neither capable of reducing nitrate nor producing indole or

hydrogen sulfide (Carrión et al., 2011). Interestingly, *P. deceptionensis* M1 produces dimethylsulphide (DMS) by a novel dimethylsulphoniopropionate-independent DMS production pathway (Carrión et al., 2015).

2.4.2.2 *Pseudomonas fluorescens*

Pseudomonas fluorescens is a physiologically and genetically diverse, Gram-negative, bacterium (Trippe et al., 2013) with aerobic, motile and rod-shaped cells (Scales et al., 2014). It is ubiquitous in terrestrial habitats and is found predominantly in moist environments, including soil, leaves, water and animals (Sun et al., 2016; Trippe et al., 2013). While the optimal temperature range for growth is 25 - 30 °C (Liu et al., 2021), cells can grow in temperatures between 4 - 32 °C (Scales et al., 2014). If incubation temperatures are too high, *Pseudomonas fluorescens* can transition to a viable but non-culturable state (Scales et al., 2014). It is a bacterial pathogen that can grow in mammalian hosts, including humans, where it causes diseases such as bacteremia (Scales et al., 2014; Sun et al., 2016) and pneumonia (Liu et al., 2021).

Pseudomonas fluorescens strain SBW25 is a plant-associated, plasmid-free and non-pathogenic bacterium that was isolated from the phytosphere of sugar beet plants (Bailey et al., 1995). It exhibits biocontrol activities and plant growth promoting properties and is widely used as a model organism for evolution and plant colonization studies (Trippe et al., 2013) as well as for studies on biofilm formation (Preston et al., 2003). In addition, strain SBW25 produces and secretes the non-proteinogenic amino acid furanomyacin, a ninhydrin-reactive compound with selective antimicrobial activities not previously known to be produced by members of the genus *Pseudomonas* (Trippe et al., 2013).

2.4.2.3 *Pseudomonas putida*

Pseudomonas putida is an ubiquitous, Gram-negative, strictly aerobic, rod-shaped bacterium isolated predominately from soil, plants and water (Weimer et al., 2020). It has enormous biotechnological potential for industrial production and as a host for synthetic biology due to its metabolic capabilities, genetic accessibility, low maintenance demands, rapid growth, high biomass yields, as well as robustness and stress-resistance, e.g., tolerance towards oxidative stress due to a high redox capacity, organic solvents and toxic chemicals (Ankenbauer et al., 2020; Nikel et al., 2016; Weimer et al., 2020). To date, *Pseudomonas putida* has already been engineered to perform diverse functions and the growing toolbox available has highly benefited from the introduction of modular pSEVA vectors (Lammens et al., 2021; Weimer et al., 2020).

Pseudomonas putida KT2440 is a saprophytic soil bacterium (Nelson et al., 2002) and a TOL plasmid pWWO free derivative of the mt-2 strain isolated in Japan (Nakazawa, 2002), capable of colonizing the

rhizosphere of crops (Espinosa-Urgel et al., 2000). It represents the best-studied *Pseudomonas putida* strain, is used as a model laboratory organism and as a model species for industrial applications and is certified as HV1 by the US Food and Drug Regulation Administration (FDA) (Kampers et al., 2019; Weimer et al., 2020).

2.4.3 *Halopseudomonas* Genus

In 2021, the transfer of species from the Pertucinogena clade into the novel *Halopseudomonas* genus within the family *Pseudomonadaceae* was proposed. Members of the *Halopseudomonas* genus are halophilic or halotolerant, which is the eponymous characteristic for this novel genus – it includes salt-loving or -tolerating *Pseudomonas* spp. – and can be distinguished from other species of the family *Pseudomonadaceae* by 24 conserved signature indels (CSIs). Most *Halopseudomonas* spp. have been isolated from the marine environment, but also from desert sand, food waste, soil, air sample, aquatic plants, and algae. Members are Gram-negative, aerobic, or facultative anaerobic, non-spore forming rods, and most species are motile by a single polar flagellum. They grow at temperatures ranging between 5 - 50 °C, with optimal growth achieved between 25 - 37 °C. Furthermore, most species require a pH value between 6 and 10 and salt concentrations between 1 - 10 % (w/v) for optimal growth. Colonies have been described as circular, convex, and pale white to pale yellow after incubation in nutrient agar. The G+C content of DNA of representative species ranges from 57.5 - 63 mol % with genome sizes of 3.0 to 4.6 Mbp. (Rudra & Gupta, 2021)

2.4.3.1 *Halopseudomonas aestusnigri*

Halopseudomonas aestusnigri strain VGXO14, first validly published under the name *Pseudomonas aestusnigri*, was isolated from crude oil-contaminated intertidal sand from the Atlantic shore of Spain in 2004 after the Prestige oil spill in November 2002. The bacterial cells are Gram-negative, strictly aerobic, rod-shaped (1.6 - 2.0 µm long and 0.6 - 0.7 µm wide) and grow at temperatures of 18 - 42 °C. Optimal growth was observed at 25 - 30 °C, pH 6 - 10 and 2 - 10 % (w/v) NaCl. Primary characterization experiments have revealed a limited carbon utilization compared to other species (Sánchez et al., 2014).

Recently, a novel and highly organic-solvent-tolerant esterase of great relevance for biocatalytic applications was identified from the marine crude oil-degrading (hydrocarbonoclastic) bacterium *Halopseudomonas aestusnigri* VGXO14 (Bollinger, Molitor, et al., 2020). Furthermore, strain VGXO14 also encodes a novel carboxylic polyester hydrolase (PE-H) that shows hydrolytic activity towards various polyethylene terephthalate (PET) substrates (Bollinger, Thies, Knieps-Grünhagen, et al., 2020).

2.4.3.2 *Halopseudomonas oceani*

Halopseudomonas oceani (basonym: *Pseudomonas oceani*) strain KX20 was isolated in 2014 from deep seawater in the northwestern Pacific Ocean. The cells are Gram-negative, aerobic and non-pigmented rods (0.4 μm wide and 2.1-2.6 μm long) that are motile by a single polar flagellum. The bacterium can grow in temperature ranges between 4 - 41 $^{\circ}\text{C}$, 0 - 10 % (w/v) NaCl and pH values between 6 - 10 and can assimilate carbon sources other species of the genus cannot, e.g., L-alanyl-glycine and D-Mannose. Polar lipids produced by the KX20 strain include phosphatidylethanolamine (PE), diphosphatidylglycerol (DPG) and phosphatidylglycerol (PG). Growth in King B medium showed no production of fluorescent pigments (M. Wang & Sun, 2016). *Halopseudomonas oceani* KX20 also shows hydrolytic activity with respect to different polyester substrates (Molitor et al., 2020).

2.5 The Open Science Framework (OSF)

Despite the competitive environment in the natural sciences, there is currently an emerging trend towards open sharing of research results and collaboration, which is becoming increasingly important in the scientific community under the term “Open Science” (Sanjana, 2021). Open Science aims to promote transparency at every stage of research and increase the reproducibility of data to make knowledge and research more accessible and to exploit new ways of communicating science (Sanjana, 2021; Sullivan et al., 2019), thereby influencing the way research is conceived, conducted and recorded (Vicente-Saez & Martinez-Fuentes, 2018).

The Center for Open Science (COS), a non-profit organization, has launched the Open Science Framework (OSF) to create an open-source platform for researchers and scientists of all disciplines to promote the reproduction and openness of research projects, including methods, relevant data, and results on a global scale. The OSF platform enables the centralization of workflows by providing a platform for the (joint) development, management, storage, and sharing of research ideas, study designs, data and written outputs such as reports and papers (Foster & Deardorff, 2017). An overview of the tools and functions of the OSF platform and a detailed description on how it can be used to increase the transparency of one’s own research is provided by the work of Sullivan et al. (Sullivan et al., 2019).

3 Materials and Methods

3.1 Bacterial Strains and Cultivation Conditions

The bacterial wild-type strains used in this study include *Escherichia coli* DH5 α (DSMZ 6897), *Halopseudomonas aestusnigri* VGXO14 (DSMZ 103065), *Halopseudomonas oceani* KX20 (DSMZ 100277), *Pseudomonas deceptionensis* M1 (DSMZ 26521), *Pseudomonas fluorescens* SBW25, and *Pseudomonas putida* KT2440 (DSMZ 6125). *Pseudomonas fluorescens* SBW25 was donated to the M2 Research Group (M2RG, Microalgae and Microbiomes Research Group, UIT – The Arctic University of Norway) by Rosemarie Wilton from the Argonne National Laboratory, Illinois, USA (Chan et al., 2023). Unless otherwise stated, all bacterial wild-type strains were cultured in autoclave sterilized Lauria-Bertani (LB) medium (MP Biomedicals, Santa Ana, Ca, USA) at 30 °C with constant shaking in an incubator. Plasmid bearing strains were grown in LB medium with an appropriate antibiotic (100 μ g/mL kanamycin or 25 μ g/mL chloramphenicol in ethanol). A negative control (LB medium without bacterial inoculum) was included with each cultivation to check for contamination. Inoculation and handling of liquid cultures was always performed with aseptic technique under a laminar flow hood. LB agar plates inoculated from glycerol stocks were streaked under the laminar flow hood, while inoculation of LB agar plates from liquid cultures – e.g., after transformation, was performed near a Bunsen burner flame to secure sterility.

Antibiotic stock solutions were prepared by complete dissolution of kanamycin powder (BioChemica, K1377-5G) in MilliQ-water to a final concentration of 100 mg/mL and by dissolving chloramphenicol powder (BioChemica, C1919-5G) in ethanol to a concentration of 25 mg/mL. The antibiotic stock solutions were then filter-sterilized into sterile 1.5 mL Eppendorf tubes using a sterile syringe and sterile 0.22 μ m syringe filter unit. Aliquots were stored at -20 °C.

3.2 BASIC DNA Assembly

The broad-host-range reporter plasmids were assembled in the Biopart Assembly Standard for Idempotent Cloning (BASIC). This is a linker-guided DNA assembly method for efficient and parallel assembly of bioparts integrated into the BASIC standard (see 2.1.3). The DNA parts used in this study were sourced from the M2RG synthetic biology library kit. The starting material consisted of six pre-assembled promoter-reporter cassettes stored in a pSEVA331-derived backbone with a chloramphenicol selection marker. These contigs were excised and assembled into a pSEVA231-derived backbone containing a kanamycin selection marker. The first step was therefore to isolate the plasmids carrying the contigs and backbone of interest from *E. coli* DH5 α , which is used as host for

long-term vector storage. Glycerol stocks of the respective *E. coli* DH5 α strains were used to each inoculate 7 mL LB medium supplemented with an appropriate antibiotic and cultured at 37 °C with constant shaking overnight, followed by plasmid preparation (see 3.6) and storage of isolated plasmids at -20 °C until used for BASIC clip reactions.

3.2.1 BASIC Clip Reaction

BASIC clip reactions were performed in 0.2 mL PCR tubes to digest the DNA parts of interest out of their storage vectors and ligate the linkers. For each clip reaction 17 μ L MilliQ-water, 3 μ L 10X T4 DNA Ligase Reaction Buffer (New England Biolab, Ipswich, USA, Cat. No.: B0202S), 1 μ L of suffix linker, 1 μ L of prefix linker and 200 nmol of the BASIC biopart DNA (50 ng per 1kb total plasmid size) were mixed and topped up with MilliQ-water to a total volume of 28.5 μ L. Afterwards, 1 μ L BsaI-HFv2 20 U (New England Biolabs, Ipswich, USA, Cat. No.: R3733) and 0.5 μ L T4 DNA Ligase (New England Biolab, Ipswich, USA, Cat. No.: M0202L) were added to each reaction. The resulting reaction mix (total volume of 30 μ L) was then carefully mixed by pipetting up and down and subsequently incubated using a PCR thermocycler with the following temperature program: cycle 20x (37 °C for 2 min, 20 °C for 1 min), 60 °C for 20 min. The clipped parts were then stored at -20 °C until purification. In total, seven clip reactions were performed. L1-P and L2-S linkers were clipped to the promoter-reporter cassettes and the L2-P and L1-S linkers were attached to the pSEVA231-derived backbone.

3.2.2 BASIC Clip Purification

The restriction-ligation reactions (see 3.2.1) were purified using a magnetic bead purification system. Purification reactions were performed in a 96-well Flacon microplate using Mag-Bind TotalPure NGS (Omega Bio-Tek, USA, Cat. No.: M1378-01) according to the manufacturer's instructions. The total volume of 30 μ L of each restriction-ligation reaction was thoroughly mixed with 54 μ L of magnetic beads by pipetting up and down ten times, ensuring that no air bubbles were formed. After a 5-min incubation at room temperature, the Falcon plate was placed on a magnetic stand for about 2 min until the magnetic beads formed rings and the solution cleared. Once the solution in each well had cleared, it was completely removed from the center of the wells using a 200 μ L pipette tip and 190 μ L of fresh 70 % ethanol solution were added to the beads. After an incubation step of 30 sec, the solution was removed again. This washing step was repeated one more time. The Falcon microplate was then left to dry for approximately 5 min and was subsequently removed from the magnetic stand. The magnetic beads were resuspended in 32 μ L MilliQ-water, incubated at room temperature for 1 min to allow for DNA to elute and the Falcon plate placed back on the magnetic stand. After magnetic bead rings were formed and the solution cleared, 30 μ L of the solution containing the eluted DNA were transferred into a fresh 1.5 mL Eppendorf tube. The purified clipped parts were stored at -20 °C until they were used in BASIC clip assembly reactions.

3.2.3 BASIC Clip Assembly

A total of six BASIC clip assemblies were performed, each with two parts. For each BASIC assembly reaction, a reaction mixture was prepared in a 200 μL PCR tube consisting of: 2 μL MilliQ-water, 1 μL 10X rCutSmart Buffer (New England Biolab, Ipswich, USA, Cat. No.: B6004S), 1 μL of purified linker ligated BASIC part A and 1 μL of purified linker ligated BASIC part B, topped up with MilliQ-water to a total reaction volume of 10 μL . The 10 μL reaction mix was then mixed by pipetting up and down and subsequently incubated in a PCR thermocycler at 50 °C for 45 min to run the assembly reaction. The *in vitro* assembled plasmids were then stored at -20 °C until transformation and propagation in competent *E. coli* DH5 α cells.

3.2.4 Heat-Shock Transformation of BASIC Constructs and Assembly Confirmation

The six reporter plasmids constructed with BASIC were then transformed into *E. coli* DH5 α for propagation and plating of transformed strains on LB agar with kanamycin. Single colonies of plasmid bearing cells were then used to verify the correct assembly and to inoculate clonal population of the respective strains for cryopreservation. For the transformation of the six *in vitro* assembled BASIC constructs, competent *E. coli* DH5 α cells stored at -80 °C were thawed on ice. Meanwhile, a volume of 5 μL of each BASIC assembly reaction (see 3.2.3) was transferred into pre-autoclaved 1.5 mL Eppendorf tubes and cooled on ice. Then, 50 μL of thawed competent *E. coli* DH5 α cells were added to each pre-cooled 5 μL BASIC assembly reaction and incubated on ice for 20 min. Afterwards, the tubes were placed in a water bath at 42 °C for 45 sec to heat shock the cells and subsequently placed back on ice for 2 min. A total volume of 200 μL LB medium was added to each tube to enhance the recovery of cells, which were then incubated for one hour at 37 °C with shaking.

After recovery, the transformed cells were plated onto pre-warmed LB agar plates with kanamycin using an ethanol sterilized cell spreader. For each of the six transformation reactions, 100 μL transformed cells were plated. The remaining volume of each cell culture was centrifuged at 8000 rpm for 3 min at room temperature. The cell pellets were resuspended in 100 μL LB medium and plated out on LB agar plates containing kanamycin. All plates were incubated overnight at 37 °C. The next day, 4 single colonies of each strain were taken from the transformation plates and screened by colony-PCR (cPCR) to confirm the presence of the respective promoter-reporter cassettes (see 3.4). For each transformation, one of the screened colonies that was shown to contain the correct assembled plasmid was selected and used to inoculate 7 mL LB medium with kanamycin for overnight cultivation. These overnight cultures were then used to make 25 % glycerol stocks and isolate the new plasmid constructs by miniprep (see 3.6) for later transformation of the five remaining host species (see 3.3). For cryopreservation of transformed *E. coli* DH5 α strains, 1 volume of overnight culture and 1 volume of 50 % glycerol were transferred into a 2 mL cryotube (VWR International, Leuven, Belgium, Cat. No.: 479-1239), mixed thoroughly by repetitive inversion and subsequently stored at -80 °C. As an

additional conformation that the plasmids were correctly assembled, LB agar plates with chloramphenicol and LB plates with kanamycin were streaked from previously made glycerol stock using sterile inoculation loops.

3.3 Electroporation

All *Pseudomonas* and *Halopseudomonas* spp. were transformed by electroporation with each of the six broad-host-range reporter plasmids. First, a clonal population of the desired species was inoculated from a single colony in a sterile glass tube and incubated at 30 °C with shaking overnight. While all *Pseudomonas* spp. were inoculated in 5 mL LB medium, both *Halopseudomonas* spp. were inoculated in 7.5 mL LB medium (one overnight culture was needed for each transformation reaction). The next day, fresh LB medium was added to each culture to a total volume of 10 mL per glass tube. The cultures were incubated for an additional 1 - 2 h at 30 °C with shaking and the bacterial cells were then harvested by centrifugation. Therefore, a volume of 1.5 mL of overnight culture per transformation reaction was transferred into an autoclave sterilized 1.5 mL Eppendorf tube and centrifuged for 3 min at 8000 rpm and room temperature for all *Pseudomonas* spp.. For *Halopseudomonas* spp., the entire volume of the overnight culture (10 mL) was transferred into a sterile 15 mL Falcon tube and centrifuged for 15 min at 4400 rpm and room temperature. After centrifugation, the supernatants were discarded, and the cell pellets resuspended in 1.5 mL autoclave sterilized sucrose electroporation buffer (300 mM Sucrose, 1 mM MgCl₂). Resuspended *Halopseudomonas* spp. were additionally transferred into sterile 1.5 mL Eppendorf tubes.

Resuspended bacterial pellets in 1.5 mL Eppendorf tubes were then centrifuged for 3 min at 8000 rpm and room temperature and supernatants discarded. Afterwards, the pellet was resuspended in 1.5 mL sucrose electroporation buffer, centrifuged for 3 min at 8000 rpm and room temperature and the supernatant discarded. This washing step was repeated twice. The final bacterial cell pellet was resuspended in 80 µL sucrose electroporation buffer, transferred into sterile, pre-labelled 1-mm gap electroporation cuvettes (VWR International, Leuven, Belgium, Cat. No.: 732-1135) and incubated with 50 - 75 ng of the respective plasmid DNA for 30 min at room temperature. A negative control was included for each species that was transformed. These were treated in the same way as the other samples, with the only exception that no plasmid DNA was added before electroporation.

After incubation, the cells were electroporated at 1250 V with high voltage setting using an ECM 399 Exponential Decay Wave Electroporation System (BTX Harvard Apparatus, 45-0000). Immediately after electroporation, 750 µL of LB medium were added to the electroporated cells in the cuvette and mixed gently by pipetting up and down. The electroporated cells were then transferred into a sterile glass tube with 5 mL LB medium and incubated at 30 °C with shaking for 1 - 2 h for recovery. The electroporation was performed near a Bunsen burner flame to secure sterility.

After recovery, 100 μ L of each cell culture were plated on LB agar plates with kanamycin using an ethanol sterilized cell spreader. In addition, the remaining cells of all *Halopseudomonas* spp. were harvested by centrifugation at 4000 rpm and room temperature for 10 min, the cell pellet resuspended in approximately 100 μ L LB medium and plated as described above. The streaked plates were then incubated at 30 °C for 1-2 days until the colonies had grown sufficiently large. To confirm the successful transformation of host species, 4 to 8 single colonies were picked from each transformation plate and screened by cPCR (see 3.4). Subsequently, one of the colonies that tested positive for each strain was used to inoculate 5 mL of LB medium with kanamycin in a sterile glass tube, which was then incubated overnight at 30 °C with shaking. The next day, three 25% glycerol stocks of each plasmid bearing strain were prepared by thoroughly mixing 1 volume of 50 % glycerol and 1 volume of overnight culture in a 2 mL cryogenic vial (VWR International, Leuven, Belgium, Cat. No.: 479-1239) followed by immediate storage at -80 °C.

3.4 Colony-PCR (cPCR)

After heat-shock transformation of *E. coli* DH5 α and electroporation of the other host species, cPCR was performed to confirm the successful incorporation of plasmids by amplification and detection of the respective promoter-reporter cassettes. In total, between four and eight colonies of each transformant were picked and screened by cPCR. In addition, negative controls for each species and a PCR-negative control were included for each cPCR. While no DNA was added to the PCR-negative controls to exclude possible contamination, the respective wild-type counterparts of the plasmid bearing strains screened was used as a negative control. Since the wild-type strain does not carry a plasmid and therefore does not contain the target sequence to be amplified, any amplification products indicate artifacts due to nonspecific primer binding in the bacterial genome.

Colony-PCR amplification reactions were performed in 0.2 mL PCR tubes. For each reaction, 6.75 μ L PCR-grade water, 0.375 μ L 10 μ M L1-F primer (5'- GACTCTCCGAGACAGTCAGAGGGTA-3'), 0.375 μ L 10 μ M L2-R primer (5'- GAACTACACGACTGGATACTGACTTTTCACAC-3') and 7.5 μ L Taq Plus 2X Master Mix with 1.5 mM MgCl₂ from VWR Life Science (Leuven, Belgium, Cat. No.: 733-2599) were mixed to a total reaction volume of 15 μ L. To avoid premature activity of the polymerase, the reaction mixtures were pipetted on ice. Then each colony to be screened was picked with a pipette tip, briefly tapped on a marked spot on a LB agar plate with kanamycin and subsequently dipped into the reaction mixture of the corresponding PCR tube and separated from the pipette. After all colonies had been picked, the pipette tips were carefully removed from the PCR tubes and discarded. The reaction mixtures were then incubated in a PCR thermocycler using a heated lid with the following temperature settings: initial denaturation: 95 °C for 5 min, cycle 25x (denaturation: 95 °C for 30 sec, annealing: 57 °C for 30 sec, elongation: 72 °C for 2 min), final elongation: 72 °C for 5 min. Afterwards, the PCR products were separated according to their size and analyzed by gel electrophoresis (see 3.5). The LB plate with the

inoculum of the screened colonies was incubated at 30 °C overnight. The next day, one colony tested positive for each plasmid bearing strain was used to inoculate 5 mL LB medium with kanamycin in a sterile glass tube, which was then cultured at 30 °C with shaking overnight. Glycerol stocks of the different plasmid bearing strains were made from these overnight cultures (see 3.3).

3.5 Agarose Gel Electrophoresis

To confirm the correct assembly of the broad-host-range reporter plasmids and the successful transformation of hosts, cPCR was performed and the amplification products were visualized in 0.8 % agarose gels. Therefore, 0.8 g of UltraPure™ Agarose (Invitrogen, Carlsbad, CA, USA) were boiled in 100 mL 1x TAE (Tris-acetate-EDTA) buffer until the agarose was completely dissolved and a clear agarose gel solution obtained. A total volume of 10 µL of GelRed Nucleic Acid Stain 10000X in water (Biotium, Hayward, CA, USA) was then added, mixed gently, and poured into an appropriate gel chamber with comb for the agarose to set at room temperature. Once the gel had solidified, the samples were applied. For this purpose, a volume of 5 µL of each amplification product to be analyzed was each mixed with 1 µL of 6X loading buffer on parafilm and the resulting total volume of 6 µL was subsequently pipetted into the gel pockets. Using the GeneRuler 1 kb Plus DNA Ladder from ThermoFisher Scientific (Waltham, USA, Cat. No.: SM1331), the DNA fragments were electrophoretically separated in the agarose gel at 150 V for 20 - 35 min and subsequently evaluated by band detection under UV light in a VWR Gel Documentation System Smart3.

3.6 Plasmid Preparation

The isolation of plasmids from *E. coli* DH5α was performed with the QIAprep Spin Miniprep Kit from Qiagen (Hilden, Germany), which uses silica spin columns for selective purification of plasmid DNA after alkaline cell lysis. This was done according to the manufacturer's instructions. No LyseBlue reagent was added to the resuspension buffer P1.

Prior to plasmid purification, the bacterial cells were harvested by centrifugation. Therefore, 5 mL of overnight culture of plasmid bearing *E. coli* DH5α strains were transferred into a sterile 15 mL falcon tube and centrifuged for 10 min at 4 °C and 5400 x g. The supernatant was then discarded, the cell pellet resuspended in 250 µL Buffer P1 and transferred to a 1.5 mL Eppendorf tube (step 1). After lysis of the bacterial cells (step 2 - 3), lysate was then cleared by centrifugation (step 4) and applied to provided spin columns (step 5) in which the plasmid DNA adsorbs to the silica membrane. Two washing steps were performed to remove impurities (step 6 - 9) before the DNA was eluted with 50 µL Buffer EB (step 10). The concentration of the isolated plasmid DNA was then determined fluorometrically using a Qubit fluorometer (see 3.7) and the eluted DNA was subsequently stored at -20 °C.

3.7 Fluorometric Quantification of DNA

The isolated plasmid DNA was quantified using a Qubit fluorometer (Invitrogen, Waltham, USA, Cat. No.: Q32857) and the corresponding Qubit™ 1X dsDNA HS Assay Kit from ThermoFisher (Waltham, USA, Cat. No.: Q32854). First, the Qubit fluorometer was calibrated according to the manufacturer's instructions using the two DNA standards included in the kit. After successful calibration, the Qubit working solution was prepared by diluting the Qubit reagent 1:200 in Qubit buffer. For each sample, 197 μ L of Qubit working solution were transferred into a Qubit™ Assay Tube (Cat. No. Q32856) and 3 μ L of sample was added to each tube respectively. The tubes were then vortexed for 3 - 5 sec and incubated for 2 min at room temperature before the concentration of plasmid DNA was measured.

3.8 Growth Assays

The data needed to characterize the new plasmid bearing strains and to infer population dynamics were collected by growth experiments in sterile black Thermo Scientific™ Nunc MicroWell 96-Well Optical-Bottom Microplates (Cat. No.: 165305). Due to the black upper structure of the microplates, back-scattering of light and background fluorescence is minimized during fluorescence measurements. Both, optical density, and strain-specific fluorescence were measured over time as surrogates for biomass.

Prior to the growth experiments, fresh overnight cultures were prepared in sterile glass tubes by inoculating the respective strains in 5 mL LB medium from single colonies on agar plates and incubating them overnight. For the cultivation of plasmid bearing strains, the LB medium was supplemented with kanamycin. For both mono- and co-culture growth assays, 96-well microplates were prepared according to the plate design depicted in Figure 5, which allows for timesaving with multi-channel pipettes. The use of a standardized plate layout facilitated the subsequent transfer and processing of experimental data in R. In each microplate, the wild-type counterparts of the plasmid bearing strains were grown as a reference.

Monoculture growth experiments were prepared by aliquoting 199 μ L of LB medium into each well. Kanamycin was added to the wells in which plasmid bearing strains were to be cultured. The wells of the last row (row H) served as negative controls to check for contamination (Figure 5). Only LB medium and no cell culture was added to these wells. The other wells were then inoculated in biological replicates of seven with 1 μ L of overnight culture and the microplates subsequently sealed with a gas permeable Breathe-Easy sealing membrane (Sigma-Aldrich, Cat. No.: Z380059).

	A: Monocultures						B: Co-Cultures					
	1	2	3	4	5	6	7	8	9	10	11	12
A	<i>E. coli</i> WT	<i>E. coli</i> GFP	<i>E. coli</i> Kate	<i>E. coli</i> EYFP	<i>E. coli</i> Cit	<i>E. coli</i> Cer	Combo1 good	Combo1 bad	Combo1 WT	Combo2 good	Combo2 bad	Combo2 WT
B	<i>E. coli</i> WT	<i>E. coli</i> GFP	<i>E. coli</i> Kate	<i>E. coli</i> EYFP	<i>E. coli</i> Cit	<i>E. coli</i> Cer	Combo1 good	Combo1 bad	Combo1 WT	Combo2 good	Combo2 bad	Combo2 WT
C	<i>E. coli</i> WT	<i>E. coli</i> GFP	<i>E. coli</i> Kate	<i>E. coli</i> EYFP	<i>E. coli</i> Cit	<i>E. coli</i> Cer	Combo1 good	Combo1 bad	Combo1 WT	Combo2 good	Combo2 bad	Combo2 WT
D	<i>E. coli</i> WT	<i>E. coli</i> GFP	<i>E. coli</i> Kate	<i>E. coli</i> EYFP	<i>E. coli</i> Cit	<i>E. coli</i> Cer	Combo1 good	Combo1 bad	Combo1 WT	Combo2 good	Combo2 bad	Combo2 WT
E	<i>E. coli</i> WT	<i>E. coli</i> GFP	<i>E. coli</i> Kate	<i>E. coli</i> EYFP	<i>E. coli</i> Cit	<i>E. coli</i> Cer	Combo1 good	Combo1 bad	Combo1 WT	Combo2 good	Combo2 bad	Combo2 WT
F	<i>E. coli</i> WT	<i>E. coli</i> GFP	<i>E. coli</i> Kate	<i>E. coli</i> EYFP	<i>E. coli</i> Cit	<i>E. coli</i> Cer	Combo1 good	Combo1 bad	Combo1 WT	Combo2 good	Combo2 bad	Combo2 WT
G	<i>E. coli</i> WT	<i>E. coli</i> GFP	<i>E. coli</i> Kate	<i>E. coli</i> EYFP	<i>E. coli</i> Cit	<i>E. coli</i> Cer	Combo1 good	Combo1 bad	Combo1 WT	Combo2 good	Combo2 bad	Combo2 WT
H	blank	blank	blank	blank	blank	blank	blank	blank	blank	blank	blank	blank

Figure 5: Standardized 96-well microplate layout for all monoculture and co-culture growth experiments.

Monocultures (A) and co-cultures (B) were cultivated in 96-well microplates in biological replicates of seven (well row A - G). In well row H, controls without bacterial inoculum (blanks) were run. In monoculture growth experiments, all six strains of a species (wild-type strain and five plasmid bearing strains) were cultivated in parallel. This is illustrated with *E. coli* in well column 1 - 6. In total, 15 different species combinations (combo 1 - combo 15) were co-cultured. For each species combination, three different strain combinations were tested, which are denoted here as “good”, “bad” and “WT”. All three strain combinations for each binary combination were run together on the same plate, as illustrated in well column 7 - 8 and 10 - 12. “good” refers to strains whose estimates of specific growth rate calculated from optical density and fluorescence match, while “bad” refers to strains whose specific growth rates estimates given by optical density and fluorescence strongly differ from each other (for more information see 4.3.1). “WT” refers to the co-culturing of two wild-type strains.

The 96-well microplates were incubated at constant 30 °C in a Synergy H1 plate reader (Agilent Biotek, Winooski, USA, Serial Number 21031715). After reaching the incubation temperature of 30 °C, the plates were shaken linearly at a frequency of 1096 cpm (1 mm) for 10 sec followed by an initial measurement of optical density at 600 nm (OD600) as well as four different fluorescence types. This initial measure of OD600 served as an additional control step for the early detection of any conditions that could affect the measurements, such as air bubbles in wells, scratches on the bottom of the plate or culture medium on the breathable membrane. After the initial measurements, the 96-well microplates were continuously shaken linear (1096 cpm, 1 mm). OD600, sfGFP fluorescence (excitation: 485, emission: 515, gain: 75), mKate fluorescence (excitation: 585, emission: 615, gain: 125), mEYFP and mCitrine fluorescence (excitation: 505, emission: 535, gain: 75) and mCerulean fluorescence (excitation: 430, emission: 475, gain: 75) were continuously measured every 7.5 min up to 24 h growing cells through all phases of bacterial growth. The cultivation of individual strains was sometimes repeated in a different plate.

The growth experiments with binary co-cultures were prepared and performed under almost identical conditions. Instead of 199 μ L only 198 μ L LB medium with or without kanamycin were added to each well and inoculated with 1 μ L overnight culture of each of the two partnered strains. No bacterial

inoculum was added to the blanks. As a reference for each binary combination, the two corresponding wild-type strains were grown together (Figure 5).

3.9 Data Processing and Quantitative Analysis

Processing and manipulation of growth curve and fluorescence curve data from monoculture and co-culture growth assays, statistics and data visualizations were done in R (R Core Team, 2022). The fluorescence data measured for all cell cultures over time was not normalized by optical density as part of the characterization process of this synthetic biology toolkit as a normalization of fluorescence by strain-specific optical density is not viable when using polycultures. Descriptive statistics used for the visual display of quantitative data included measures of central tendency and variability, such as the mean, median, standard deviation, and interquartile range, as well as the depiction of all data points. To quantify uncertainty, Tukey's Honest Significance Tests were conducted using the package `'multcomp'` (Hothorn et al., 2008). The Tukey HSD test is a statistical test based on pairwise comparison of sample means to test observed differences among pairs for significance. Differences with a p-value < 0.05 were considered statistically significant.

3.9.1 Modelling Growth and Estimating Growth Parameters

Growth parameter estimates were determined by fitting growth models to the experimental data collected during growth assays with the package `'growthrates'` (Petzoldt, 2022) in R. The growth models used are further described in Chapter 3.9.1.1 and Chapter 3.9.1.2.

3.9.1.1 Estimating Specific Growth Rates

Throughout this thesis work, species biomass was estimated using the indirect measures of OD600 and fluorescence. Thus, all first order rate constants are estimates calculated from OD600 or fluorescence data and will be further referred to as specific growth rates μ . The estimates of specific growth rates were calculated based on a regression method using the `'all_easylinear'` function from the `'growthrates'` package, which fits the linear solution (Equation 5) of the ordinary differential equation describing exponential cell growth (Equation 4) to experimental data, where N is the population size at a time t , μ is a constant given in units of inverse time, and N_0 represents the initial population size at timepoint zero (corresponding to the initial condition used for the solution).

$$\frac{dN}{dt} = \mu N \quad (4)$$

$$\ln(N(t)) = \mu t + \ln(N_0) \quad (5)$$

The function ``all_easylinear`` log-transforms the OD600 and fluorescence measurements and subsequently fits a linear regression to all windows of h consecutive data points, where h can be determined by the user, and calculates the slopes. To calculate the final slope, *i.e.*, specific growth rate, an extended data window is determined. This includes the data point of the window with the steepest slope and all data points of adjacent windows that have at least a defined percent of the maximum slope, previously specified by the quota, *e.g.*, 95 %. The linear solution of the exponential growth model (Equation 5) is then fitted to the extended data window considered for the overall linear fit by linear regression, its slope being the specific growth rate estimate. In this study, the parameter h was chosen so that each window contained enough data points to capture approximately two hours of growth. Afterwards, the final linear regression models for all estimates were visually checked for reasonable fitting of the model. All linear regression model of specific growth rates estimated from strain-specific fluorescence in co-cultures had to pass the threshold of R^2 values > 0.75 in addition to visual assessment.

3.9.1.2 Estimating Carrying Capacity

The ecological carrying capacity, which is a measure of the maximum population density that a given environment can support, was estimated using two different approaches. For both approaches, measurements of fluorescence and optical density were used as a proxy for biomass. First, the maximum fluorescence (F_{max}) and the maximum optical density (OD_{max}), which represent measurements of the maximum value the plate reader observed, were used as surrogates for the carrying capacity. Documented F_{max} and OD_{max} values correspond to the highest fluorescence or OD600 value from the mean growth curve data of seven biological replicates.

In addition, the carrying capacity was estimated by fitting a parametric logistic differential equation (Equation 6) to the experimental data, which has a parameter K that functionally acts as ecological carrying capacity. The parameter N represents the populations size at a time t , μ is a constant (*i.e.*, the specific growth rate) given in units of inverse time, and K is the carrying capacity.

To determine the parameter K from the datasets of all growth assays, the function ``all_growthmodel``, with the mathematical growth formula ``grow_logistic`` was used from the ``growthrates`` package. This function fits the logistic growth model written as an analytical solution to the logistic differential equation (Equation 7), where N_0 is the initial population size at time zero, corresponding to the initial conditions used for the solution. The parameters are estimated by least squares regression.

$$\frac{dN}{dt} = \mu N \left(1 - \frac{N}{K}\right) \quad (6)$$

$$N(t) = \frac{KN_0}{N_0 + (K - N_0)e^{(-\mu t)}} \quad (7)$$

The estimated K values determined from optical density are reported as K_{OD} in units of OD600, while K values estimated from fluorescence curve data are given as K_{fl} and have the unit RFU. Prior to nonlinear regression analysis and determination of maximum fluorescence values, growth and fluorescence curve data for co-cultures were truncated at 16 h because the occurrence of artifacts in some individual wells affected the further downstream processing of the data.

3.9.2 Calculating Metabolic Burden

To investigate the effect of plasmid maintenance and heterologous protein expression on the growth of the different host species in monocultures, the metabolic burden (m_B) was calculated from specific growth rates estimated from OD600 measurements according to Equation 8. Here, $\mu_{OD,WT}$ is the reference specific growth rate estimated from OD600 of the wild-type strain in units of inverse time and $\mu_{OD,synth}$ is the specific growth rate estimated from OD600 of the plasmid bearing strain, also in units of inverse time.

$$m_B = \frac{\mu_{OD,WT} - \mu_{OD,synth}}{\mu_{OD,WT}} \cdot 100\% \quad (8)$$

While positive percentage values indicate a decrease in growth of the plasmid bearing strain compared to the wild-type strain, meaning that the plasmid poses a burden to the host growth, negative percentages refer to an increase in growth compared to the wild-type strain. The metabolic burden of strains cultivated in co-cultures was calculated according to Equation 8, with specific growth rates determined from the combined optical density measurements taken during combinatorial growth. The pairwise cultivation of the respective wild-type strains was used to obtain the reference specific growth rate for all binary co-cultures.

3.9.3 Inferring Co-Culture Growth Dynamics and Binary Interactions

The growth dynamics in all binary co-cultures were investigated in a successive procedure. Firstly, the species-specific measures of fitness μ_{fl} , K_{fl} and F_{max} were estimated from strain-specific fluorescence curve data obtained during combinatorial growth assays (see 3.8) according to the approaches described in Chapter 3.9.1.1 and Chapter 3.9.1.2. By comparing the values of the growth parameters

of the co-cultivated species, the more fit species of each combinatorial co-culture was determined in terms of specific growth rate and carrying capacity. The species that achieved the higher specific growth rate or carrying capacity was defined as the fitter interaction partner.

Subsequently, the proportion of fitness maintained by each species during combinatorial growth, defined as the fitness maintenance, was quantified by the metric Ξ . The metric Ξ was determined in relation to all three measures of fitness considered in this thesis work and is therefore referred to as Ξ_{μ} , Ξ_K and Ξ_F , respectively. The three measures of fitness maintenance, Ξ_{μ} , Ξ_K and Ξ_F , were calculated using Equation 9, Equation 10 and Equation 11 from the respective means of seven biological replicates. While μ_{fl} is the specific growth rate estimated from fluorescence in units of inverse time and K_{fl} is the carrying capacity in units of RFU determined by fitting a logistic growth model to the fluorescence data, F_{max} denotes the reference carrying capacity as given by the maximum fluorescence value measured and has units of RFU.

$$\Xi_{\mu} = \frac{\mu_{fl,co-culture}}{\mu_{fl,monoculture}} \cdot 100 \% \quad (9)$$

$$\Xi_K = \frac{K_{fl,co-culture}}{K_{fl,monoculture}} \cdot 100 \% \quad (10)$$

$$\Xi_F = \frac{F_{max,co-culture}}{F_{max,monoculture}} \cdot 100 \% \quad (11)$$

To assess the impact of interspecies interactions on species-specific growth, a threshold of 5 % was implemented in this work. Thus, fitness maintenance values < 95 % were defined as an indication of a distinct reduction in the fitness of a species compared to its fitness in monoculture, whereas fitness maintenance values > 105 % implied a beneficial effect of combinatorial growth on the species fitness. The underlying nature of the interspecies growth interaction was then deduced from the categorical classification of each species growth outcome as beneficial (+), impaired (-) or neutral (0, Ξ values of $100 \pm 5 \%$). Overall, interspecies interactions were classified into mutualistic, commensal, and antagonistic relationships. Thus, the fitness maintenance of species had to be below or above the previously described threshold of 5 % for a distinct mutualistic or antagonistic interaction.

3.10 Conducting Open Science and Reproducible Research

With the intention of practicing transparent and reproducible science, all experimental OD600 and fluorescence raw data from monoculture and co-culture growth assays, as well as the R Markdown scripts used for data analysis and visualization, have been made publicly available on the Open Science Framework website in the OSF project: “Broad-Host-Range Genetic Tools for Observing Microbial Consortia”, which can be accessed via the following link: <https://osf.io/h7ndk/>.

4 Results

In this study, a synthetic biology device platform for the interrogation of population dynamics was established and experimentally tested for its applicability. The functionality of this platform is based on a combinatorial toolkit consisting of different broad-host-range reporter plasmids and bacterial hosts, which allows population growth dynamics, *e.g.*, strain-specific fitness, to be decoupled and inferred based on fluorescence measurements. The results of the development, the subsequent characterization of this device platform, and its testing using model co-cultures are presented below.

4.1 Broad-Host-Range Device Platform

One objective of this study was to implement a platform that uses fluorescence as a tool for the high throughput monitoring of growth dynamics of microbial communities. This concept was implemented by transforming bacterial hosts with reporter plasmids that constitutively express fluorescent proteins with differential excitation and emission wavelengths, such that the growth of the plasmid bearing strains can be simultaneously assessed with high temporal resolution in combinatorial liquid cultures. To this end, broad-host-range fluorescent reporter plasmids were constructed and subsequently transformed into a collection of host species, including: *Escherichia coli* DH5 α (*E. coli*), *Halopseudomonas aestusnigri* VGXO14 (*H. aestusnigri*), *Halopseudomonas oceani* KX20 (*H. oceani*), *Pseudomonas deceptionensis* M1 (*P. deceptionensis*), *Pseudomonas fluorescens* SBW25 (*P. fluorescens*) and *Pseudomonas putida* KT2440 (*P. putida*).

4.1.1 Reporter Plasmids Integrated into the BASIC Standard

The use of fluorescence as a surrogate measure for the assessment of bacterial growth requires that the bacteria are first transformed with a genetic tool that allows the targeted measurement of a known fluorophore. Thus, an important goal in the development of this synthetic biology toolkit was to build a set of plasmids that can be transformed across a wide range of hosts and whose functionality is based on the properties of fluorescent reporter proteins. Some of the bacteria selected as microbial chassis from the M2RG host library are resistant to chloramphenicol. Therefore, kanamycin was chosen as the selection marker for all reporter plasmids to be included into this kit, as all chosen strains are sensitive to kanamycin and do not exhibit natural resistance. Furthermore, kanamycin is a more stable and routine antibiotic than chloramphenicol, which can benefit the robustness and thus the general handling and use of the genetic tools.

Six pre-assembled J23104 promoter-reporter cassettes stored in pSEVA331 vectors integrated into the **B**iopart **A**ssembly **S**tandard for **I**dempotent **C**loning (BASIC) cloning environment with a chloramphenicol selection marker (Cm^R) and pBBR1 origin of replication (backbone BB33) encoding the fluorescent proteins sfGFP, mRFP, mKate, mEYFP, mCitrine and mCerulean were assembled with a BASIC integrated pSEVA231 derived backbone with a kanamycin selection marker (Kan^R) and pBBR1 origin of replication (backbone BB23), according to the BASIC DNA assembly method (Figure 6A). This resulted in the generation of the six broad-host-range reporter plasmids built in the BASIC environment that are listed in Table 1. The schematic of the plasmids is shown in Figure 6B. The exchange of genetic parts was facilitated by the modularity of constructs integrated into the BASIC standard.

The correct assembly of plasmids was verified in two steps, upon heat-shock transformation of competent *E. coli* DH5 α cells. To confirm the presence of the J23104-reporter cassettes in the assembled constructs, colony-PCR was performed with the L1-F forward and L2-R reverse PCR primers (Figure 6C). The associated gels can be found in Appendix A. For each strain, one of the colonies screened positive for the presence of the promoter-reporter cassette was used to inoculate an overnight culture for subsequent cryopreservation of a clonal population of the respective strain. In addition, strains with J23104-reporter cassettes stored in vectors with chloramphenicol selection marker and the new broad-host-range reporter plasmids were streaked from glycerol stocks on LB agar plates with chloramphenicol and plates with kanamycin, respectively, which is exemplarily shown in Figure 7 (images of all streaked LB plates can be found in Appendix A). All strains carrying the newly assembled plasmids were sensitive to chloramphenicol and resistant to kanamycin. The observed sensitivity of strains with the Cm^R gene towards kanamycin and their resistance to chloramphenicol proves that the observed resistance is linked to the presence of the antibiotic resistance gene and thus confirms the correct integration of the BB23-backbone.

Table 1: Overview of constructed broad-host-range reporter plasmids.

All plasmids have a backbone with a kanamycin selection marker and pBBR1 origin of replication (backbone BB23) derived from the BASIC integrated pSEVA231 plasmid. The plasmids function by constitutive expression of the respective fluorescent reporter protein. P3 refers to the promoter cassette, which includes a terminator, J23104 promoter, RiboA encoding sequence, and a ribosome binding site.

Plasmid Name	Plasmid ID	Cargo	Plasmid Size
BB23-P3-sfGFP	pCPgfp	P3-sfGFP	3854 bp
BB23-P3-mRFP	pCPrfp	P3-mRFP	3821 bp
BB23-P3-mKate	pCPkate	P3-mKate	3839 bp
BB23-P3-mEYFP	pCPeyfp	P3-mEYFP	3863 bp
BB23-P3-mCitrine	pCPcit	P3-mCitrine	3857 bp
BB23-P3-mCerulean	pCPcer	P3-mCerulean	3857 bp

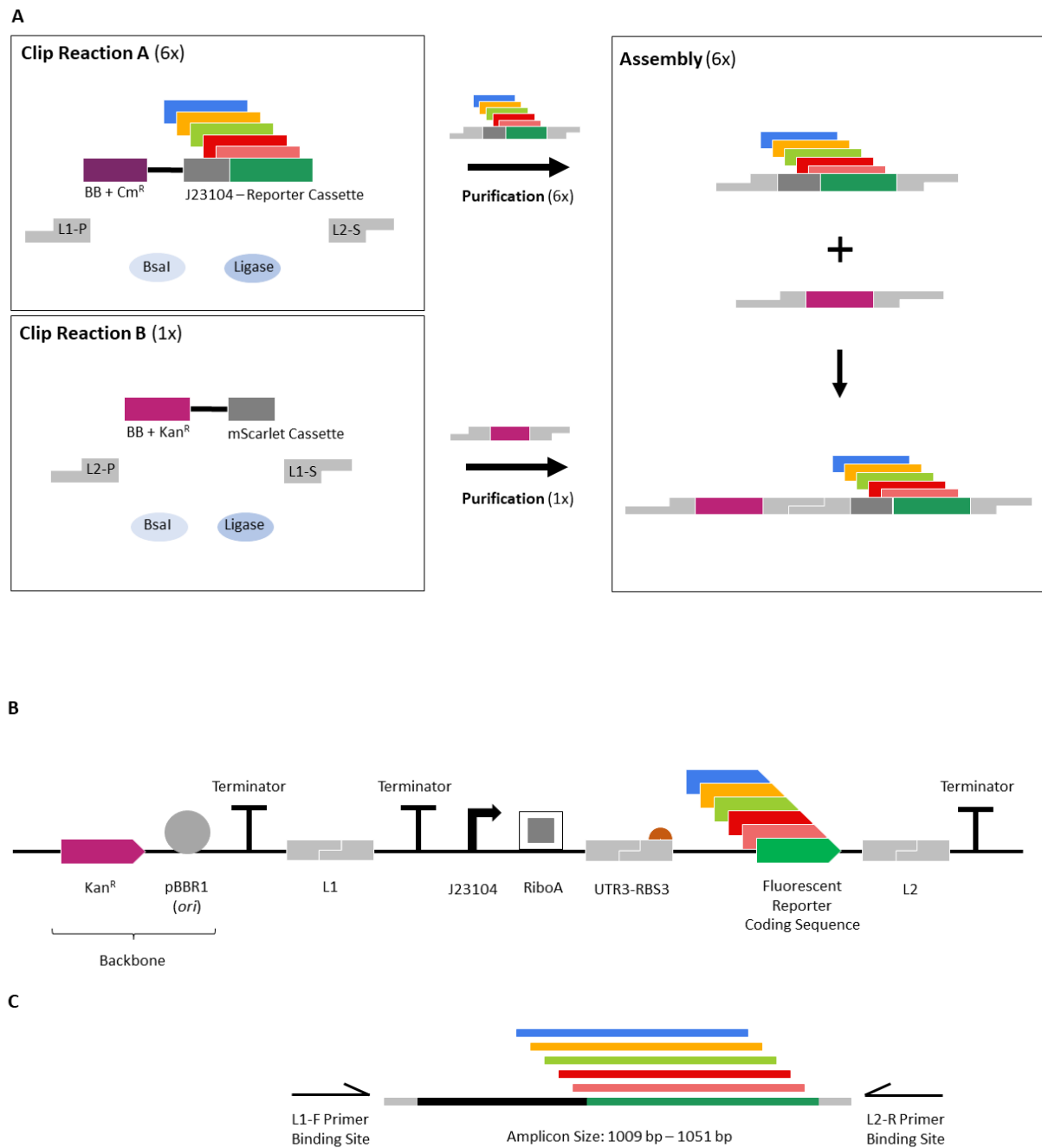


Figure 6: BASIC DNA assembly workflow and schematic of linearized broad-host-range reporter plasmids.

A: The Prefix and Suffix half-linkers were clipped to J23104 promoter-reporter cassettes by simultaneous Bsal digestion and ligation in six distinct clip reactions. The corresponding half-linkers were clipped to a backbone with a kanamycin selection marker and pBBR1 origin of replication (backbone BB23). After magnetic bead purification, the purified clipped parts were annealed in BASIC assembly reactions generating six broad-host-range reporter plasmids. Plasmids used for clip reactions and final constructs are shown in linearized form.

B: Schematic of broad-host-range reporter plasmids. The J23104 – reporter cassettes and the backbone with the kanamycin selection marker are assembled with the linkers L1 and L2. The constitutive promoter J23104 promotes the constant expression of the reporter genes and thus production of fluorescent proteins. RiboA is an autocatalytic ribozyme that standardizes the length of transcribed mRNA molecules by cleaving the upstream 5'-UTR region after it has been transcribed. UTR3-RBS3 is a linker encoding a ribosome binding site (RBS) sequence with strong translational strength in its adapter region. The backbone consists of a kanamycin selection marker and pBBR1 origin of replication (*ori*).

C: PCR primers L1-F and L2-R binding to BASIC L1 and L2 linker DNA sequences yielding amplicons of different lengths, depending on the length of the fluorescent protein encoding genes.

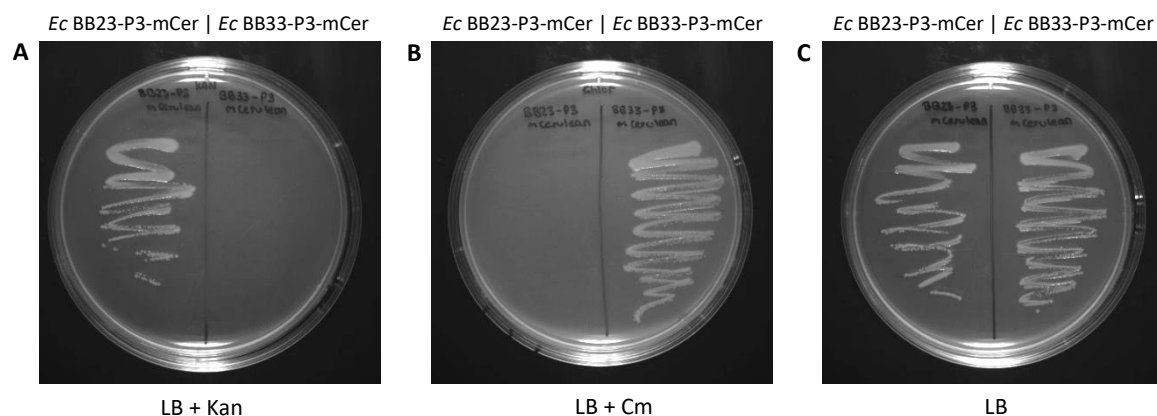


Figure 7: Confirmation of successful integration of the BB23-backbone into the pCPcer plasmid.

Ec BB23-P3-mCer (*E. coli* DH5 α carrying the pCPcer plasmid) and *Ec BB33-P3-mCer* (*E. coli* DH5 α carrying the J23104-mCerulean cassette stored in the BASIC integrated pSEVA331 vector) were streaked on LB agar plates with kanamycin (A), with chloramphenicol (B) and without antibiotics (C), respectively. While *Ec BB23-P3-mCer* is sensitive to chloramphenicol, *Ec BB33-P3-mCer* only exhibits sensitivity towards kanamycin.

4.1.2 Bacterial Hosts for Fluorescent Reporter Plasmids

As the core of this device platform, a library of all possible host-plasmid combinations was established. Therefore, each of the six broad-host-range fluorescent reporter plasmids was transformed by electroporation across three *Pseudomonas* spp. and two *Halopseudomonas* spp., which were chosen as primary hosts to characterize and test the device platform for its applicability. *E. coli* DH5 α served as additional host for all genetic devices and was transformed by the heat-shock method while cloning the plasmids according to the BASIC DNA assembly method. After propagation in *E. coli* DH5 α the plasmids were isolated for subsequent transformation of the other species by electroporation. Therefore, this study evaluated the broad-host-range plasmid reporter kit across both well-established model organisms, e.g., *E. coli* and *P. putida*, and non-traditional hosts being developed within the M2RG synthetic biology library (Chan et al., 2023; Verusevski, 2022).

The transformation of all host species with each of the six reporter plasmids pCPgfp, pCPprfp, pCPkate, pCPeyfp, pCPcit and pCPcer was successful, resulting in a collection of 36 distinct plasmid bearing strain combinations (Table 2). Transformants were validated by colony-PCR with the L1-F and L2-R PCR primers (Figure 6C), screening for the respective promoter-reporter cassettes of the individual plasmids (see Appendix B - Appendix F). The successful transformation of all *Pseudomonas* spp. and *Halopseudomonas* spp. indicates that the transformation protocol can likely be transferred to further members of these species, allowing the kit to be easily expanded by new hosts.

Table 2: Overview of plasmid bearing strains and their IDs used hereinafter.

Plasmid Bearing Strain ID	Host Species	Plasmid
<i>Ec</i> pCPgfp	<i>Escherichia coli</i> DH5 α	BB23-P3-sfGFP
<i>Ec</i> pCPrfp	<i>Escherichia coli</i> DH5 α	BB23-P3-mRFP
<i>Ec</i> pCPkate	<i>Escherichia coli</i> DH5 α	BB23-P3-mKate
<i>Ec</i> pCPeyfp	<i>Escherichia coli</i> DH5 α	BB23-P3-mEYFP
<i>Ec</i> pCPcit	<i>Escherichia coli</i> DH5 α	BB23-P3-mCitrine
<i>Ec</i> pCPcer	<i>Escherichia coli</i> DH5 α	BB23-P3-mCerulean
<i>Ha</i> pCPgfp	<i>Halopseudomonas aestusnigri</i> VGXO14	BB23-P3-sfGFP
<i>Ha</i> pCPrfp	<i>Halopseudomonas aestusnigri</i> VGXO14	BB23-P3-mRFP
<i>Ha</i> pCPkate	<i>Halopseudomonas aestusnigri</i> VGXO14	BB23-P3-mKate
<i>Ha</i> pCPeyfp	<i>Halopseudomonas aestusnigri</i> VGXO14	BB23-P3-mEYFP
<i>Ha</i> pCPcit	<i>Halopseudomonas aestusnigri</i> VGXO14	BB23-P3-mCitrine
<i>Ha</i> pCPcer	<i>Halopseudomonas aestusnigri</i> VGXO14	BB23-P3-mCerulean
<i>Ho</i> pCPgfp	<i>Halopseudomonas oceani</i> KX20	BB23-P3-sfGFP
<i>Ho</i> pCPrfp	<i>Halopseudomonas oceani</i> KX20	BB23-P3-mRFP
<i>Ho</i> pCPkate	<i>Halopseudomonas oceani</i> KX20	BB23-P3-mKate
<i>Ho</i> pCPeyfp	<i>Halopseudomonas oceani</i> KX20	BB23-P3-mEYFP
<i>Ho</i> pCPcit	<i>Halopseudomonas oceani</i> KX20	BB23-P3-mCitrine
<i>Ho</i> pCPcer	<i>Halopseudomonas oceani</i> KX20	BB23-P3-mCerulean
<i>Pd</i> pCPgfp	<i>Pseudomonas deceptionensis</i> M1	BB23-P3-sfGFP
<i>Pd</i> pCPrfp	<i>Pseudomonas deceptionensis</i> M1	BB23-P3-mRFP
<i>Pd</i> pCPkate	<i>Pseudomonas deceptionensis</i> M1	BB23-P3-mKate
<i>Pd</i> pCPeyfp	<i>Pseudomonas deceptionensis</i> M1	BB23-P3-mEYFP
<i>Pd</i> pCPcit	<i>Pseudomonas deceptionensis</i> M1	BB23-P3-mCitrine
<i>Pd</i> pCPcer	<i>Pseudomonas deceptionensis</i> M1	BB23-P3-mCerulean
<i>Pp</i> pCPgfp	<i>Pseudomonas putida</i> KT2440	BB23-P3-sfGFP
<i>Pp</i> pCPrfp	<i>Pseudomonas putida</i> KT2440	BB23-P3-mRFP
<i>Pp</i> pCPkate	<i>Pseudomonas putida</i> KT2440	BB23-P3-mKate
<i>Pp</i> pCPeyfp	<i>Pseudomonas putida</i> KT2440	BB23-P3-mEYFP
<i>Pp</i> pCPcit	<i>Pseudomonas putida</i> KT2440	BB23-P3-mCitrine
<i>Pp</i> pCPcer	<i>Pseudomonas putida</i> KT2440	BB23-P3-mCerulean
<i>Pf</i> pCPgfp	<i>Pseudomonas fluorescens</i> SBW25	BB23-P3-sfGFP
<i>Pf</i> pCPrfp	<i>Pseudomonas fluorescens</i> SBW25	BB23-P3-mRFP
<i>Pf</i> pCPkate	<i>Pseudomonas fluorescens</i> SBW25	BB23-P3-mKate
<i>Pf</i> pCPeyfp	<i>Pseudomonas fluorescens</i> SBW25	BB23-P3-mEYFP
<i>Pf</i> pCPcit	<i>Pseudomonas fluorescens</i> SBW25	BB23-P3-mCitrine
<i>Pf</i> pCPcer	<i>Pseudomonas fluorescens</i> SBW25	BB23-P3-mCerulean

4.2 Characterization of the Genetic Device Platform

This section characterizes the new device platform described in Chapter 4.1, which enables interrogation of population dynamics by using both static and time-course measurements of fluorescence as a proxy for strain-specific biomass. Two ecologically important growth outputs were estimated from these datasets – the specific growth rate and the carrying capacity. In total, three different measurements of fitness were used to estimate these parameters from monoculture growth. While the specific growth rate μ was estimated by fitting a first order growth model representing exponential cell growth (Equation 4) to fluorescence and OD600 growth curve data respectively, two measures for comparative evaluation served as surrogates for the carrying capacity. These comprise the parameter K (K_{fl} and K_{OD}) extrapolated from a logistic equation (Equation 6) by nonlinear regression

and the maximum fluorescence and optical density measured by the plate reader (F_{max} and OD_{max}). Due to the high redundancy of the pCPrfp and pCPkate plasmids, the plasmid pCPrfp was excluded from all growth experiments and consecutive analysis.

4.2.1 Observation of Batch Effects and Reproducibility

During the characterization experiments of the plasmid bearing strains, some growth experiments were split across different plates. For each experiment, *i.e.*, plate, the respective wild-type strains were included as reference. The data obtained was used for a short experiment designed to investigate whether batch effects could be expected on different plates that could affect the reproducibility of the introduced genetic device system. Therefore, the specific growth rates of three different wild-type strains estimated from OD600 from two growth experiments were used as metrics to investigate batch effects. This was done by using descriptive statistics and statistical Tukey's Honest Significance Test to quantify uncertainty.

The evaluation of the data has shown that significant batch effects can be observed for all three tested wild-type strains of *H. oceani*, *P. deceptionensis* and *P. fluorescens* (Figure 8), which consequently affect the reproducibility of the system. The comparative visualization of the corresponding specific growth rate estimates shows a distinct difference in the specific growth rate between plates for all strains, a trend that is consistent among all biological replicates. These observed differences in specific growth rates between plates are statistically significant for each strain examined. The results therefore indicate that batch effects are very likely to occur with the cultivation of all wild-type strains and potentially with plasmid bearing strains as well. Thus, the occurrence of batch effects on reproducibility should be considered during experimental design. The observed batch effects were managed by data evaluation based on plate comparisons. This means that data points from the seven biological replicates of both plates for *H. oceani*, *P. deceptionensis* and *P. fluorescens* were included in the reference specific growth rate estimates for all subsequent characterizations, which refers to the specific growth rates of the corresponding wild-type strains. Further studies on batch effects were not performed within the scope of this thesis work.

4.2.2 Growth Parameters from Monoculture Growth Data

The strain-specific growth parameters μ and K were estimated by fitting growth models to monoculture OD600 and fluorescence curve data. Therefore, all plasmid bearing, and wild-type strains were cultured in biological replicates of seven in 96-well microplates under the same experimental conditions in an automated plate reader (see 3.8). The bacterial growth over time was measured via optical density in 7.5-min intervals as well as four different fluorescent outputs, respectively. The estimated growth parameters of the wild-type strains were used as reference values.

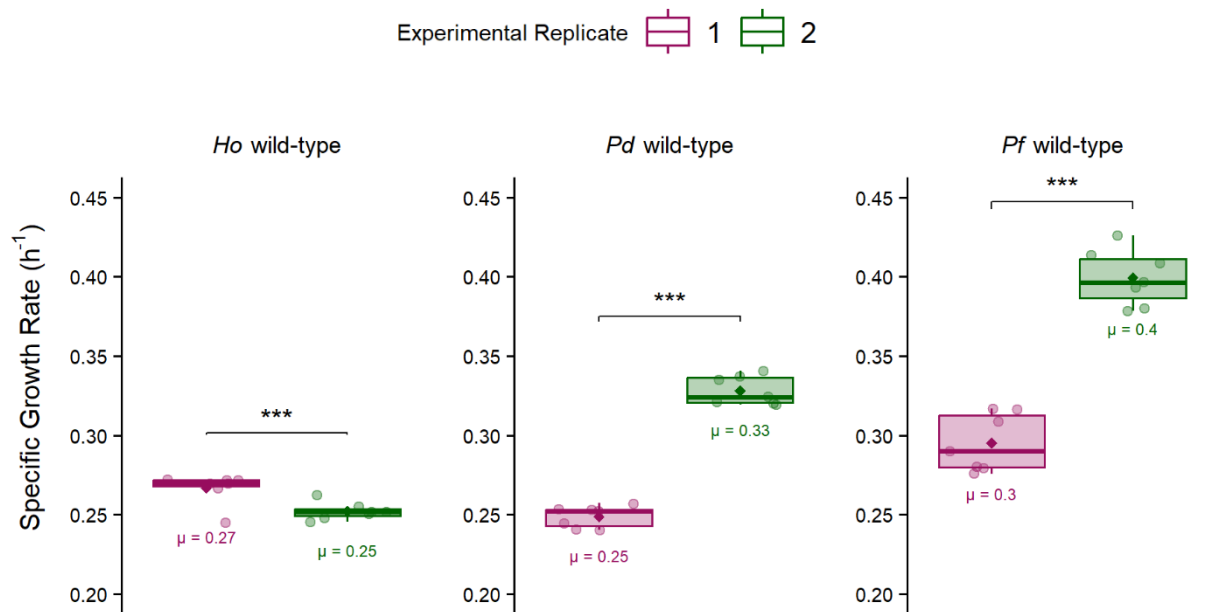


Figure 8: Quantification of statistically significant batch effects for three wild-type strains based on the comparison of their specific growth rates from two experimental replicates.

The descriptive comparison of the specific growth rates (μ) estimated from OD600 reveals significant batch effects for the wild-type strains of *H. oceanii*, *P. deceptionensis* and *P. fluorescens*. This is also confirmed by the results of the Tukey's Honest Significance tests performed. Estimates of the specific growth rates of the biological replicates ($n = 7$) are indicated by semi-transparent circles while their mean is shown as filled rhombus. The data of experimental replicates is color coded. Significance levels are marked by asterisks (***: $p < 0.001$).

4.2.2.1 Specific Growth Rate Estimates

The specific growth rate μ is a measure of fitness that describes the velocity of growth and can be estimated from either direct or indirect measurements of population density. Both, optical density, and fluorescence used in this study are considered indirect measures and are therefore tools used as a proxy for monitoring biomass concentration and assessing microbial growth. While optical density is a turbidity measurement based on light scattering, which is proportional to biomass in planktonic cultures, fluorescence is a measurement of photon generation. Thus, using fluorescence as an indirect measure to estimate bacterial growth assumes that the amount of photon releasing fluorophores present in a sample, as measured by fluorescence emission upon relaxation from an excited state, is also proportional to biomass. To validate the correctness of this statement, a comparison of the specific growth rates estimated from OD600 and strain-specific fluorescence for every plasmid bearing strain was made. Optical density measurements were therefore used as reference for bacterial growth.

Overall, a statistically significant match between the specific growth rates estimated from OD600 and the strain-specific fluorescence could only be observed for six of the total of 30 plasmid bearing strains, which are listed in Table 3. While several plasmid bearing strains with matching estimates of specific growth rate were identified for *P. fluorescens*, the difference between both estimates was statistically significant for all *P. putida* and *H. oceanii* strains (Table 3). This suggests that the suitability of

fluorescence as a surrogate for bacterial growth is limited and strongly dependent on the combination of fluorescent reporter protein and host species used.

It is also noticeable that there is no statistically significant match between the two specific growth rates for any of the strains carrying the pCPkate plasmid, which might suggest that the mKate protein is not suited for approximating bacterial growth by the methodology applied in these studies (Table 3). However, there is a caveat that all μ values are estimates and that some bias is likely due to the uncertainty in fitting models across large datasets. Therefore, it is important to also consider the magnitude of difference between the specific growth rates estimated from both surrogate measures. The estimated specific growth rates for all strains are graphically visualized in Chapters 4.2.2.1.1 to 4.2.2.1.6. Nevertheless, accounting that optical density is proportional to biomass, it can be expected that the greater the difference between the two estimates of specific growth rate, the more likely it is that the specific growth rates obtained from fluorescence do not closely resemble the true velocity of bacterial growth during log-phase. This also supports the inference, that the applicability of fluorescence to assess species-specific growth in polycultures potentially depends on the selection of plasmid bearing strains and therefore is to be considered during strain selection for combinatorial growth (see 4.3.1).

Table 3: Overview of plasmid bearing strains with statistically non-significant differences between the specific growth rates determined from OD600 and strain fluorescence, indicating a proportionality between fluorescence and biomass that makes them highly suitable strains for approximating the growth performance of the corresponding species.

For each plasmid bearing strain a Tukey HSD test was performed between the specific growth rates obtained from OD600 and strain-specific fluorescence. P-values > 0.05 were considered statistically non-significant.

Strain	Compared Pairs of Outputs	p-Value	Strain	Compared Pairs of Outputs	p-Value
<i>Ec</i> pCPcit	OD600 – Citrine fluorescence	0.73013	<i>Pf</i> pCPgfp	OD600 – GFP fluorescence	0.55
<i>Ha</i> pCPcer	OD600 – Cerulean fluorescence	0.6755	<i>Pf</i> pCPeyfp	OD600 – EYFP fluorescence	1
<i>Pd</i> pCPeyfp	OD600 – EYFP fluorescence	0.89972	<i>Pf</i> pCPcit	OD600 – Citrine fluorescence	0.8382

4.2.2.1.1 *Escherichia coli*

The specific growth rates for all *E. coli* strains estimated from experimental OD600 and fluorescence data collected during monoculture growth assays are shown in Figure 9. The mean specific growth rates determined from OD600 data for all plasmid bearing strains are only marginally lower than the reference mean specific growth rate from the wild-type strain, ranging between 0.28 h⁻¹ and 0.29 h⁻¹. This indicates that all plasmid bearing strains grow well, suggesting that the viability and proliferation of the hosts was not significantly impaired upon introduction of the genetic devices and expression of heterologous proteins. Overall, the observed background fluorescence, which represents the noise obtained with this methodology, is low. This is important for separating the fluorescence signals during combinatorial cultivation. The only exception is observed with the strain *Ec* pCPgfp (Figure 9B). The background EYFP and Citrine fluorescence increases similarly as fast compared to the specific GFP fluorescence, which is implied by the statistically non-significant difference between the specific

growth rates estimated from the corresponding fluorescence signals. A relatively high GFP background fluorescence can be further observed for *Ec* pCpcit (Figure 9E). This can be attributed to overlapping excitation and emission spectra of the sfGFP and mCitrine proteins. Spectral scan growth assays have shown that it is not possible to separate the fluorescence signals from both proteins with the Biotek Synergy H1 plate reader used (data not shown). Thus, the combinatorial cultivation of strains with the pCPgfp and pCPcit plasmids should be avoided when using the methodology developed in this study. In addition, a statistically significant match between the specific growth rates estimated from OD600 and fluorescence was observed for *Ec* pCPcit, suggesting that the growth of *E. coli* DH5 α is best assessed with the pCPcit plasmid.

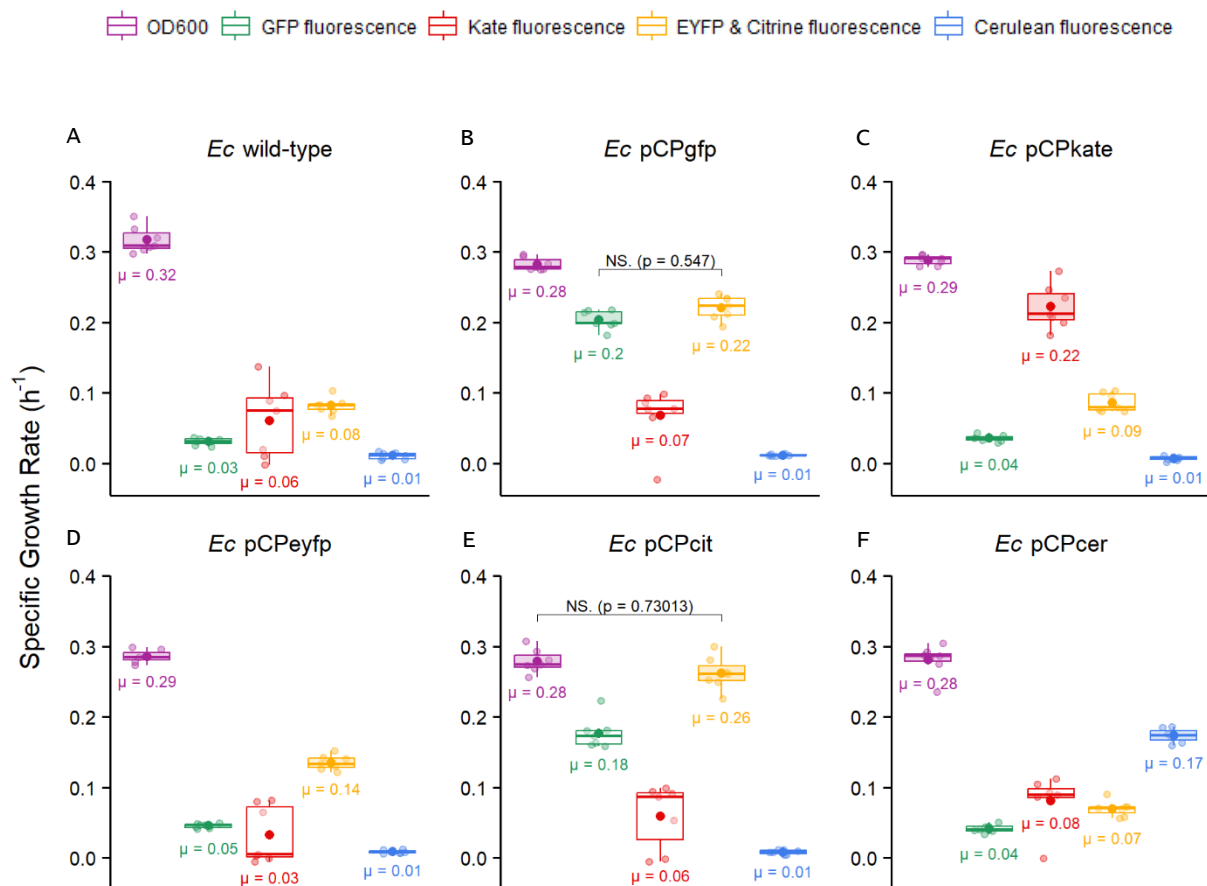


Figure 9: The comparison of the specific growth rates estimated from OD600 and fluorescence reveals that the growth of *E. coli* DH5 α can be best assessed using the pCPcit plasmid. In addition, the measurement of background fluorescence for *Ec* pCPgfp and *Ec* pCPcit unveils a signal overlap of the sfGFP and mCitrine proteins.

The specific growth rates for the biological replicates ($n = 7$) are indicated by semi-transparent circles while their mean is shown as filled circle. The OD600 and fluorescence data is color coded. In each panel, boxes displaying the distribution of data, *i.e.*, specific growth rates, ascribed to OD600 and strain-specific fluorescence measurements are filled. The specific growth rate obtained from the specific fluorescence was pairwise compared to all other estimates of specific growth rate of the same strain by Tukey HSD tests. All differences among pairs are statistically significant (p -value < 0.05) unless otherwise indicated in the figure.

4.2.2.1.2 *Pseudomonas putida*

The descriptive statistics for the estimated specific growth rates of all *P. putida* strains are visualized in Figure 10. The comparison of the specific growth rates as given by optical density reveals that the fitness of the plasmid bearing strains is reduced by approximately 20 % with respect to the wild-type reference (*Pp* pCPkate, Figure 10C), indicating that the plasmids negatively influence growth. Although this slight, consistent decrease in fitness can be observed among all plasmid bearing strains, no significant impairment was ascertained. The overlapping signals of the sfGFP and mCitrine proteins are also observed for *Pp* pCPgfp, as signified by statistically non-significant difference in the specific growth rates determined from GFP and Citrine fluorescence (Figure 10B). The growth of *P. putida* was approximated best with the pCPcer plasmid, indicated by the smallest difference of 0.06 h⁻¹ between the specific growth rates estimated from OD600 and strain fluorescence.

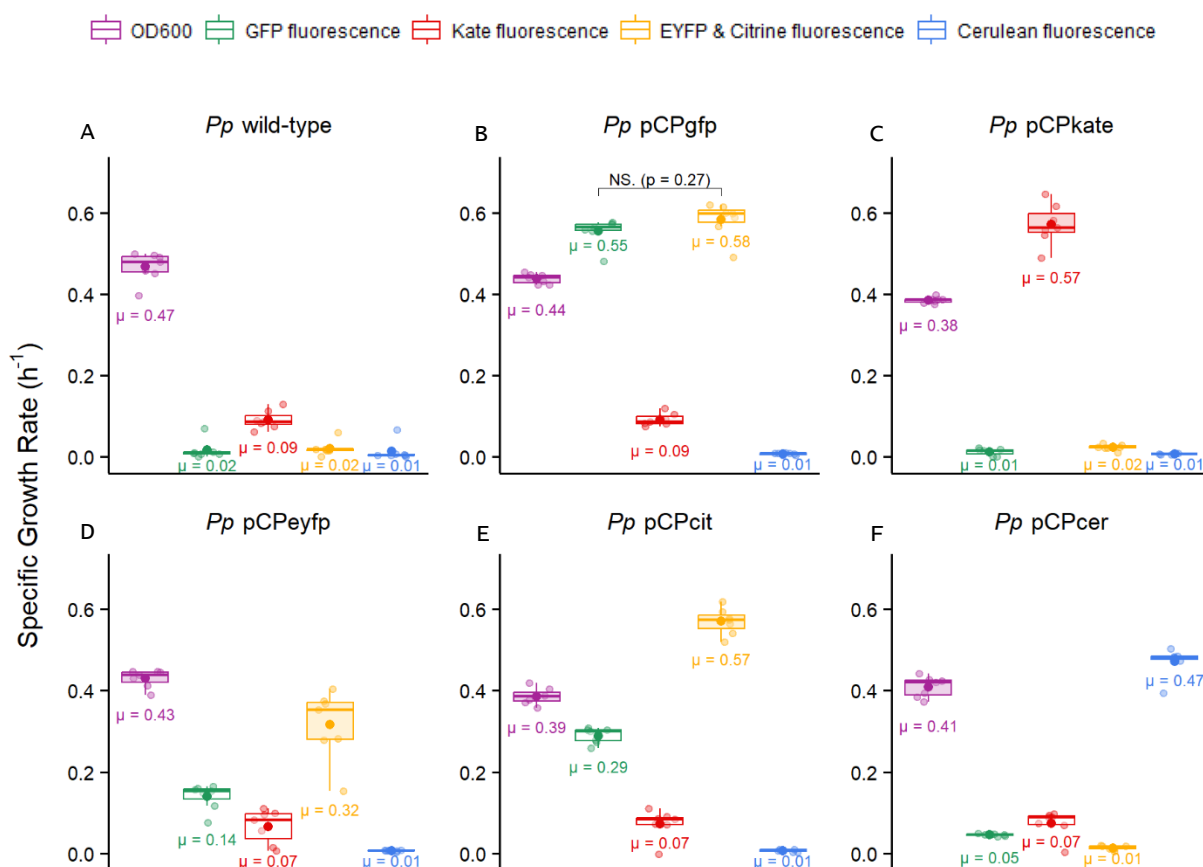


Figure 10: The comparative analysis of the specific growth rates obtained from OD600 and fluorescence data for all strains shows that the growth of *P. putida* can be best approximated using the mCerulean fluorescent reporter protein.

The specific growth rates of $n = 7$ biological replicates are indicated by semi-transparent dots while their mean is shown as filled dot. The data related to the different fluorescence and optical density measurements is color coded. In each panel, boxes displaying the distribution of data, *i.e.*, specific growth rates, ascribed to OD600 and strain-specific fluorescence measurements are filled. The specific growth rate obtained from the specific fluorescence was pairwise compared to all other estimates of specific growth rate of the same strain by Tukey HSD tests. All differences among pairs are statistically significant (p -value < 0.05) unless otherwise indicated in the figure.

4.2.2.1.3 *Halopseudomonas aestusnigri*

The fitting of an exponential growth model to experimental optical density and fluorescence data for the characterization of plasmid bearing *H. aestusnigri* strains has resulted in a set of specific growth rate estimates determined from five different measures and are depicted in Figure 11. While a statistically significant match between the specific growth rates estimated from optical density and Cerulean fluorescence is observed for *Ha* pCPcer (Figure 11F), the other strain-specific fluorescence estimates of the specific growth rate appear to be considerably higher than the corresponding estimates determined from optical density, especially for the strains *Ha* pCPkate and *Ha* pCPcit (Figure 11C and E). This may indicate that the use of the reporter plasmids pCPkate and pCPcit is less suitable for assessing the growth of *H. aestusnigri*. Compared to the *Pseudomonas* spp., the reference specific growth rate from *Ha* wild-type is lower, but not substantially reduced upon transformation with the reporter plasmids as implied by the specific growth rates obtained from OD600 of the plasmid bearing strains.

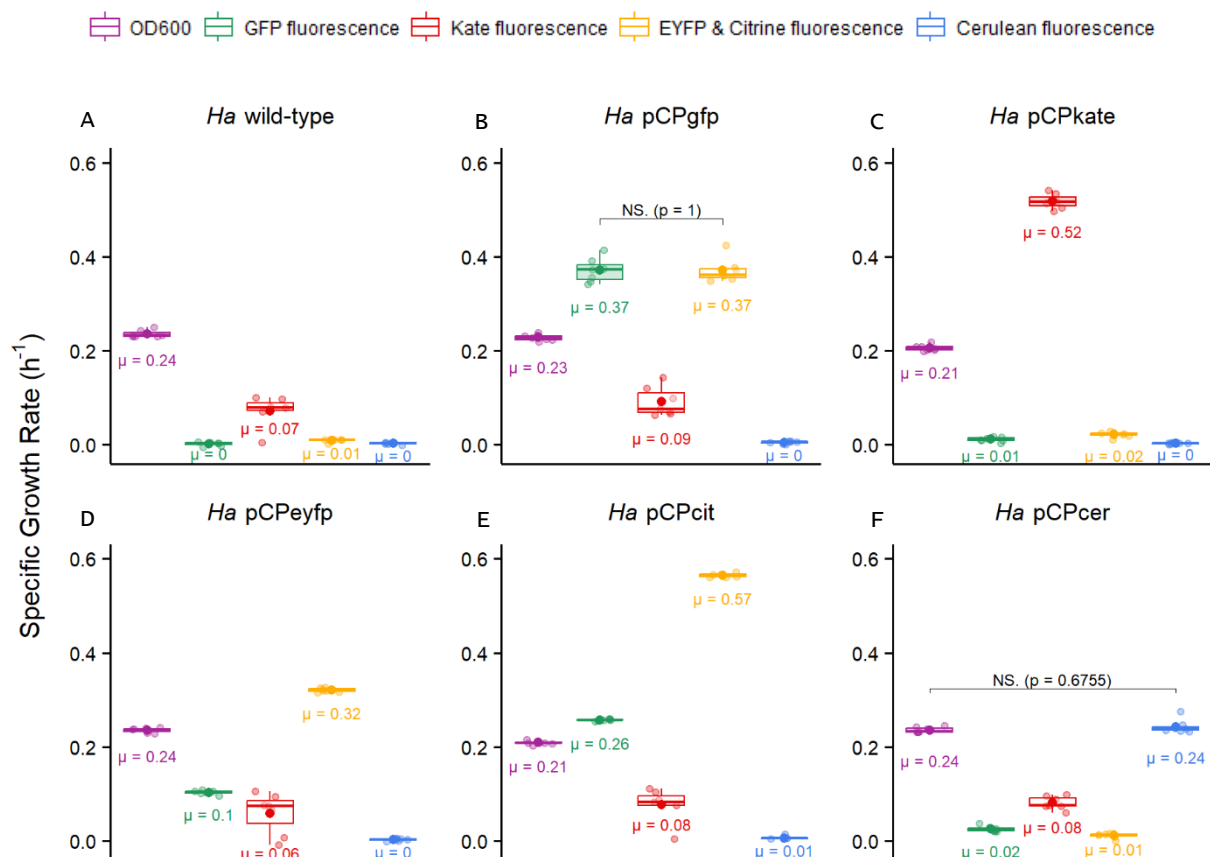


Figure 11: The statistically non-significant difference between the specific growth rates determined from OD600 and Cerulean fluorescence for *Ha* pCPcer signifies a proportionality between fluorescence and biomass and thus implies that the pCPcer plasmid is the tool of choice to assess the growth of *H. aestusnigri*.

All estimates of specific growth rate ($n = 7$) obtained from OD600 and fluorescence measurements for all *H. aestusnigri* strains are indicated by color coded, semi-transparent dots. The means are shown as filled dots. In each panel, boxes displaying the distribution of data ascribed to OD600 and strain-specific fluorescence measurements are filled. The specific growth rate obtained from the specific fluorescence was pairwise compared to all other estimates of specific growth rate of the same strain by Tukey HSD tests. All differences among pairs are statistically significant (p -value < 0.05) unless otherwise indicated in the figure.

4.2.2.1.4 *Halopseudomonas oceani*

The monoculture growth assays for the preliminary characterization of plasmid bearing strains revealed that all transformed *H. oceani* strains exhibit a considerable difference between the specific growth rates determined from OD600 and strain-specific fluorescence (Figure 12). For example, the specific growth rate obtained from Kate fluorescence for *Ho* pCPkate has an almost three times higher value compared to that estimated from OD600 growth curve data (Figure 12C). Thus, it can be argued that the pCPkate plasmid is not particularly suited for monitoring biomass concentration of *H. oceani* over time. As visible in Figure 12B and E, the overlap of the GFP and EYFP and Citrine fluorescence signals of the sfGFP and mCitrine proteins can be seen.

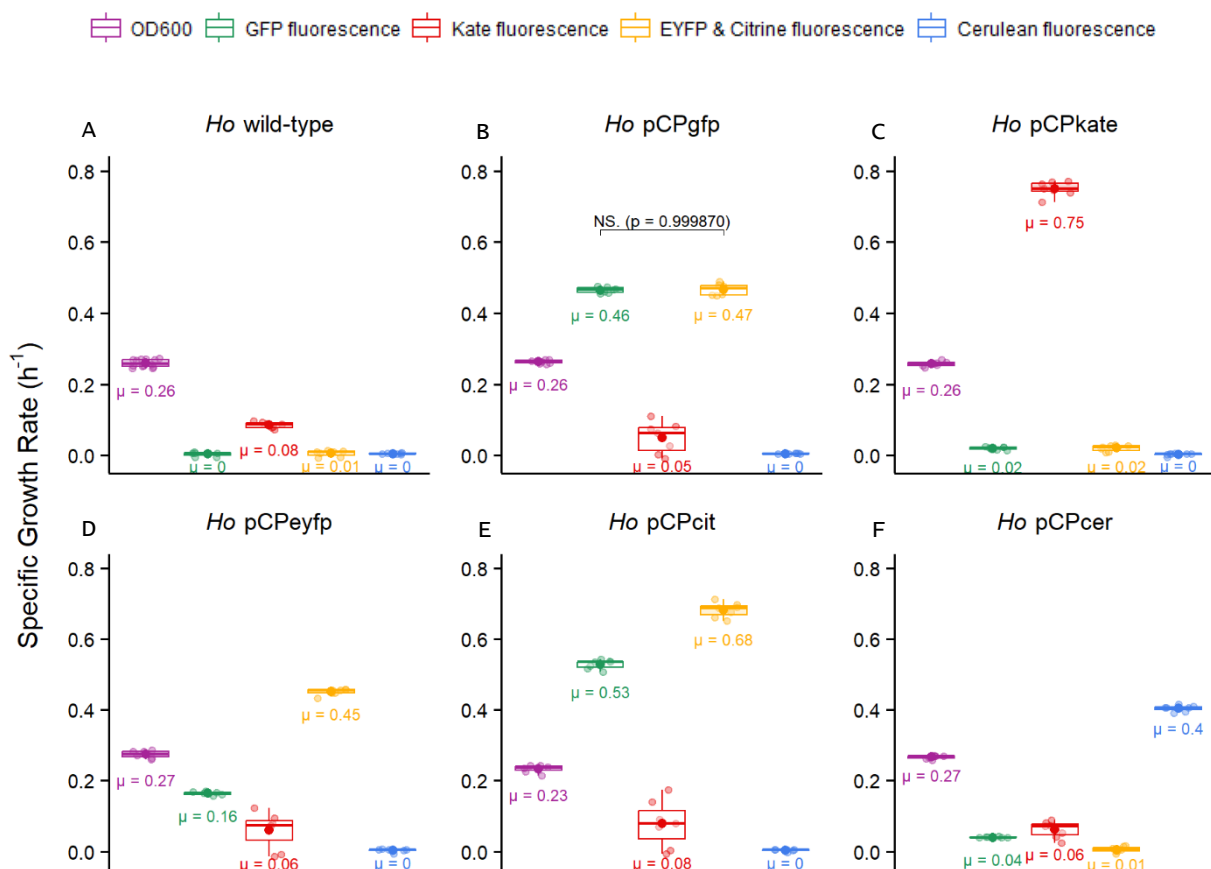


Figure 12: The estimates of specific growth rate obtained from OD600 and fluorescence measurements for all plasmid bearing *H. oceani* strains show statistically significant differences in their values.

The specific growth rates for $n = 7$ biological replicates (indicated by semi-transparent dots) and the corresponding means (filled dot) are shown for all *H. oceani* strains. The different fluorescence types and optical density are color coded. In each panel, boxes displaying the distribution of data ascribed to OD600 and strain-specific fluorescent measurements are filled. The specific growth rate obtained from the specific fluorescence was pairwise compared to all other estimates of specific growth rate of the same strain by Tukey HSD tests. All differences among pairs are statistically significant (p -value < 0.05) unless otherwise indicated in the figure.

4.2.2.1.5 *Pseudomonas deceptionensis*

The quantitative data for specific growth rate estimates for each *P. deceptionensis* strain was visualized using descriptive statistics as shown in Figure 13. As depicted in Figure 13D, there was no statistically significant difference between the specific growth rates calculated from OD600 and EYFP and Citrine fluorescence for the strain carrying the pCPeyfp plasmid. This implies, that the *Pd* pCPeyfp strain is probably best to assess the growth of *P. deceptionensis* by the indirect measure of fluorescence. It is noticeable that the mean specific growth rate of the different strains as given by optical density takes on values between $0.15 \pm 0.03 \text{ h}^{-1}$ and $0.32 \pm 0.01 \text{ h}^{-1}$, which indicates up to twice as high fitness between different plasmid bearing strains. Thus, it can be suggested that *P. deceptionensis* as a host reacts more sensitively to the transformation with different reporter plasmids compared to other species, e.g., *H. aestusnigri* (Figure 11). Opposing the observations from the five other hosts the GFP fluorescence measured during the cultivation of *Pd* pCPcit must have been very low as indicated by the low value of the corresponding specific growth rate (Figure 13E).

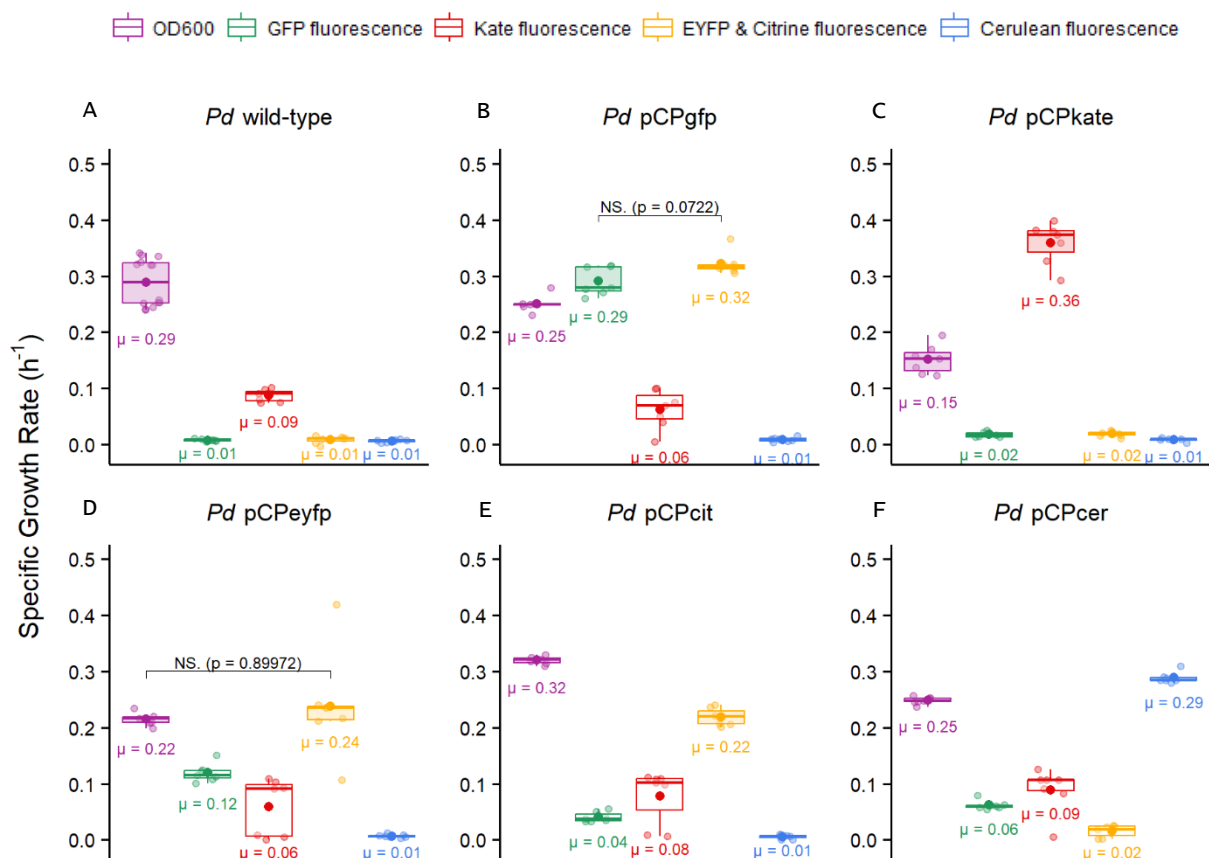


Figure 13: The growth of *P. deceptionensis* is best assessed by tracking of EYFP fluorescence as signified by the statistically non-significant difference between the specific growth rates obtained from OD600 and EYFP fluorescence for *Pd* pCPeyfp. The specific growth rates estimated from all five color coded measures for all biological replicates ($n = 7$) are shown as semi-transparent dots. The means are indicated by filled dots. In each panel, boxes displaying the distribution of data ascribed to OD600 and strain-specific fluorescent measurements are filled. The specific growth rate obtained from the specific fluorescence was pairwise compared to all other estimates of specific growth rate of the same strain by Tukey HSD tests. All differences among pairs are statistically significant (p -value < 0.05) unless otherwise indicated in the figure.

4.2.2.1.6 *Pseudomonas fluorescens*

The processing of experimental growth and fluorescence curve data revealed large differences in the specific growth rates estimated from OD600 between the plasmid bearing strains, ranging from $0.19 \pm 0.02 \text{ h}^{-1}$ (*Pf* pCPcer) to $0.41 \pm 0.04 \text{ h}^{-1}$ (*Pf* pCPeyfp), with the reference specific growth rate estimated at a value of $0.35 \pm 0.02 \text{ h}^{-1}$ (Figure 14). No statistically significant difference between the specific growth rates estimated from fluorescence and OD600 was detected for *Pf* pCPgfp, *Pf* pCPeyfp and *Pf* pCPcit. Considering that optical density is proportional to biomass concentration in planktonic liquid cultures, this suggests that the GFP, EYFP and Citrine fluorescence measured is proportional to biomass and thus the fluorescent proteins sfGFP, mEYFP and mCitrine are highly suited to assess the growth of *P. fluorescens*.

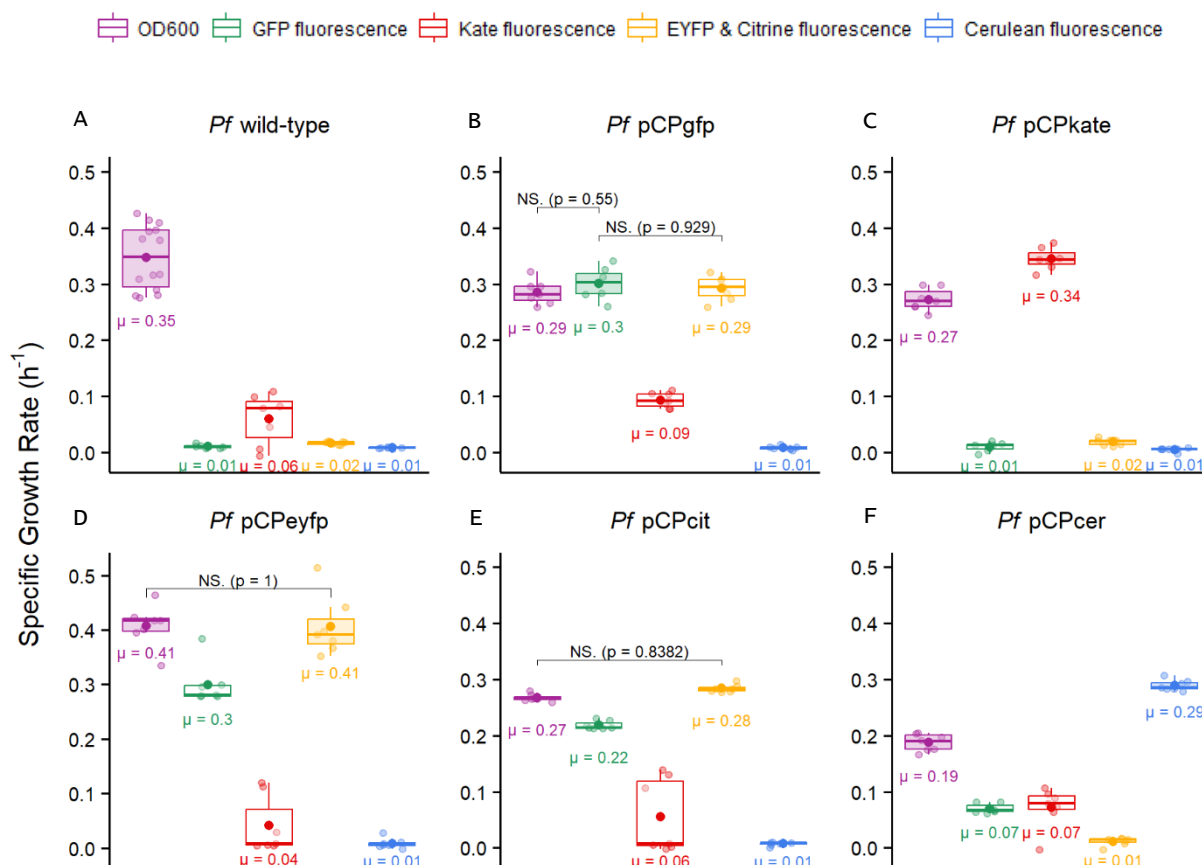


Figure 14: The comparison of specific growth rates obtained from growth curve and fluorescence curve data for *Pf* pCPgfp, *Pf* pCPeyfp and *Pf* pCPcit reveals statistically non-significant differences, indicating that GFP, EYFP and Citrine fluorescence are proportional to the population density of *P. fluorescens* making the pCPgfp, pCPeyfp and pCPcit plasmids good reporter tools to assess growth performance.

The specific growth rates for all biological replicates ($n = 7$) are shown as semi-transparent dots. The means are indicated by filled dots. In each panel, boxes displaying the distribution of data ascribed to OD600 and strain-specific fluorescent measurements are filled. The specific growth rate obtained from the specific fluorescence was pairwise compared to all other estimates of specific growth rate of the same strain by Tukey HSD tests. All differences among pairs are statistically significant (p -value < 0.05) unless otherwise indicated in the figure.

4.2.2.2 Estimates of Carrying Capacity

The ecological carrying capacity is a measure of fitness and refers to the maximum number of cells an environment can hold and sustain. To approximate this growth metric by fluorescence, a logistic growth model with the parameter K accounting for the maximum population density was fitted to experimental growth and fluorescence curve data (Equation 6). The growth model K estimates obtained from fluorescence data are denoted as K_{fl} while estimates obtained from OD600 measurements are referred to as K_{OD} . The K values were further compared to the maximum measurement of fluorescence and optical density (F_{max} and OD_{max}), which served as a second surrogate for the ecological carrying capacity.

First, the K_{OD} and OD_{max} values were compared to investigate the difference between the two metrics resulting from the different approaches used to estimate the ecological carrying capacity of strains. Since OD_{max} is a measure of light scattering that is proportional to biomass, it is considered the more accurate approximation of the actual ecological carrying capacity and was therefore used as a reference for evaluating the precision of the K_{OD} values derived from the logistic growth model.

The comparative evaluation of the surrogate measures revealed that both approaches provide similar estimates for the carrying capacity, with K_{OD} values deviating in a range of ± 0.1 OD600 from their respective reference value, with a few exceptions (Figure 15). The strains *Ho* wild-type and *Ho* pCPkate reached K_{OD} values $> 10^4$ OD600, which can easily be recognized as an artifact representing values outside of what is biologically possible. Therefore, they can clearly be classified as errors derived from the nonlinear fitting of the logistic growth model to the experimental data. Even though the observations indicate an overall decent model fit with the logistic growth equation, they also reveal a certain degree of uncertainty and error rate related to this approach, which can be quantified to at least 5.6 % based on the data shown in Figure 15. Since all the obvious erroneous estimates can be ascribed to *H. oceanii* strains, this could be an indication that fitting a logistic growth model to diauxic growth curve data entails a potentially higher error rate. Furthermore, the relatively large standard deviation of K_{OD} estimates observed for all *Pseudomonas* spp. and *E. coli*, indicated by error bars in Figure 15, implies a high degree of dispersion of the data which emphasizes the importance of biological replicates within the experimental design for extrapolating the carrying capacity in form of the parameter K from a logistic growth model.

E. coli and *P. putida* strains reached population densities ranging between approximately 0.8 - 1 OD600. In contrast, the *Halopseudomonas* spp. exhibited around twofold lower OD_{max} and K_{OD} values (strains *Ho* wild-type and *Ho* pCPkate excluded), which corresponds to turbidity observations made during the cultivation of strains in liquid cultures. Interestingly, the strains of both *Halopseudomonas* spp. also exhibited the lowest specific growth rates of all strains (Figure 11 and Figure 12), indicating an overall lower relative fitness with regards to the cultivation conditions.

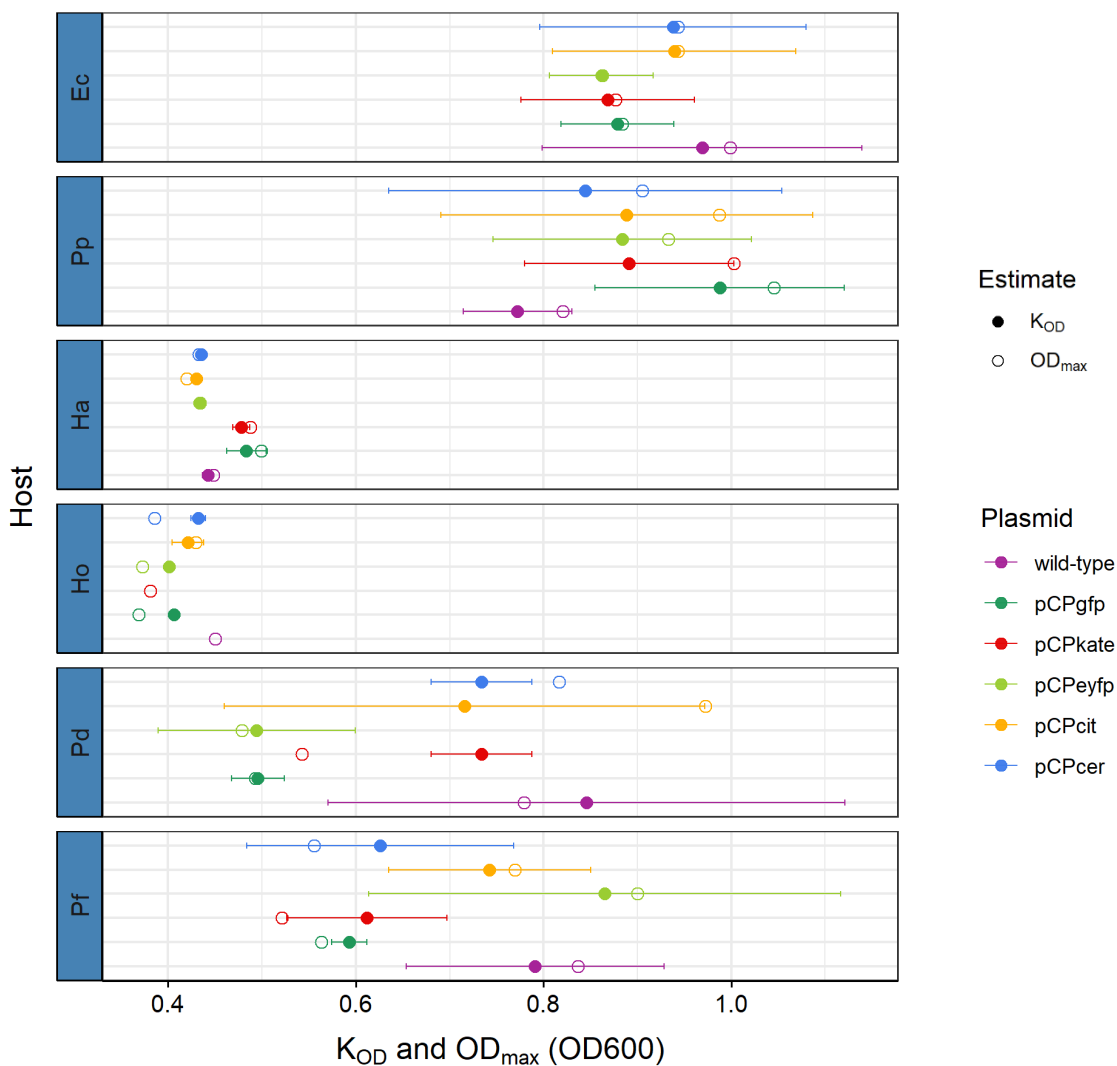


Figure 15: Two metrics of carrying capacity determined from optical density growth curve data reveal an overall reasonable model fit of the logistic equation used to estimate the ecological carrying capacity of strains despite some observed errors related to model fitting.

The estimates of carrying capacity obtained from the logistic growth model (K_{OD}) are depicted as filled dots. Estimates corresponding to the maximum optical density measured (OD_{max}) are illustrated as empty dots. Dots represent means of $n = 7$ biological replicates. Strains are color coded based on their genotype. Error bars represent standard deviations. K_{OD} estimates for *Ho* wild-type and *Ho* pCPkate strains are not mapped as their values exceeded 10000 OD600, emphasizing the existence of error rates related to the model fitting approach.

K_{fl} and F_{max} values obtained from fluorescence curve data show a high degree of similarity, except for *Pd* pCPkate (Figure 16). For this strain, a difference of about 30000 RFU between the estimated F_{max} and K_{fl} value can be observed, which can be attributed to a poor model fit. The relative relationship of the K estimates obtained from OD600 and fluorescence to each other is consistent for most strains of each host species. However, the relative relationship of K_{OD} and K_{fl} as well as OD_{max} and F_{max} estimates diverges between species, which is particularly noticeable for both *Halopseudomonas* spp.. Thus, it can be inferred that both approaches should be used with caution for the qualitative approximation of the carrying capacity and some margin of error in fitting the growth model should be anticipated. It is important to consider that both estimates, F_{max} and K_{fl} , represent measures of fluorescence and not

biomass, and therefore have no quantitative and only limited qualitative validity with regards to the assessment of the ecological carrying capacity. However, these measurements are advantageous because they readily lend themselves to combinatorial assays needed to screen larger design spaces associated with the construction and observation of synthetic populations, co-cultures, and higher order consortia.

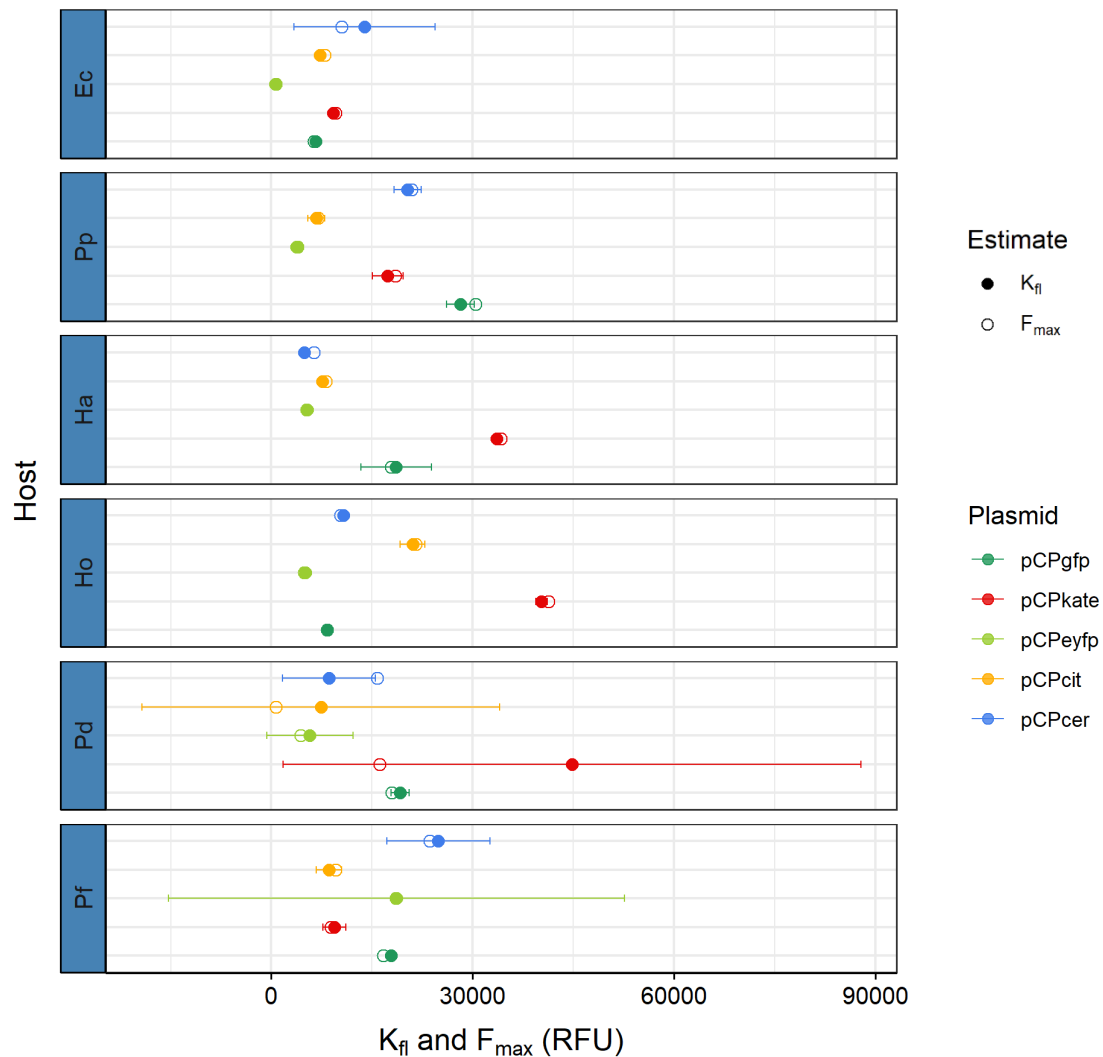


Figure 16: The carrying capacity between host strains shows an effect of metabolic burden from different plasmids and a limited qualitative validity.

The estimates derived from the nonlinear regression of the logistic growth model (K_{fl}) are depicted as filled dots. Estimates corresponding to the maximum fluorescence measured (F_{max}) are illustrated as empty dots. Dots represent means of $n = 7$ biological replicates. Strains are color coded based on their genotype. Error bars represent standard deviations.

Interestingly, the host strains have reached different carrying capacities (Figure 16). This suggests that the carrying capacity of the host is modified by the metabolic burden imposed by the different reporter plasmids upon transformation. Plasmid maintenance and expression of heterologous genes draws host cell's energy and raw material resources that could otherwise be allocated to support cell growth. This metabolic load causing a shift in resource availability burdens the hosts own machineries, thereby

affecting the specific growth rate of strains and making it reasonable to assume that all growth metrics, including the carrying capacity, are influenced by the metabolic burden. Nevertheless, any difference in the carrying capacity between strains is also likely to be biased due to the uncertainty arising from the nonlinear regression of the logistic growth model across datasets.

4.2.3 Quantification of the Metabolic Burden

A shortcoming associated with the use of this broad-host-range plasmid reporter kit is that the bacteria experience a plasmid-dependent metabolic load, the effect of which on host growth physiology can vary greatly. Thus, the metric m_B was introduced to quantify the burden of maintaining the reporter plasmids and expressing the encoded heterologous genes on the growth of different hosts. The metric m_B is defined as the percent difference in the specific growth rate of the plasmid bearing strain and wild-type strain compared to the specific growth rate of the reference wild-type strain obtained from OD600 measurements (Equation 8). While a positive metabolic burden indicates that the plasmid bearing strain has a lower specific growth rate compared to the wild-type strain, a negative m_B value implies a higher growth rate of the plasmid bearing strain compared to its wild-type control. Tukey HSD tests were performed on all pairs of host strains metabolic burdens to investigate whether significant differences could be observed.

E. coli and *P. putida* strains experienced a similar amount of reduction in growth upon transformation, which is implied by the statistically non-significant differences in m_B values. Thus, it can be concluded that the growth of *E. coli* and *P. putida* is similarly impacted by all reporter plasmids (Figure 17A and B). In contrast, their specific growth rates estimated from fluorescence, which are proxy measures of the first order rate change in biomass, differ quite strongly, in particular the *P. putida* strains (Figure 10). This implies a different growth behavior and is consistent with previous observations that fluorescence is not generically proportional to biomass.

The greatest range of influence on the host growth phenotype was observed for *P. deceptionensis* and *P. fluorescens* (Figure 17E and F). *Pd* pCPkate and *Pf* pCPcer experienced the highest metabolic burdens upon transformation with the respective reporter plasmids, indicated by the reduction of their growth rates by $47.6 \pm 8.5 \%$ and $45.9 \pm 4.7 \%$. Interestingly, even though *Pd* pCPkate showed the highest growth inhibition of all plasmid bearing strains, it managed to overcome this burden, indicated by a high relative fitness inferred from fluorescence curve data in terms of carrying capacity (Figure 16) and specific growth rate (Figure 13).

Contrary to expectations, the growth rate of some hosts was increased upon introduction of some reporter plasmids. *Pf* pCPeyfp exhibited the highest increase in growth, implied by the most negative m_B value of $-17.2 \pm 8.6 \%$. It also reached the highest specific growth rate of all *P. fluorescens* strains (Figure 14) and a high carrying capacity (Figure 16), suggesting an overall high fitness. In contrast,

Pd pCPcit experienced an increase in growth rate compared to its wild-type control ($m_b = -0.9 \pm 1.4 \%$), but only achieved a moderate relative carrying capacity (Figure 16) and specific growth rate (Figure 13). These observations can possibly be attributed to different relative strengths in the OD600 and Citrine fluorescence signals.

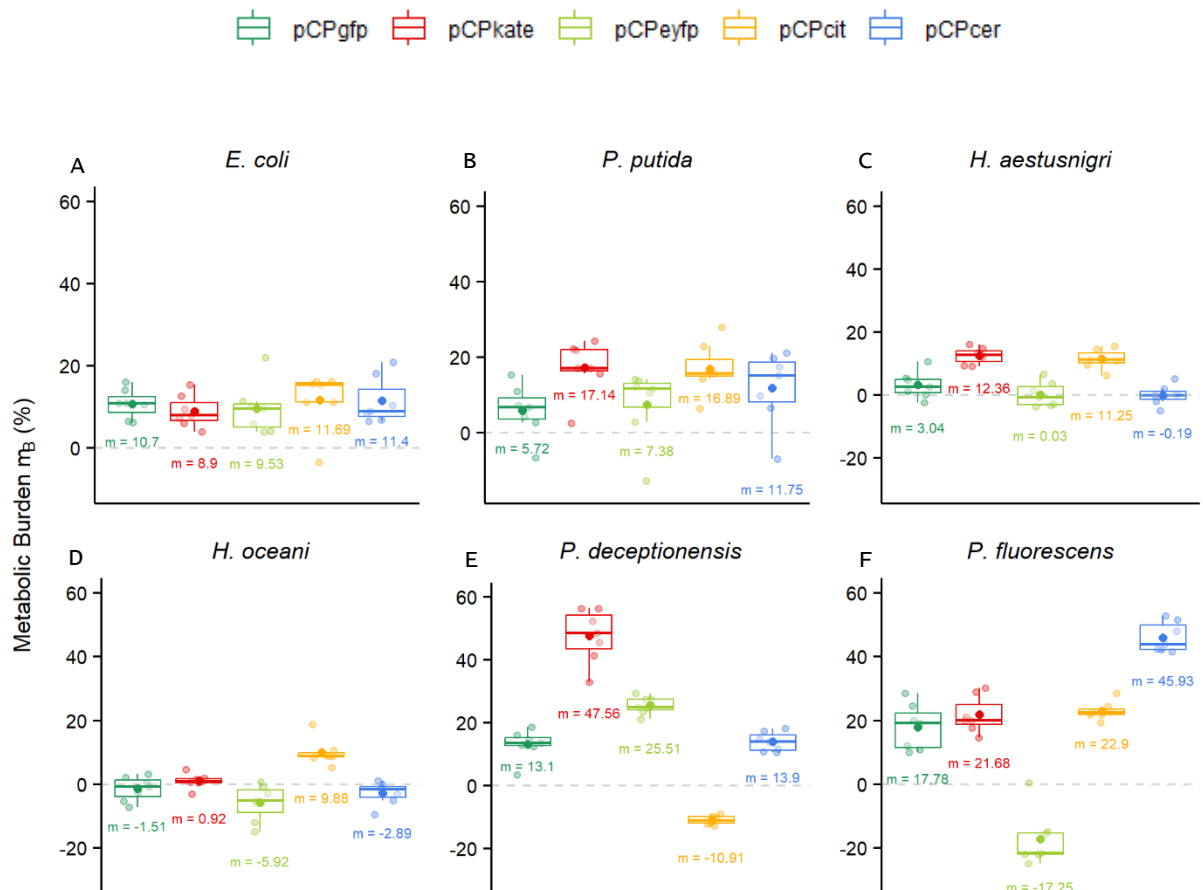


Figure 17: The visual representation of metabolic burdens shows that the growth of *P. deceptionensis* and *P. fluorescens* is most strongly affected upon transformation with the reporter plasmids, signified by large differences in the m_b values.

The percent metabolic burdens of $n = 7$ biological replicates are indicated by semi-transparent dots for every species-plasmid combination. The reporter plasmids are color coded and filled dots represent the mean metabolic burdens. The grey dashed, horizontal lines, plotted at $m_b = 0 \%$, visually mark where no difference in growth rates between plasmid bearing strains and their wild-type control exists. Tukey HSD tests revealed no statistically significant difference between all pairs of metabolic burdens calculated for different strains of *E. coli* (A) and *P. putida* (B). In panel C, the metabolic burden of *Ha* pCPkate differs statistically significantly from the metabolic burdens of all other strains ($p < 0.001$) except for *Ha* pCPcit. The metabolic burdens of *Ha* pCPcit and *Ha* pCPgfp, *Ha* pCPeyfp and *Ha* pCPcer also differ significantly from each other ($p < 0.01$). The metabolic burden of *Ho* pCPcit is statistically significant from all other strains ($p < 0.001$) and the m_b value of *Ho* pCPeyfp is statistically significant from *Ho* pCPkate ($p < 0.05$, panel D). In panel E, the differences between metabolic burdens of all *P. deceptionensis* strains are statistically significant from each other ($p < 0.001$), except for *Pd* pCPgfp and *Pd* pCPcer ($p > 0.05$). In panel F, the metabolic burden of *Pf* pCPeyfp and *Pf* pCPcer differs statistically significantly from all strains ($p < 0.001$).

The performance and amount of pressure a plasmid puts on a host cell, *e.g.*, by drawing resources away from growth, is dependent on that host's specific physiology, the chassis. To identify chassis-effects, Tukey HSD tests were performed on all pairs of metabolic burdens between the different hosts with respect to each broad-host-range reporter plasmid. Hence, any of the statistically relevant relationships ($p < 0.05$) depicted in Figure 18 display a chassis-effect.

The data suggests that *P. deceptionensis* and *P. fluorescens* are the most unique chassis with respect to host physiology. Chassis-effects between both *Pd* and *Pf* strains and minimum three other strains were observed for each of the six reporter plasmids. While *P. deceptionensis* exhibited the highest metabolic burden with respect to the pCPkate and pCPeyfp plasmid, *P. fluorescens* experienced a high metabolic burden with respect to the pCPgfp, pCPcit and pCPcer plasmids. The other species displayed a more shared consistency of the broad-host-range plasmids on growth behavior, indicated by similar degrees of growth burden. This could be attributed to the relative simplicity and similarity in the design of the reporter plasmids.

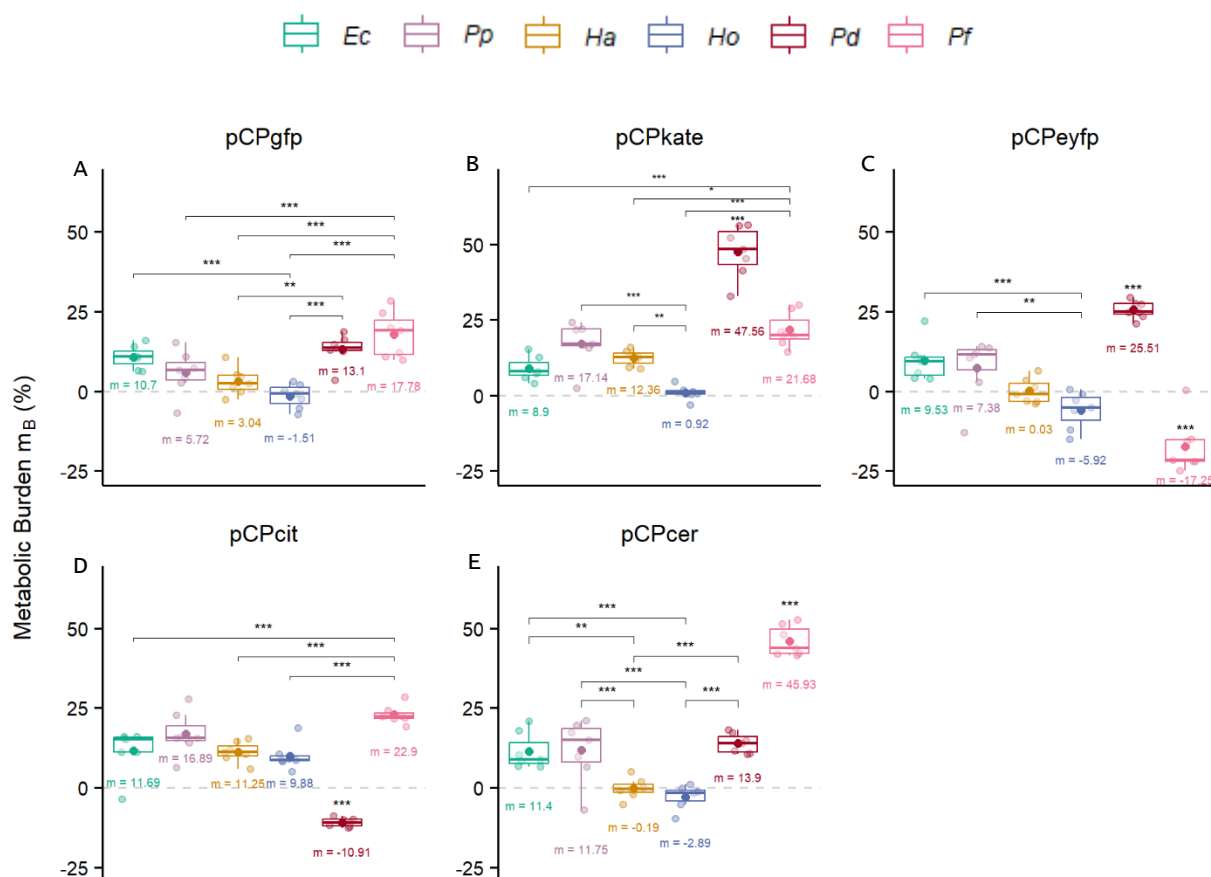


Figure 18: Statistically significant relationships show the chassis-effects between species for each of the broad-host-range reporter plasmids.

The distribution of metabolic burden values is visually shown by box plots. Host species are color coded. Semi-transparent dots show data of $n = 7$ biological replicates while dots represent the mean value of metabolic burdens. The grey dashed, horizontal lines, plotted at $m_B = 0\%$, visually mark where no difference in growth rates between the plasmid bearing strains and their wild-type controls exists. Significance levels that indicate chassis-effects between strains are displayed by asterisks (***: $p < 0.001$, **: $p < 0.01$, *: $p < 0.05$). Boxes marked directly with asterisks represent strains that have a significant relationship with all other hosts. In panel C, the significance level between *P. fluorescens* and *H. oceanus* is '*'.

4.3 Inference of Combinatorial Growth Dynamics by Fluorescence

The purpose of this section is to investigate whether interspecies growth dynamics can be decoupled using fluorescence to simultaneously assess and track strain-specific growth in liquid cultures within a certain time span. This involves evaluating whether the methodology developed in this thesis work can be used to estimate the ecologically important growth parameters μ and K for each bacterial species in combinatorial co-cultures, and whether the binary growth interactions between these fluorescently labelled species can be inferred in terms of specific growth rate and carrying capacity. Another key objective is to examine if the choice of plasmid bearing strains has an impact on the interrogation of interspecies growth dynamics, which is central to the applicability of the genetic device platform described in Chapter 4.1.

4.3.1 Selection of Suitable Binary Co-Cultures

To test whether this device platform can be used to capture and decouple combinatorial growth dynamics, an experiment was designed to track species-specific growth in co-cultures based on measurements of fluorescence. The previously characterized plasmid bearing strains and their wild-type counterparts result in a selection of 36 distinct strains that can be pairwise combined and cultivated in a total of 630 different ways. This is a relatively large number of possible combinations with certainty that some of the strain-strain combinations would not yield significant results. It was therefore deemed infeasible to test them and only a limited number of selective combinations were chosen based on systematic criteria (Figure 19).

Firstly, it was specified that only two-species combinations would be tested, resulting in 15 different combinatorial co-cultures. For a meaningful analysis and interpretation of the dynamic competitive interaction of two species over time the assumption was made that the estimates of specific growth rate obtained from fluorescence should be in accordance with the estimates of specific growth rate given by OD600 ($\mu_{fl} \approx \mu_{OD}$, referred to as “good” combinations). Since the preliminary growth characterization of the plasmid bearing strains has revealed large deviations between the specific growth rate obtained from OD600 and the strain-specific fluorescence, it is assumed that the choice of plasmid bearing strains interferes with the inference of population dynamics (see 4.2.2.1). To investigate whether the choice of tools has an influence on the prediction of growth dynamics, plasmid bearing strains with great differences in their fluorescence and OD600 estimates of specific growth rate ($\mu_{fl} \ll \mu_{OD}$ and $\mu_{fl} \gg \mu_{OD}$, referred to as “bad” combinations) were also combined into all two-species co-cultures. Thus, the initial filtering of plasmid bearing strains for co-culturing was based on the correlation of the two specific growth rate estimates associated with each respective strain and divided into two categories each of 15 combinations – A: strains with $\mu_{fl} \approx \mu_{OD}$ and B: strains with $\mu_{fl} \ll \mu_{OD}$ or $\mu_{fl} \gg \mu_{OD}$.

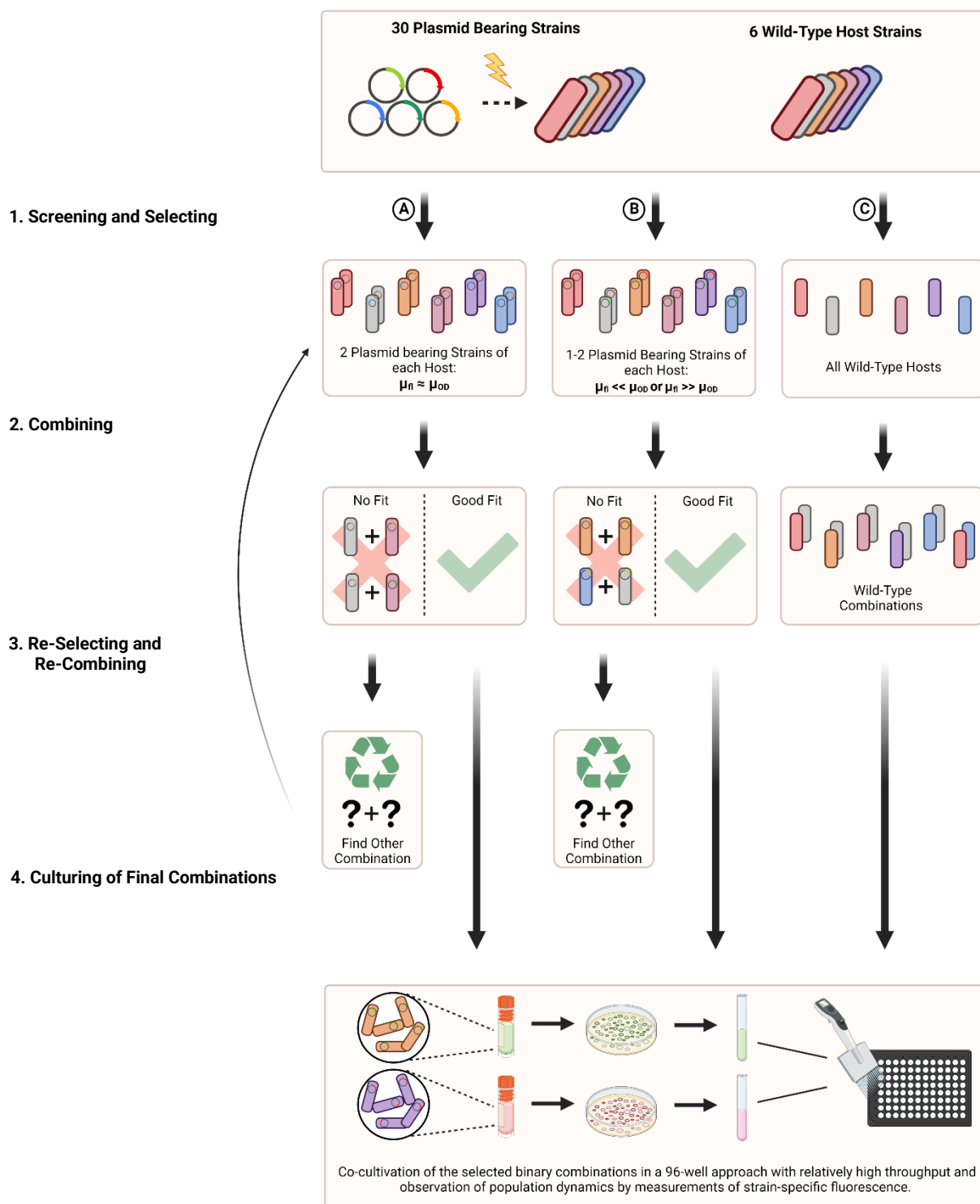


Figure 19: Selection procedure to determine suitable pairs of plasmid bearing strains for combinatorial two-species co-cultures.

First, all plasmid bearing strains were screened and two strains from each host species were selected that best met the selection criteria (A) $\mu_{fl} \approx \mu_{OD}$ and (B) $\mu_{fl} \ll \mu_{OD}$ OR $\mu_{fl} \gg \mu_{OD}$. Selected strains in each category were then combined into pairs of all possible binary combinations. If no appropriate match with the selected strains was possible, the next best strains were selected and combined into pairs. In addition, all two-species combinations were formed with the wild-type strains (C). The final combinations for all three categories A - C were then cultured in 96-well plates and both OD600 and fluorescence measurements taken over time by an automated plate reader.

(Created with BioRender.com)

After screening and selecting up to two plasmid bearing strains for each host species that best met the primary selection criteria for categories A and B, strains had to be combined into pairs. Therefore, strains selected to be combined were not allowed to have overlapping fluorescence signals, such as strains carrying the pCPgfp and pCPeyfp or pCPcit plasmids, to ensure the separation of measured fluorescence outputs by the methodology developed and applied in this study. Moreover, the strains *Ec* pCPcer and *Pd* pCPkate were preferred over the strains *Ec* pCPeyfp and *Pd* pCPcit during selection and combining. If no combination could be formed with the previously selected strains, the next best strain was used. All fifteen binary combinations were additionally cultured using the wild-type hosts as reference to determine the metabolic load and possible influences of the interaction partners on it (category C). Thus, a total of 45 combinations were chosen (15 combinations for each category). These final choices of strain-strain combinations for combinatorial cultivation in 96-well plates that originated from this selection process depicted in Figure 19 are listed in Table 4.

Table 4: Final choices of strain-strain combinations for binary co-cultures.

Selected combinations (combo 1 - 15) for each of the following categories: **A:** plasmid bearing strains with $\mu_{fl} \approx \mu_{OD}$, **B:** plasmid bearing strains with $\mu_{fl} \ll \mu_{OD}$ or $\mu_{fl} \gg \mu_{OD}$, **C:** wild-type strains.

	A		B		C	
	Strain A	Strain B	Strain A	Strain B	Strain A	Strain B
Combo 1	<i>Ec</i> pCPcit	<i>Pp</i> pCPcer	<i>Ec</i> pCPcer	<i>Pp</i> pCPeyfp	<i>Ec</i> wild-type	<i>Pp</i> wild-type
Combo 2	<i>Ec</i> pCPcit	<i>Ha</i> pCPcer	<i>Ec</i> pCPcer	<i>Ha</i> pCPcit	<i>Ec</i> wild-type	<i>Ha</i> wild-type
Combo 3	<i>Ec</i> pCPcit	<i>Ho</i> pCPcer	<i>Ec</i> pCPcer	<i>Ho</i> pCPkate	<i>Ec</i> wild-type	<i>Ho</i> wild-type
Combo 4	<i>Ec</i> pCPkate	<i>Pd</i> pCPeyfp	<i>Ec</i> pCPcer	<i>Pd</i> pCPkate	<i>Ec</i> wild-type	<i>Pd</i> wild-type
Combo 5	<i>Ec</i> pCPkate	<i>Pf</i> pCPeyfp	<i>Ec</i> pCPcer	<i>Pf</i> pCPkate	<i>Ec</i> wild-type	<i>Pf</i> wild-type
Combo 6	<i>Pp</i> pCPgfp	<i>Ha</i> pCPcer	<i>Pp</i> pCPkate	<i>Ha</i> pCPcit	<i>Pp</i> wild-type	<i>Ha</i> wild-type
Combo 7	<i>Pp</i> pCPcer	<i>Ho</i> pCPeyfp	<i>Pp</i> pCPeyfp	<i>Ho</i> pCPkate	<i>Pp</i> wild-type	<i>Ho</i> wild-type
Combo 8	<i>Pp</i> pCPcer	<i>Pd</i> pCPeyfp	<i>Pp</i> pCPeyfp	<i>Pd</i> pCPkate	<i>Pp</i> wild-type	<i>Pd</i> wild-type
Combo 9	<i>Pp</i> pCPcer	<i>Pf</i> pCPeyfp	<i>Pp</i> pCPeyfp	<i>Pf</i> pCPcer	<i>Pp</i> wild-type	<i>Pf</i> wild-type
Combo 10	<i>Ho</i> pCPeyfp	<i>Ha</i> pCPcer	<i>Ho</i> pCPkate	<i>Ha</i> pCPcit	<i>Ho</i> wild-type	<i>Ha</i> wild-type
Combo 11	<i>Ha</i> pCPcer	<i>Pd</i> pCPeyfp	<i>Ha</i> pCPcit	<i>Pd</i> pCPkate	<i>Ha</i> wild-type	<i>Pd</i> wild-type
Combo 12	<i>Ha</i> pCPcer	<i>Pf</i> pCPeyfp	<i>Ha</i> pCPcit	<i>Pf</i> pCPcer	<i>Ha</i> wild-type	<i>Pf</i> wild-type
Combo 13	<i>Ho</i> pCPcer	<i>Pd</i> pCPeyfp	<i>Ho</i> pCPcit	<i>Pd</i> pCPkate	<i>Ho</i> wild-type	<i>Pd</i> wild-type
Combo 14	<i>Ho</i> pCPcer	<i>Pf</i> pCPeyfp	<i>Ho</i> pCPkate	<i>Pf</i> pCPcer	<i>Ho</i> wild-type	<i>Pf</i> wild-type
Combo 15	<i>Pd</i> pCPeyfp	<i>Pf</i> pCPkate	<i>Pd</i> pCPkate	<i>Pf</i> pCPcer	<i>Pd</i> wild-type	<i>Pf</i> wild-type

4.3.2 Evaluation of Experimental Data from Combinatorial Growth Experiments

All 45 previously selected co-cultures were grown in biological replicates of seven in 96-well microplates in an automated plate reader under the same experimental conditions as for the monocultures (see 3.8). The overall change in biomass in each co-culture was monitored by regular measurements of optical density, while the strain-specific biomasses were tracked by proxy measurements of fluorescence. Both the OD600 and four different fluorescence measurements were taken at 7.5-min intervals over a maximum period of 24 h. Experimental growth and fluorescence curve data were truncated at 16 h before growth parameters were estimated (see 3.9.1.2).

A two-step procedure consisting of the decoupling and inference of binary growth interactions was then used to evaluate the experimental OD600 and fluorescence curve data obtained during the high throughput combinatorial growth experiments of all two-species co-cultures listed in Table 4. First, for each competing species, all three measures of fitness, *i.e.*, the bacterial growth parameters μ_{fl} , K_{fl} and F_{max} , were estimated from the corresponding strain-specific fluorescence datasets obtained during the combinatorial growth of the plasmid bearing strains of categories A and B. In doing so, it was also investigated whether the individual growth of both bacterial species in each co-culture could be successfully tracked by measuring the different types of fluorescence output. This was done by plotting the strain-specific fluorescence curves of the two competing species against time. The μ_{fl} and K_{fl} values were estimated by regression analysis of the respective growth models (Equation 4 and Equation 6), whereas the F_{max} values were determined as the highest fluorescence value measured within the first 16 hours of growth. To quantify the observed metabolic burden, the specific growth rate was further estimated from the OD600 data (μ_{OD}) for all combinations of categories A, B and C. All model fits for the linear regression analysis were visually inspected and had to pass a threshold of $R^2 > 0.75$ to be considered a sufficiently good model fit. Furthermore, the competitive fitness winners in terms of carrying capacity and specific growth rate of the same co-cultures from categories A and B were compared to evaluate whether the choice of plasmid bearing strains has an influence on the prediction of interspecies growth interactions.

After the strain-specific growth parameters were determined, the second step was to quantify the effect of co-cultivation on the fitness of the individual species by comparing their fitness in monoculture with their fitness in co-culture. This was done by introducing the metric Ξ , referred to as fitness maintenance, which was calculated in terms of all three measures of fitness under investigation in this thesis work (see 3.9.3). Based on the fitness maintenance, which indicates whether a species is positively, negatively, or neutrally influenced in its fitness by interspecies interaction (one-way interactions), the underlying bidirectional interactions were derived hereafter. For a pronounced positive or negative fitness maintenance as well as a distinct mutualistic or antagonistic interspecies interaction, a 5 % threshold had to be exceeded (see 3.9.3). The investigation of combinatorial growth dynamics was only conducted for co-cultures of category A with $\mu_{fl} \approx \mu_{OD}$. All results related to the interrogation of population dynamics are presented in the following Chapters 4.3.2.1 to 4.3.2.4.

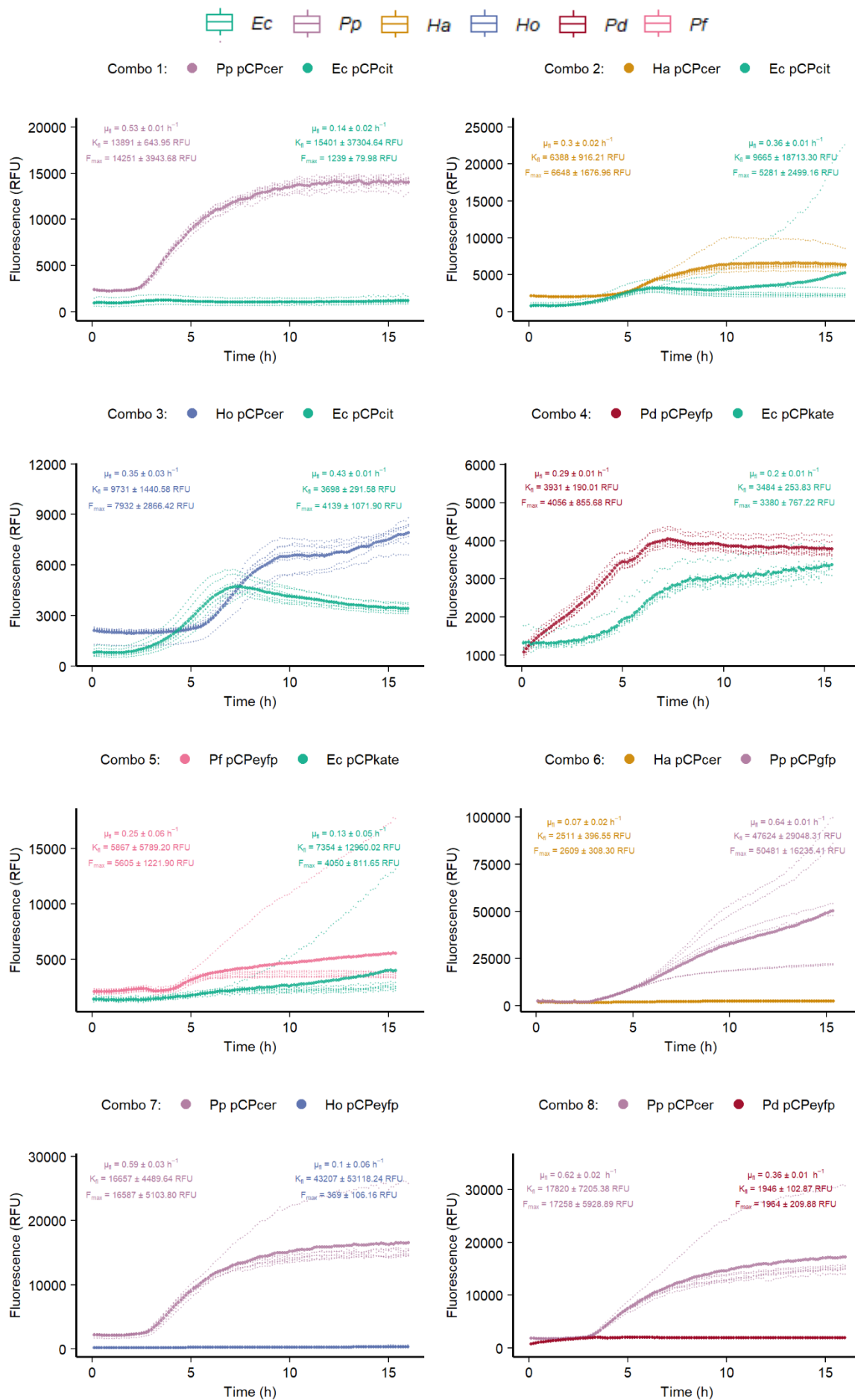
4.3.2.1 Estimates of Bacterial Fitness in Combinatorial Co-Cultures

To obtain an initial and holistic view of the strain-specific growth monitored by fluorescence measurements in two-species co-cultures, the specific fluorescence data of all seven biological replicates and their mean values were plotted over time and the corresponding growth parameters μ and K were determined according to the approaches described in Chapter 3.9.1. The fluorescence curves and all three measures of bacterial fitness μ_{fl} , K_{fl} and F_{max} for the “good” combinations (category A with $\mu_{fl} \approx \mu_{OD}$) are graphically visualized in Figure 20.

As shown in Figure 20, reasonable looking fluorescence curves with a typical microbial growth pattern could be plotted for each co-culture based on the fluorescence measurements of the two competing strains. The graphical representation of the growth curves for all seven biological replicates of each combination further showed that the fluorescence measurements were mostly consistent between replicates. For some combinations, however, individual replicates differ significantly from the other replicates and the mean ($n = 7$). Nonetheless, with two exceptions, all biological replicates showed consistent results in terms of growth trajectory and their relative relationship to the competitor's growth curves. In combination 2 (*Ec* pCPcit and *Ha* pCPcer) and combination 5 (*Ec* pCPkate and *Pf* pCPeyfp), individual replicates reach very high RFU values, which could lead to inaccurate predictions of growth interaction if not considered in conjunction with the other replicates – *e.g.*, by calculating the mean. Hence, this is another indication of the importance of considering a sufficient number of biological replicates in the experimental design process when applying the tools and methods developed under this thesis project. These aforementioned replicates, which reach very high RFU values and can be classified as outliers, adversely influence the determination of the growth parameter estimates and could possibly account for the partly high standard deviations observed for the F_{max} measure (Figure 20).

The comparison of the two surrogate measures of ecological carrying capacity obtained from fluorescence data, K_{fl} and F_{max} , has shown that the K_{fl} values sometimes deviate strongly from their reference value F_{max} . These K_{fl} values also have high standard deviations, which may indicate a poor fit of the logistic growth model to the experimental data. The comparison of the K_{fl} values and the corresponding F_{max} reference values of the co-cultured strains for combinations 1, 2, 5, and 7 revealed different fitness winners in terms of carrying capacity (Figure 20). Combination 7 is the most prominent example of this. While the K_{fl} value for *Ho* pCPeyfp was estimated to be 43207 ± 53118.24 RFU, the corresponding reference, the highest measured fluorescence value F_{max} , reached only 369 ± 106.16 RFU. This clearly demonstrates a high level of uncertainty associated with fitting the logistic growth model to large datasets and how this can potentially lead to misrepresentations of bacterial growth phenotypes. These results therefore suggest that the logistic growth function should be used with caution to estimate the carrying capacity and that the measured F_{max} value appears to be the more consistent and reliable of the two metrics.

The visualization of the fluorescence curves, as seen in Figure 20, caused sporadic distortions in the representation of the fluorescence-based growth curves, which can be noted by the absence of visible slopes in some of the plotted fluorescence curves despite the presence of growth as indicated by the μ values, *e.g.*, in combinations 1, 8, 9 and 10. To illustrate this with an example, Figure 21 shows the fluorescence curves and the corresponding graphs of the model fit for determining the estimates of specific growth rate for the combination 8 (*Pp* pCPcer and *Pd* pCPeyfp). All linear regression models for the estimation of specific growth rates are provided in the R Markdown file published as part of the OSF project: "Broad-Host-Range Genetic Tools for Observing Microbial Consortia" (<https://osf.io/h7ndk/>).



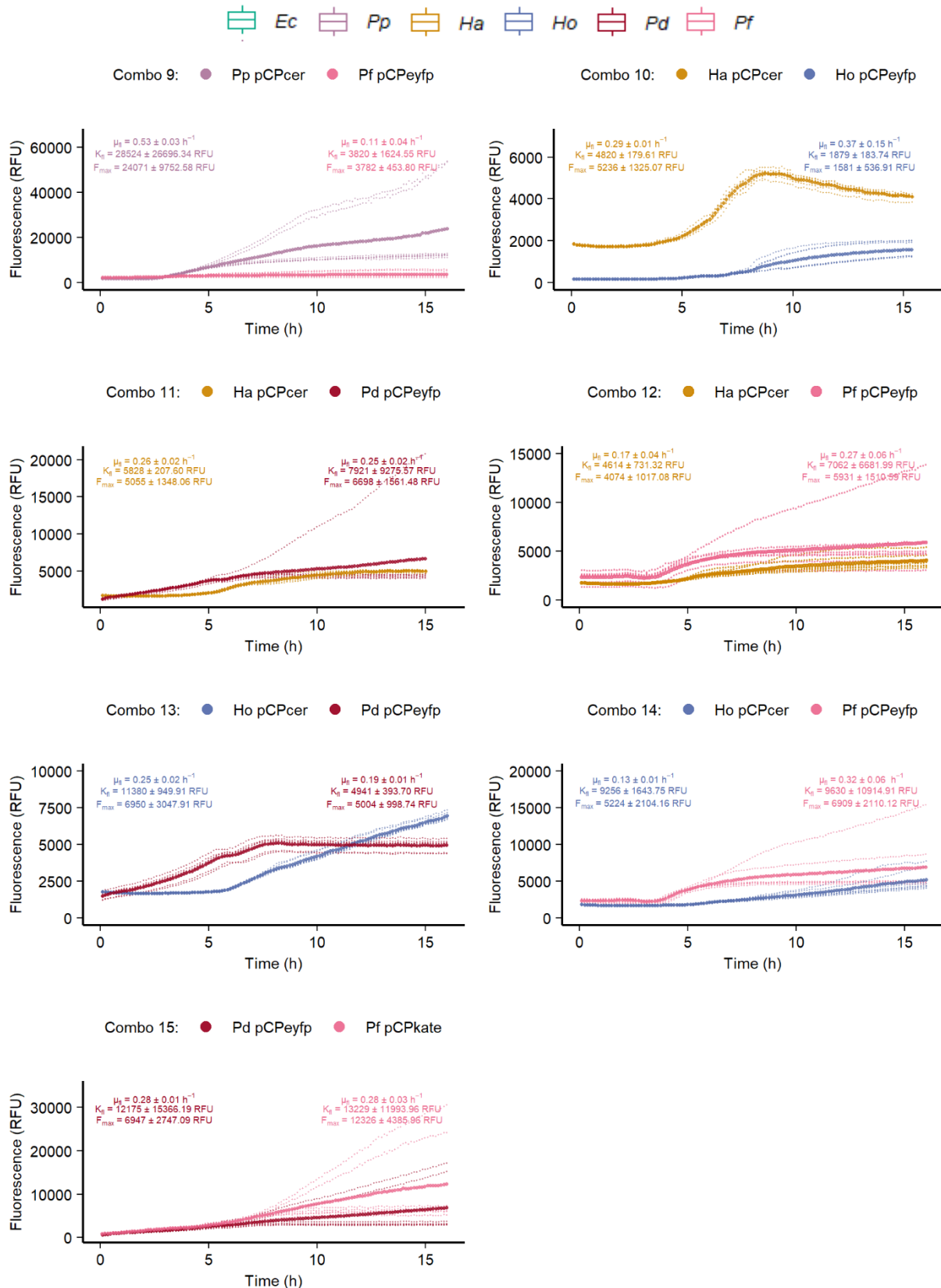


Figure 20: Growth curves of co-cultivated species plotted from strain-specific fluorescence measurements show consistency between replicates, whereas the derived growth parameters μ_{fi} , K_{fi} and F_{max} indicate some inconsistencies between the two measures of carrying capacity.

The data truncated at 16 hours represents the strain-specific fluorescence measured over time. Semi-transparent dots indicate measurements from $n = 7$ biological replicates, and the dots represent the mean. Species are color coded and the co-cultivated strains are named in the header of each graph. All three measures of fitness estimated for each strain are depicted in each graph and color coded according to the species.

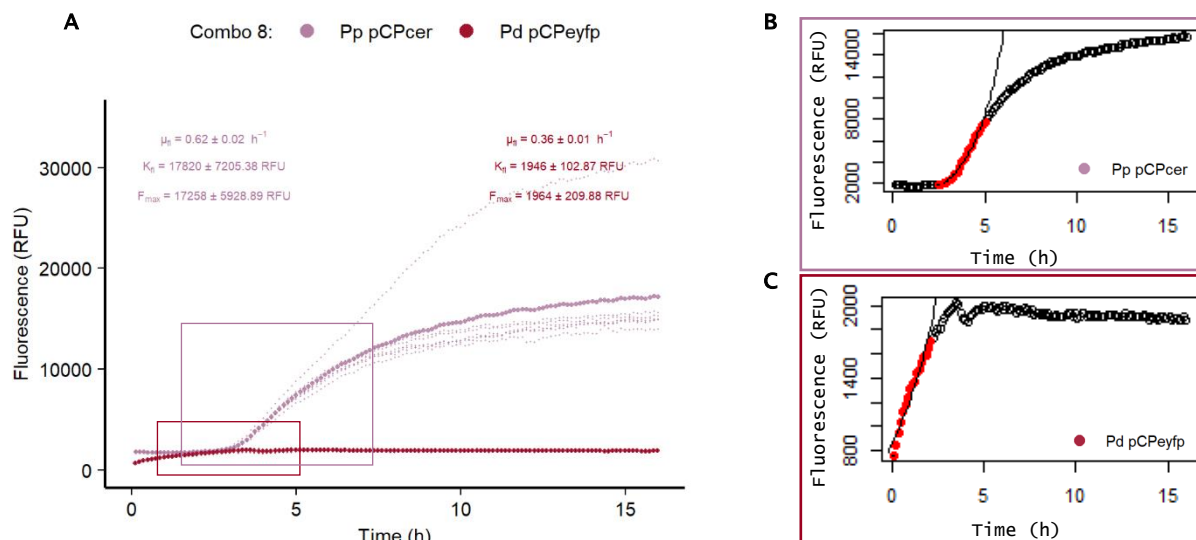


Figure 21: The individual examination of the fluorescence curves shows that due to the different size ranges of the measured RFU values, the increase in fluorescence of *Pd pCPeyfp* cannot be clearly identified in the joint diagram.

The fluorescence curves in figure part A show the RFU values of EYFP and Cerulean fluorescence measured over time during combinatorial growth and display the growth trajectory of *Pp pCPcer* and *Pd pCPeyfp*. Semi-transparent dots indicate the data of all $n = 7$ biological replicates for each strain and the dots represent the mean. In figure parts B and C, the individual fluorescence curves are illustrated with a magnification. The parts of the two fluorescence curves marked in red show the extended data window considered for the final model fit for the estimation of the specific growth rate μ . The exponential functions running through the red area represent the mathematical regression models fitted to the experimental data after re-transformation.

4.3.2.2 Influence of Plasmid Bearing Strains on the Prediction of Growth Dynamics

To investigate whether the choice of fluorescent reporter proteins has an impact on the fluorescence-based prediction of growth dynamics, strains with great differences in their specific growth rates estimated from fluorescence and OD600 were paired into binary co-cultures (category B, $\mu_{fl} \ll \mu_{OD}$ or $\mu_{fl} \gg \mu_{OD}$). The comparative evaluation of fluorescence curve data and derived growth parameters from the “good” and “bad” combinations of the same two-species co-cultures (categories A and B) revealed that the choice of plasmid bearing strains influenced the prediction of species-specific fitness and thus bacterial growth interactions in 60 % of the combinations tested. Thus, in nine out of the fifteen cases, the more fit species of the two competitors varied in terms of at least one of the two metrics of bacterial fitness between the strain combinations of categories A and B, including the combinations 1, 2, 3, 4, 10, 12, 13, 14 and 15. In six of these nine binary combinations, the species that achieved both higher specific growth rates and carrying capacities in category A and B co-cultures varied. This change in the competitive fitness outcome is graphically visualized in Figure 22 for combination 14 (*H. oceanii* and *P. fluorescens*). While *P. fluorescens* constitutes the more fit competitor in the “good” combination with $\mu_{fl} \approx \mu_{OD}$ (*Pf pCPeyfp*: $\mu_{fl} = 0.32 \pm 0.06 \text{ h}^{-1}$, $K_{fl} = 9630 \pm 10914.91 \text{ RFU}$, $F_{max} = 6909 \pm 2110.12 \text{ RFU}$), *H. oceanii* achieved a higher specific growth rate and carrying capacity in

the “bad” combination of category B with $\mu_{fl} \ll \mu_{OD}$ or $\mu_{fl} \gg \mu_{OD}$ (*Ho* pCPkate: $\mu_{fl} = 0.78 \pm 0.03 \text{ h}^{-1}$, $K_{fl} = 25198 \pm 13182.94 \text{ RFU}$, $F_{max} = 26140.17 \pm 9903.53 \text{ RFU}$). It can therefore be concluded that the estimates of specific growth rate as given by strain-specific fluorescence of the plasmid bearing strains used should be as close as possible to the estimates of specific growth rate obtained from the OD600 to use fluorescence as a proxy for strain-specific biomass and as a tool to effectively decouple population dynamics.

Combination 14: *H. oceanii* & *P. fluorescens*

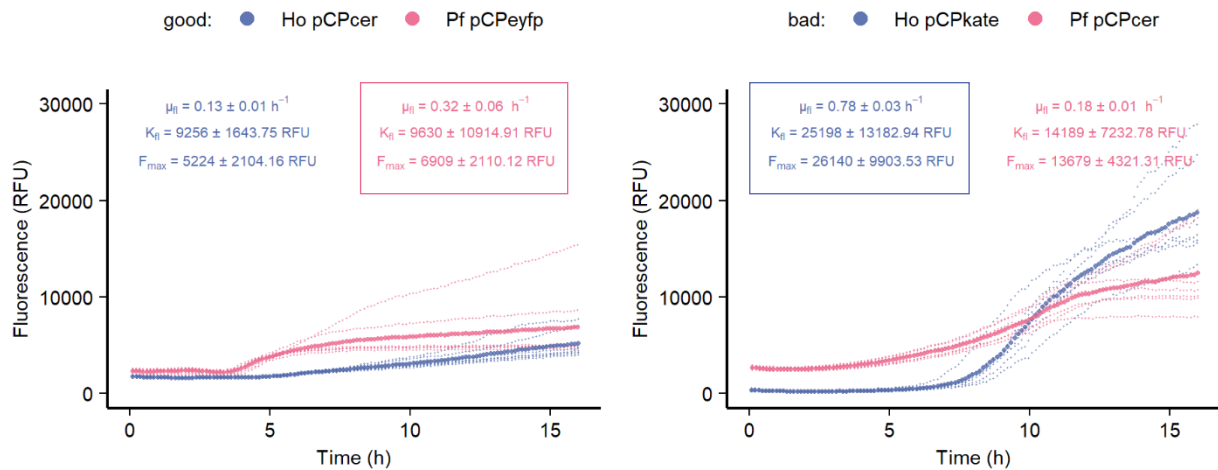


Figure 22: The comparison of the fluorescence curves and growth parameters μ and K for the “good” and “bad” strain combinations of the same binary co-cultures reveals that the prediction of fitness competition depends on the choice of plasmid bearing strains for each species.

In the “good” combination ($\mu_{fl} \approx \mu_{OD}$) *P. fluorescens* achieved a higher specific growth rate and carrying capacity compared to its competitor *H. oceanii*. A complete reversal of the competitive fitness outcome between both species can be seen for the “bad” combination (category B), where *H. oceanii* reached a higher specific growth rate and carrying capacity. The data represents the strain-specific fluorescence measured over time. Semi-transparent dots indicate measures of $n = 7$ biological replicates and the dots represent the mean. Co-cultured strains are color coded. The colored boxes indicate the strain that reached a higher specific growth rate and carrying capacity during co-cultivation.

4.3.2.3 Quantification of the Metabolic Burden

As shown in Chapter 4.3.2.1, the monitoring of the individual growth of fluorescently tagged bacterial species in combinatorial co-cultures is possible. However, the bacteria must be loaded with plasmids that carry the genetic information for the constitutive production of fluorescent proteins. The host is likely to experience a metabolic burden that can reduce its overall fitness depending on how energetically expensive and resource consuming plasmid maintenance and the expression of heterologous genes is. Thus, the fluorescence data and derived growth parameter estimates represent quantities of relative population dynamics under burden. When different species or strains are grown together, their growth can be further influenced by bacterial interactions, *e.g.*, the competition for limited resources or syntrophy, which can affect the growth, reproduction and survival of the individual species or strain and thus the competitive dynamics of the system (Bernstein et al., 2012; Kehe et al., 2021). To quantify the overall metabolic burden of the individual co-culture systems imposed by the broad-host-range reporter plasmids the metric m_B was used. This was defined as the

quotient of the difference in the specific growth rates of the reference co-culture system and the co-culture with plasmid bearing strains and the specific growth rate of the reference control system (Equation 8). All specific growth rates used to calculate the metabolic burdens are quantities given by OD600 data.

The total growth burden of the “good” co-cultures (category A) ranges from $m_B = 16.4 \pm 6.7\%$ to $m_B = -3.6 \pm 4.3\%$, with most combinatorial cultures showing a growth reduction of up to 10% compared to their wild-type reference co-cultures (Figure 23). In contrast, the metabolic burdens observed for the “bad” co-cultures (category B) ranged from $m_B = 46.6 \pm 3.7\%$ to $m_B = -15.0 \pm 5.3\%$. While positive percentages indicate a reduction in the overall growth rate of the co-culture system compared to the wild-type reference system, a negative percentage implies an increase in the overall growth and thus the fitness of the system. No direct correlation could be identified between the metabolic load and the combinations where the choice of plasmid bearing strains had a qualitative influence on the determination of the fitter competitor with respect to at least one of the two metrics of bacterial fitness (see 4.3.2.2). For example, the choice of plasmid bearing strains impacted the prediction of interspecies growth interactions in both combination 2, which has the smallest observed difference in metabolic burden between the good and bad combination, and combination 14, which displays the largest recorded difference in metabolic burdens.

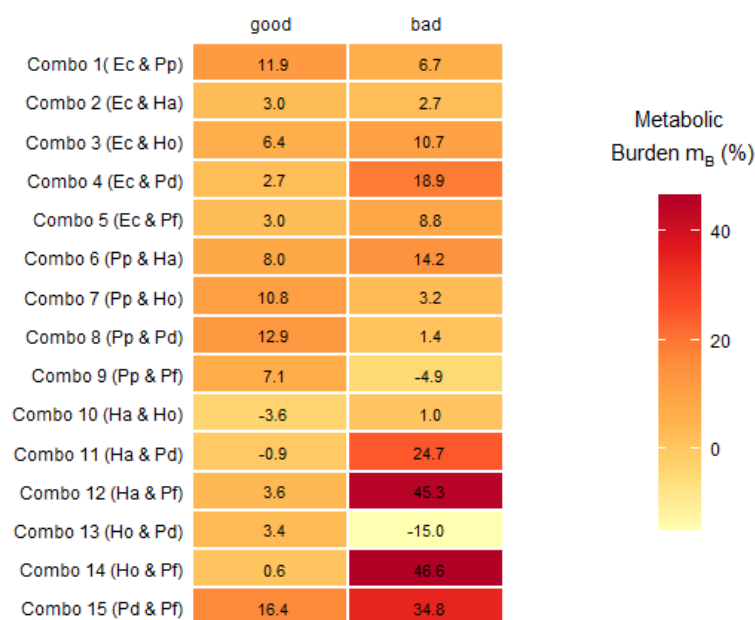


Figure 23: The metabolic burdens of the “bad” combinations show the greatest variance, yet no correlation can be inferred between the metabolic load and combinations where the outcome of competitive growth between species depended on the choice of plasmid bearing strains.

The highest m_B values, indicating the greatest reduction in overall growth of the co-culture system, are marked in red, while the negative percentages, shown in yellow, signify enhanced growth compared to the reference co-culture system. Tukey HSD tests were performed between the metabolic burdens of the “good” and “bad” combination for all fifteen co-culture combinations. All differences between pairs are statistically significant ($p < 0.001$).

4.3.2.4 Growth Interactions Derived from Growth Parameter Estimates

For the evaluation of the binary growth interactions between species of all combinatorial co-cultures, the growth parameters previously estimated from fluorescence measurements (see 4.3.2.1) were used. First, the fitter species of each combination was determined by comparing one of the three metrics of fitness μ_{fi} , K_{fi} and F_{max} of the two interacting strains at a time. The comparison showed that *P. putida* achieved the highest specific growth rate and carrying capacity in terms of measured maximum fluorescence F_{max} , implying the highest overall fitness (Table 5 and Table 7). When considering the second surrogate measure used to approximate the carrying capacity, the K_{fi} values derived from nonlinear regression analysis, *P. putida* only reached the higher carrying capacity with three out of the five other species (Table 6). Overall, in four of the fifteen combinations tested (combinations 1, 2, 5 and 7), the comparative assessment of the F_{max} and K_{fi} measures listed in Table 6 and Table 7 revealed a disparity in the species achieving the higher carrying capacity. It can therefore be concluded that the determination of the dominant species in terms of carrying capacity is biased by the proxy measure used. This tendency to bias is consistent with previous observations made when obtaining estimates from monoculture growth (see 4.2.2.2). Consequently, both approaches used to interpret the ecological carrying capacity should be evaluated with caution. The metric F_{max} , which interprets the carrying capacity as a measure of the maximum fluorescence, is arguably a better surrogate measure of this growth output than the metric K_{fi} , as the estimate is not subject to the uncertainties of nonlinear regression. It was also observed that the fitter organism in terms of specific growth rate was not consistent with the fitter species in terms of carrying capacity for a total of either four (maximum fluorescence value F_{max}) or six (nonlinear regression estimate K_{fi}) combinations.

Furthermore, the extent to which the growth of each species was affected by interactions during combinatorial cultivation was investigated. The fitness that each species retained was compared with its fitness in monoculture and quantified by the metric Ξ , which was defined as the growth output estimated from fluorescence during co-cultivation divided by the corresponding fluorescence estimate obtained during growth in monoculture. The Ξ values were calculated from all three measures of fitness – μ , K_{fi} and F_{max} – and are referred to as Ξ_{μ} , Ξ_K and Ξ_F , respectively (Equation 9, Equation 10 and Equation 11). Calculated Ξ values below 100 % indicate reduced or antagonized fitness and thus a negative impact on species growth. Conversely, Ξ values above 100 % imply a positive or beneficial effect on the species fitness through binary interactions. For a distinct positive or negative impact on bacterial fitness, a 5 % threshold must be exceeded, as defined in this thesis work (see 3.9.3). Therefore, Ξ values of 100 ± 5 % indicate a neutral impact on species fitness. Based on the observed effects on the fitness of both interaction partners in the combinatorial two-species co-cultures, the underlying nature of the interaction between the species was inferred, referred to here as bidirectional interactions. The types of interspecies interactions differentiated in this thesis are mutualism, commensalism, and antagonism. If both species benefit from the interaction, the relationship is considered mutualistic, whereas if the fitness of one species is impaired, the relationship is regarded as antagonistic. Analogous to fitness maintenance, a 5 % threshold had to be exceeded for a distinct

mutualistic or antagonistic interaction. In a commensal relationship, neither species is harmed and one or neither species benefits from combinatorial growth.

The analysis of all co-culture systems with $\mu_{fl} \approx \mu_{OD}$ (category A) showed that *E. coli* experienced the greatest growth benefit of all species in terms of specific growth rate when co-cultured with *H. oceanii* (combo 3), as signified by the highest Ξ_{μ} value ($\Xi_{\mu} = 162.31\%$) observed (Table 5). The bidirectional interactions derived from fitness maintenance Ξ_{μ} are shown in Table 5 and indicate that most binary interactions are antagonistic in nature, *i.e.*, at least one of the two partners is inhibited in its fitness by interactions. In the pairings *E. coli* and *H. aestusnigri* (combo 2) and *P. putida* and *P. deceptionensis* (combo 8), both interacting species benefit from their coexistence, as indicated by Ξ_{μ} values that are well above the 105 % threshold for a distinct mutualistic interaction. A commensal relationship was only observed in combination 11, where *H. aestusnigri* benefited from co-cultivation, while *P. deceptionensis* was not affected in its fitness.

The comparative analysis of the growth parameters K_{fl} and F_{max} , the fitness maintenance measures Ξ_K and Ξ_F as well as the underlying growth interactions has shown that the results are biased depending on the two different measures used as surrogates for the ecological carrying capacity. For seven of the fifteen co-cultures, highlighted in blue in Table 6 and Table 7, the interrogation of growth dynamics based on the parameters K_{fl} and F_{max} has yielded different results with respect to at least one of the measures examined. For combinations 2 and 11, the ascertained type of interaction is not consistent with both approaches used to derive the carrying capacity. For example, the interactions derived from both measures of carrying capacity indicate a mutualistic relationship between *P. deceptionensis* and *P. fluorescens* (combination 15), whereas a mutualistic relationship between *E. coli* and *H. aestusnigri* (combo 2) and *H. aestusnigri* and *P. deceptionensis* (combination 11) emerged only from the analysis of the carrying capacity estimated by the parameter K of the logistic growth model. Furthermore, the one-way beneficial, antagonistic, or neutral influences on each of two interacting species determined from the Ξ_K and Ξ_F values are not consistent with the two surrogate measures of the carrying capacity in a total of five combinations (combinations 1, 2, 10, 11 and 13). It can be concluded that the dynamics of population growth can be inferred from fluorescence measurements, which serve as proxy for species-specific biomass for estimating the two growth outputs examined in this thesis work—specific growth rate and carrying capacity. However, as with carrying capacity, the results may depend on which measures are used as proxies for ecological processes.

All strains belonging to the *Halopseudomonas* spp. were found to have low fitness relative to the others investigated in this study. This result was shown in both low specific growth rates (Figure 11 and Figure 12) and low carrying capacities (Figure 16), under the selected cultivation conditions when growing monocultures for strain characterization. In co-culture with *E. coli*, *H. oceanii* and *P. deceptionensis*, the species *H. aestusnigri* experienced a positive impact on its fitness in terms of specific growth rate, as indicated by Ξ_{μ} values $> 105\%$ (Table 5). In contrast, combinatorial growth with each of the five other species had a negative effect on the fitness of *H. oceanii* in terms of specific

growth rate and carrying capacity derived from maximum fluorescence measurements, as signified by Ξ_{μ} and Ξ_F values < 95 % (Table 5 and Table 7). In terms of the carrying capacity, as estimated by the parameter K , both *Halopseudomonas* spp. experienced a beneficial influence on their fitness when cultivated with *P. deceptionensis* (Table 6). In contrast, both *Halopseudomonas* spp. were antagonised in their growth to high population densities when considering the carrying capacity as interpreted by the maximum fluorescence observed (Table 7). The fitness maintenance of *H. oceani* during growth with *P. putida* (combination 7) shows about eight times better fitness compared to growth in monoculture ($\Xi_K = 845.84$ %, Table 6). However, it is reasonable to assume that the corresponding K_{fl} value is an artifact resulting from poor model fitting of the nonlinear regression model, given the trajectory of the fluorescence curves for combination 7 shown in Figure 20 and the reference Ξ_F value ($\Xi_F = 7.57$ %, Table 7). The occurrence of poor model fit and disproportionate K_{fl} estimates for *H. oceani* was already observed in the characterization of plasmid bearing strains in monoculture (see 4.2.2.2).

The result show that the fitness of a bacterial species can differ significantly in mono- and co-culture, indicating the influence of interactions between species on population dynamics. In summary, the potential of fluorescence as a tool for decoupling and inferring species-specific fitness in planktonic liquid co-cultures has been demonstrated and potential sources of error associated with the methodology used have been identified.

Table 5: Interrogation of population dynamics in terms of specific growth rate estimated from strain-specific fluorescence measurements shows that *P. putida* has the highest fitness among all species and that most bidirectional interactions between the species are antagonistic in nature.

The specific growth rate estimated from the fluorescence data (μ_{fi}) and the fitness maintenance with respect to the specific growth rate (Ξ_{μ}) were determined for each of the interacting species in all two-species co-cultures. In addition, the more fit species, *i.e.*, the species with the higher specific growth rate μ_{fi} , the one-way interactions, and the bidirectional interactions derived from the specific growth rates are displayed. (+) indicates that a species benefits from the cultivation with the respective partner, *i.e.*, it achieves a higher specific growth rate in co-culture than in monoculture characterized by Ξ_{μ} values > 105 %, (-) indicates a negative influence of combinatorial growth on the species fitness, *i.e.*, it achieves a higher specific growth rate in monoculture than in the co-culture, as implied by Ξ_{μ} values < 95 %. (0) indicates a neutral impact of the co-culture interaction on the fitness of a species, *i.e.*, the specific growth rate does not change significantly between growth in mono- and co-culture, as indicated by Ξ_{μ} values of 100 ± 5 %. Hence, for a distinct mutualistic or antagonistic interaction, the previously determined Ξ_{μ} values must be below or above a threshold value of 5 %.

	Species	Strains	μ_{fi} [h ⁻¹]	Ξ_{μ} [%]	Fitter Species	One-Way Interactions	Bidirectional Interactions
1	<i>E. coli</i>	<i>Ec</i> pCPcit	0.14	52.16	<i>P. putida</i>	- / +	Antagonism
	<i>P. putida</i>	<i>Pp</i> pCPcer	0.53	113.25			
2	<i>E. coli</i>	<i>Ec</i> pCPcit	0.36	138.68	<i>E. coli</i>	+ / +	Mutualism
	<i>H. aestusnigri</i>	<i>Ha</i> pCPcer	0.30	124.41			
3	<i>E. coli</i>	<i>Ec</i> pCPcit	0.43	162.31	<i>E. coli</i>	+ / -	Antagonism
	<i>H. oceani</i>	<i>Ho</i> pCPcer	0.35	87.53			
4	<i>E. coli</i>	<i>Ec</i> pCPkate	0.20	88.17	<i>P. deceptionensis</i>	- / +	Antagonism
	<i>P. deceptionensis</i>	<i>Pd</i> pCPeyfp	0.29	121.79			
5	<i>E. coli</i>	<i>Ec</i> pCPkate	0.13	58.44	<i>P. fluorescens</i>	- / -	Antagonism
	<i>P. fluorescens</i>	<i>Pf</i> pCPeyfp	0.25	62.24			
6	<i>P. putida</i>	<i>Pp</i> pCPgfp	0.64	116.34	<i>P. putida</i>	+ / -	Antagonism
	<i>H. aestusnigri</i>	<i>Ha</i> pCPcer	0.07	27.58			
7	<i>P. putida</i>	<i>Pp</i> pCPcer	0.59	124.56	<i>P. putida</i>	+ / -	Antagonism
	<i>H. oceani</i>	<i>Ho</i> pCPeyfp	0.10	21.24			
8	<i>P. putida</i>	<i>Pp</i> pCPcer	0.62	132.26	<i>P. putida</i>	+ / +	Mutualism
	<i>P. deceptionensis</i>	<i>Pd</i> pCPeyfp	0.36	152.53			
9	<i>P. putida</i>	<i>Pp</i> pCPcer	0.53	113.05	<i>P. putida</i>	+ / -	Antagonism
	<i>P. fluorescens</i>	<i>Pf</i> pCPeyfp	0.11	25.89			
10	<i>H. aestusnigri</i>	<i>Ha</i> pCPcer	0.29	119.67	<i>H. oceani</i>	+ / -	Antagonism
	<i>H. oceani</i>	<i>Ho</i> pCPeyfp	0.37	82.09			
11	<i>H. aestusnigri</i>	<i>Ha</i> pCPcer	0.26	107.62	<i>H. aestusnigri</i>	+ / 0	Commensalism
	<i>P. deceptionensis</i>	<i>Pd</i> pCPeyfp	0.25	104.79			
12	<i>H. aestusnigri</i>	<i>Ha</i> pCPcer	0.17	68.58	<i>P. fluorescens</i>	- / -	Antagonism
	<i>P. fluorescens</i>	<i>Pf</i> pCPeyfp	0.27	66.79			
13	<i>H. oceani</i>	<i>Ho</i> pCPcer	0.25	61.94	<i>H. oceani</i>	- / -	Antagonism
	<i>P. deceptionensis</i>	<i>Pd</i> pCPeyfp	0.19	81.82			
14	<i>H. oceani</i>	<i>Ho</i> pCPcer	0.13	33.32	<i>P. fluorescens</i>	- / -	Antagonism
	<i>P. fluorescens</i>	<i>Pf</i> pCPeyfp	0.32	79.47			
15	<i>P. deceptionensis</i>	<i>Pd</i> pCPeyfp	0.28	115.93	/	+ / -	Antagonism
	<i>P. fluorescens</i>	<i>Pf</i> pCPkate	0.28	81.58			

Table 6: Decoupling and inferring growth dynamics in terms of carrying capacity, interpreted by the parameter K of a logistic growth model, shows that most interactions between species are antagonistic. The results suggest that *H. oceani* achieves the higher carrying capacity in co-culture with four of the five other species. However, this is questionable because of the very high Ξ_k values, which are more indicative of uncertainties in the model fitting.

The carrying capacity estimated from fluorescence data (K_{fl}) and the fitness maintenance (Ξ_k) in terms of the parameter K extrapolated from the logistic growth model were determined for each of the interacting species in all binary co-cultures. In addition, the more fit species, *i.e.*, the dominant species with the higher K_{fl} value, the one-way interactions, and the bidirectional interactions derived from the carrying capacity are displayed. (+) indicates that a species benefits from cultivation with the respective partner, *i.e.*, it achieves a higher carrying capacity in co-culture than in monoculture signified by Ξ_k values > 105 %, (-) indicates a negative influence of combinatorial growth on the species fitness, *i.e.*, it achieves a higher carrying capacity in monoculture than in co-culture, as implied by Ξ_k values < 95 %. (0) indicates a neutral impact of the co-culture interaction on the fitness of a species, *i.e.*, the carrying capacity does not change significantly between growth in mono- and co-culture, as implied by Ξ_k values of 100 ± 5 %. Hence, for a distinct mutualistic or antagonistic interaction, the previously determined Ξ_k values must be below or above a threshold value of 5 %. The blue colored rows mark the combinations where decoupling of growth dynamics and inference of interactions based on the two different measures of carrying capacity yielded different results.

	Species	Strains	K_{fl} [RFU]	Ξ_k [%]	Fitter Species	One-Way Interactions	Bidirectional Interactions
1	<i>E. coli</i>	<i>Ec</i> pCPcit	15401	211.83	<i>E. coli</i>	+ / -	Antagonism
	<i>P. putida</i>	<i>Pp</i> pCPcer	13891	68.41			
2	<i>E. coli</i>	<i>Ec</i> pCPcit	9665	132.93	<i>E. coli</i>	+ / +	Mutualism
	<i>H. aestusnigri</i>	<i>Ha</i> pCPcer	6388	130.75			
3	<i>E. coli</i>	<i>Ec</i> pCPcit	3698	50.86	<i>H. oceani</i>	- / -	Antagonism
	<i>H. oceani</i>	<i>Ho</i> pCPcer	9731	90.76			
4	<i>E. coli</i>	<i>Ec</i> pCPkate	3484	37.84	<i>P. deceptionensis</i>	- / -	Antagonism
	<i>P. deceptionensis</i>	<i>Pd</i> pCPeyfp	3931	68.49			
5	<i>E. coli</i>	<i>Ec</i> pCPkate	7354	79.87	<i>E. coli</i>	- / -	Antagonism
	<i>P. fluorescens</i>	<i>Pf</i> pCPeyfp	5867	31.48			
6	<i>P. putida</i>	<i>Pp</i> pCPgfp	47624	169.00	<i>P. putida</i>	+ / -	Antagonism
	<i>H. aestusnigri</i>	<i>Ha</i> pCPcer	2511	51.39			
7	<i>P. putida</i>	<i>Pp</i> pCPcer	16657	82.04	<i>H. oceani</i>	- / -	Antagonism
	<i>H. oceani</i>	<i>Ho</i> pCPeyfp	43207	845.84			
8	<i>P. putida</i>	<i>Pp</i> pCPcer	17820	87.76	<i>P. putida</i>	- / -	Antagonism
	<i>P. deceptionensis</i>	<i>Pd</i> pCPeyfp	1946	33.91			
9	<i>P. putida</i>	<i>Pp</i> pCPcer	28524	140.48	<i>P. putida</i>	+ / -	Antagonism
	<i>P. fluorescens</i>	<i>Pf</i> pCPeyfp	3820	20.50			
10	<i>H. aestusnigri</i>	<i>Ha</i> pCPcer	4820	98.65	<i>H. aestusnigri</i>	0 / -	Antagonism
	<i>H. oceani</i>	<i>Ho</i> pCPeyfp	1879	36.78			
11	<i>H. aestusnigri</i>	<i>Ha</i> pCPcer	5828	119.29	<i>P. deceptionensis</i>	+ / +	Mutualism
	<i>P. deceptionensis</i>	<i>Pd</i> pCPeyfp	7921	138.01			
12	<i>H. aestusnigri</i>	<i>Ha</i> pCPcer	4614	94.44	<i>P. fluorescens</i>	- / -	Antagonism
	<i>P. fluorescens</i>	<i>Pf</i> pCPeyfp	7062	37.90			
13	<i>H. oceani</i>	<i>Ho</i> pCPcer	11380	106.14	<i>H. oceani</i>	+ / -	Antagonism
	<i>P. deceptionensis</i>	<i>Pd</i> pCPeyfp	4941	86.09			
14	<i>H. oceani</i>	<i>Ho</i> pCPcer	9256	86.33	<i>P. fluorescens</i>	- / -	Antagonism
	<i>P. fluorescens</i>	<i>Pf</i> pCPeyfp	9630	51.68			
15	<i>P. deceptionensis</i>	<i>Pd</i> pCPeyfp	12175	212.13	<i>P. fluorescens</i>	+ / +	Mutualism
	<i>P. fluorescens</i>	<i>Pf</i> pCPkate	13229	141.12			

Table 7: Decoupling and inferring of growth dynamics in terms of carrying capacity, interpreted as the maximum fluorescence measured during cultivation, indicates that most interactions between species are antagonistic. Furthermore, it shows that the decoupling of growth dynamics is biased depending on the approach used to interpret the ecological carrying capacity.

The carrying capacity estimated from fluorescence data (F_{max}) and the fitness maintenance (Ξ_F) with respect to the maximum fluorescence value measured during growth were determined for each of the interacting species in all binary co-cultures. The more fit species, *i.e.*, the dominant species with the higher F_{max} value, the one-way interactions, and the bidirectional interactions deduced from the carrying capacity are also displayed. (+) indicates that a species benefits from cultivation with the respective partner, *i.e.*, it achieves a higher carrying capacity in co-culture than in monoculture, which is signified by Ξ_F values > 105 %, (-) indicates a negative influence of combinatorial growth on the species fitness, *i.e.*, it achieves a higher carrying capacity in monoculture than in co-culture, as implied by Ξ_F values < 95 %. (0) indicates a neutral impact of the co-culture interaction on the fitness of a species, *i.e.*, the carrying capacity does not change significantly between growth in mono- and co-culture, as indicated by Ξ_F values of 100 ± 5 %. For a distinct mutualistic or antagonistic interaction, the previously determined Ξ_F values must therefore be below or above a threshold value of 5 %. The blue colored rows mark the combinations where decoupling of growth dynamics and inference of interactions based on the two different measures of carrying capacity gave different results.

	Species	Strains	F_{max} [RFU]	Ξ_F [%]	Fitter Species	One-Way Interactions	Bidirectional Interactions
1	<i>E. coli</i>	<i>Ec</i> pCPcit	1239	16.14	<i>P. putida</i>	- / -	Antagonism
	<i>P. putida</i>	<i>Pp</i> pCPcer	14251	68.21			
2	<i>E. coli</i>	<i>Ec</i> pCPcit	5281	66.56	<i>H. aestusnigri</i>	- / +	Antagonism
	<i>H. aestusnigri</i>	<i>Ha</i> pCPcer	6648	105.41			
3	<i>E. coli</i>	<i>Ec</i> pCPcit	4139	59.68	<i>H. oceani</i>	- / -	Antagonism
	<i>H. oceani</i>	<i>Ho</i> pCPcer	7932	76.77			
4	<i>E. coli</i>	<i>Ec</i> pCPkate	3380	35.38	<i>P. deceptionensis</i>	- / -	Antagonism
	<i>P. deceptionensis</i>	<i>Pd</i> pCPeyfp	4056	92.79			
5	<i>E. coli</i>	<i>Ec</i> pCPkate	4050	42.38	<i>P. fluorescens</i>	- / -	Antagonism
	<i>P. fluorescens</i>	<i>Pf</i> pCPeyfp	5605	30.12			
6	<i>P. putida</i>	<i>Pp</i> pCPgfp	50481	165.80	<i>P. putida</i>	+ / -	Antagonism
	<i>H. aestusnigri</i>	<i>Ha</i> pCPcer	2609	41.36			
7	<i>P. putida</i>	<i>Pp</i> pCPcer	16587	79.39	<i>P. putida</i>	- / -	Antagonism
	<i>H. oceani</i>	<i>Ho</i> pCPeyfp	369	7.57			
8	<i>P. putida</i>	<i>Pp</i> pCPcer	17258	82.60	<i>P. putida</i>	- / -	Antagonism
	<i>P. deceptionensis</i>	<i>Pd</i> pCPeyfp	1964	44.93			
9	<i>P. putida</i>	<i>Pp</i> pCPcer	24071	115.21	<i>P. putida</i>	+ / -	Antagonism
	<i>P. fluorescens</i>	<i>Pf</i> pCPeyfp	3782	20.33			
10	<i>H. aestusnigri</i>	<i>Ha</i> pCPcer	5236	83.02	<i>H. aestusnigri</i>	- / -	Antagonism
	<i>H. oceani</i>	<i>Ho</i> pCPeyfp	1581	32.40			
11	<i>H. aestusnigri</i>	<i>Ha</i> pCPcer	5055	80.16	<i>P. deceptionensis</i>	- / +	Antagonism
	<i>P. deceptionensis</i>	<i>Pd</i> pCPeyfp	6698	153.25			
12	<i>H. aestusnigri</i>	<i>Ha</i> pCPcer	4074	64.60	<i>P. fluorescens</i>	- / -	Antagonism
	<i>P. fluorescens</i>	<i>Pf</i> pCPeyfp	5931	31.87			
13	<i>H. oceani</i>	<i>Ho</i> pCPcer	6950	67.26	<i>H. oceani</i>	- / +	Antagonism
	<i>P. deceptionensis</i>	<i>Pd</i> pCPeyfp	5004	116.88			
14	<i>H. oceani</i>	<i>Ho</i> pCPcer	5224	50.55	<i>P. fluorescens</i>	- / -	Antagonism
	<i>P. fluorescens</i>	<i>Pf</i> pCPeyfp	6909	37.13			
15	<i>P. deceptionensis</i>	<i>Pd</i> pCPeyfp	6947	158.95	<i>P. fluorescens</i>	+ / +	Mutualism
	<i>P. fluorescens</i>	<i>Pf</i> pCPkate	12326	139.09			

5 Discussion

In this thesis work, a combinatorial toolkit based on practical synthetic biology tools was established to assess population dynamics in microbial populations and co-cultures in a relative high throughput manner. This was accomplished by constructing broad-host-range fluorescent reporter plasmids in the BASIC environment which were then evaluated across well-established and non-traditional bacterial hosts. The aim was to build a tractable tool and model system for investigating both microbial ecology and biotechnology applications for screening design spaces associated with synthetic microbial co-cultures. The tools and methods developed here were built for scalability and reproducibility and can be readily adopted by other researchers.

Microbial communities are ubiquitous to essentially all known ecosystems on Earth, ranging from marine and sedimentary environments to the human gut and skin surface. They are driven by complex functions and dynamic interactions that govern natural processes such as biogeochemical cycling of nutrients, climate regulation and decomposition of organic matter. The study of natural and synthetic microbial communities aims to improve the understanding of community dynamics and interspecies interactions (De Roy et al., 2014; Fredrickson, 2015). This will allow microbial consortia to be controlled and selectively engineered in the laboratory to promote applications that benefit environmental sustainability, bioproduction, or human health (Lindemann et al., 2016; H.-S. Song et al., 2019). To harness the metabolic potential of microbial communities for new applications that address contemporary needs is therefore a major challenge for modern biotechnology but the lack of tools for observing growth and inferring microbial interactions in multispecies assemblages shows the need to develop standardized methodologies.

It has been successfully demonstrated that the synthetic biology platform constructed in this thesis can be used to observe and interrogate population dynamics in bacterial co-cultures (see 4.3.2.1). An important caveat to this result is that the use of this toolkit entails several opportunities and challenges associated with the experimental design and trade-offs between the accuracy of measurements and scalability. For example, this toolkit reports data that can be used to decouple population dynamics such as strain-specific fitness based on fluorescent reporter proteins and optical density, which are not direct measures of growth, *i.e.*, change in biomass density over time. Yet, the key advantage of these proxy measurements over direct measures of biomass is scalability into 96-well plate platforms, which can eventually be automated. This thesis work is therefore intended to contribute to the development of standardizable and reproducible tools for laboratory screenings and investigations of growth dynamics and interspecies interactions associated with synthetic bacterial populations and co-cultures to advance research in scientific fields related to microbial communities.

5.1 Synthetic Microbial Communities as a Platform for Biotechnology

Natural microbial communities are complex assemblages characterized by compositional and functional heterogeneity over time and space. This makes the reproducible interrogation of community activities, the development of generalizable biological principles defining the functioning of consortia, and the testing of ecological theories highly challenging, if not impossible (Zengler et al., 2019). A popular tool used by the scientific community to address these challenges is the use of model microbial ecosystems and consortia, such as fabricated microbial ecosystems termed EcoFABs (Zengler et al., 2019). The advantage of well-defined model systems and organisms that provide platforms for standardizable and reproducible studies has already been demonstrated in the past and will clearly help to advance research related to microbial communities (Bernstein, 2019). The toolkit developed as part of this thesis can be used as a platform for inferring interspecies interactions from ecologically important measures of bacterial fitness – specific growth rate and carrying capacity, in defined laboratory environments, which was successfully demonstrated by the example of fifteen binary co-cultures (Table 5, Table 6 and Table 7). Equipped with the potential to also monitor species-specific growth and thus interactions between species in co-cultures of more than two bacterial populations – which will be discussed in more detail in Chapter 5.6 – it is suitable as a scalable system of model co-cultures for studying microbial interactions.

The increasing interest in engineered microbial communities as bioprocess platforms capable of performing functions beyond traditional monocultures (Bernstein et al., 2012; Lindemann et al., 2016) further reinforces the relevance of such tools for a variety of applications. The toolkit currently comprises a core of six bacterial species, two of which are model organisms, *i.e.*, *E. coli* DH5 α and *P. putida* KT2440, and three non-traditional marine host, *i.e.*, *H. aestusnigri* VGOX14, *H. oceani* KX20, and *P. deceptionensis* M1, which have recently been introduced as novel chassis in the field of synthetic biology (Chan et al., 2023). Members of the *Pseudomonas* and *Halopseudomonas* genus are generally known for their robustness and tremendous metabolic potential (Bitzenhofer et al., 2021; Bollinger et al., 2018). Complemented by the valuable innate phenotypes of the species listed in this toolkit, which include psychrotolerance, salinity tolerance, and polyethylene terephthalate (PET) degradation (Chan et al., 2023), they represent attractive hosts for biotechnological applications, suggesting the potential of this toolkit as a bioprocess platform. This potential is further characterized by its capacity to be used to observe the growth dynamics of individual synthetic bacterial populations and combinatorial co-cultures, and to infer the interactions between them. Both are essential prerequisites for the successful engineering of synthetic co-cultures for controllable outputs (Lawson et al., 2019; Lindemann et al., 2016).

Co-cultures are a widely used tool for ecologists and synthetic biologist to study natural, synthetic, or artificially designed interactions (Bernstein et al., 2012; Goers et al., 2014). Species interactions can significantly affect the stability and productivity of co-cultures and are therefore an important factor in their design, manipulation, and management. The growth dynamics of a species can be positively or

negatively influenced by interactions with another species, depending on the nature of relationship, which can affect the stability and desired output of the respective co-culture system (Kehe et al., 2021). Co-cultivation experiments of all binary combinations based on the six species included in this toolkit have shown that the low fitness of both *Halopseudomonas* spp. relative to the fitness of the other species, as given by both low specific growth rates (Figure 11 and Figure 12) and low carrying capacities (Figure 16), consistent with observations reported by Chan et al., (2023), can be both increased or decreased depending on which species it is partnered with. For instance, the fitness of *H. aestusnigri*, which shows the distinct phenotype of PET degradation, was almost 25 % higher in combination with *E. coli* than in monoculture, while a reduction in fitness of more than 70 % was observed when grown with *P. putida* (Table 5). Consequently, it can be suggested that co-cultures may be considered in design strategies for the development and use of *H. aestusnigri* as a microbial chassis for biotechnological applications. The growth promoting interactions observed during the interrogation of co-culture growth dynamics could be explained by different mechanisms. One likely explanation could be based on the concept of cross-feeding, an interaction in which metabolites or by-products from one species can be utilized and further metabolized by another species, creating a new niche that can be exploited for enhanced growth of the benefitting species (D'Souza et al., 2018; Pacheco et al., 2019). The investigation of model co-cultures has shown that the toolkit and methodology developed in this work provide a practical way to infer one-way and bidirectional interactions between species from measures of bacterial fitness. Nevertheless, it may be useful to randomly validate some co-cultures before using these tools to verify that the interactions derived from fluorescence measurements are correct. This could be accomplished by quantifying the species-specific biomasses at different time points using quantitative PCR (qPCR).

The interrogation of population dynamics with this combinatorial toolkit, consisting of 36 distinct plasmid bearing strains belonging to six bacterial species (Table 2) and their respective wild-type counterparts has, however, revealed a major caveat: The choice of tools, *i.e.*, reporter plasmids, used for fluorescent labelling of bacterial species has a significant impact on the estimation of growth parameters that have been used as measures for determining bacterial fitness and inferring interspecies interactions. As shown in Chapter 4.3.2.2, an experiment designed to investigate for this possibility showed that this could be observed in 60 % of the co-cultures studied. To circumvent this shortcoming of the methodology developed in this thesis when using or customizing this toolkit for alternative applications, it is important to select plasmid bearing strains for co-cultivation with estimated specific growth rates determined from OD600 and strain-specific fluorescence in monoculture growth that differ as little as possible. If used in this way this toolkit can serve as an important building block to advance the understanding, use, and control of multispecies designs, *e.g.*, as a platform for biotechnological applications.

5.2 Balancing Practicality and Uncertainty

Monitoring monoculture growth dynamics of bacterial populations in a high throughput manner is usually accomplished by measuring the change in optical density of a liquid cell culture over time. Optical density measurement owes its widespread use to its many advantages, *e.g.*, simplicity, cost-effectiveness, suitability for high throughput and automation, coupled with acceptable trade-offs in the accuracy of the measurements for many applications (Beal et al., 2020; Stevenson et al., 2016; Worthan et al., 2023). The operational suitability of methods therefore depends on their practicality and inherent uncertainties, and their development faces the challenge of a deliberate balancing of possibilities and tolerable challenges. The genetic tools and methodology developed in this thesis can be used to monitor species-specific biomass and infer population dynamics in a relatively high throughput manner offering comparable advantages and ease of use to optical density measurements.

The quantitative assessment of species-specific biomass in liquid co-cultures (being the critical limitation of optical density measurements) and scalability were two key criteria in selecting the measurement method. Fluorescence spectroscopy fulfils these two requirements and further allows – analogous to optical density – for static and time-course measurements in an automated, low-cost and high throughput manner, hence fulfilling many of the requirements for platforms in the synthetic biology pipeline, *e.g.*, for screening larger design spaces associated with synthetic co-cultures, outlined by Goers et al., (2014). The use of fluorescent reporter proteins therefore compares favourably to other methods used to quantify species-specific biomass in co-cultures, such as qPCR (Cotto et al., 2015; Junicke et al., 2014) and flow cytometry (Ogundero et al., 2022; Wallner et al., 1993), which can be more time- and labour-intensive, not readily suited for automated time-course measurements, or difficult to scale. In addition, these methods also suffer from measurement inaccuracies, *e.g.*, the error-prone conversion of gene copy number to biomass concentration in qPCR approaches (Junicke et al., 2014).

Despite its advantages, the use of fluorescence as a proxy measure for biomass comes with some challenges that must be tolerated in trade-off for the desired benefits. First, bacterial cells must be fluorescently labelled. This challenge was approached by transforming the bacteria with broad-host-range plasmids that constitutively express fluorescent reporter proteins (see 4.1), which are required to monitor species-specific biomass through fluorescence measurements. Alternatively, the fluorescent markers could have been integrated into the bacterial genome by chromosomal insertion (Schlechter et al., 2018). However, the use of plasmid vectors is more flexible and better suited for high-level protein expression, *e.g.*, by tuning promoter strength, RBS strength, or plasmid copy number (Ou et al., 2018; Schuster & Reisch, 2021; Tauer et al., 2014). The tools developed in this work therefore help to interrogate bacterial fitness as a response variable to culture conditions, interactions with other species, and the genetic device, as cells must express the plasmid-encoded genes to output their fitness. To quantify the effect of the reporter plasmids on the fitness of their recipients, both the specific growth rates determined from OD600 measurements (Figure 9 - Figure 14), and the K_{OD} and

OD_{max} values (Figure 15), which served as surrogate measures of carrying capacity, were compared between plasmid bearing strains and their wild-type counterparts. As expected, the reporter plasmids caused the species to output differential fitness, manifested in changes in specific growth rates and carrying capacities, and additionally quantified as metabolic burden based on the influence of the genetic devices on the specific growth rate of a species (Figure 17). However, no correlation between the metabolic burden imposed by a plasmid on a species and its suitability to assess that species growth performance was observed. For instance, strain characterization revealed that both the pCPeyfp and pCPcit plasmids are well suited to assess the growth of *P. fluorescens*, as indicated by statistically non-significant differences in the specific growth rates estimated from OD600 and fluorescence (Table 3). While the pCPcit plasmid caused an overall fitness reduction of approximately 23 % in *P. fluorescens*, the pCPeyfp plasmid caused the overall fitness of the same species to increase by around 17 % (Figure 17).

One of the biggest trade-offs in using fluorescence as a proxy measurement for species-specific biomass is that it is not a direct measure of population density. This means that this tool does not measure growth, *i.e.*, the changing biomass density over time, but the change in fluorescence emission intensity, which is proportional to the number of fluorophores present. The accuracy of the measurement therefore depends on the relationship between biomass and fluorescence. In this study, a first order growth model describing exponential growth (Equation 4) was used to model growth from optical density and fluorescence traces to estimate the specific growth rate. Further, a logistic growth model (Equation 6) was fitted to the same experimental data to extrapolate the parameter K as surrogate measure for the carrying capacity, which functionally accounts for the maximum amount of biomass the environment can hold. A third measure of fitness, where carrying capacity is interpreted as the maximum optical density or fluorescence observed with the plate reader, was used for comparative assessments of both proxy measurements of carrying capacity. Thus, the specific growth rate was measured as change in optical density or fluorescence over time, which is not directly equivalent to growth, and carrying capacity was estimated as maximum optical density and fluorescence, both measured and extrapolated from a logistic growth model in units of OD600 and RFU, as a surrogate metric for maximum biomass.

It was quantitatively shown that fluorescence is not generally proportional to biomass, by comparing the specific growth rate of strains estimated from optical density and fluorescence measurements. This was particularly evident in occasionally strong diverging estimates of specific growth rate obtained from OD600 and fluorescence of the same strain, suggesting that the rate of increase in fluorescent proteins over time does not correlate with the rate of increase in biomass (Figure 9 - Figure 14). It was further observed that the accuracy of fluorescence as a proxy for biomass depends on the combination of the reporter protein and species used (see 4.2.2.1). Thus, by using fluorescence emission intensity as a proxy to monitor growth the simplifying assumption is made that biomass and fluorescence are proportional, consequently introducing uncertainty to estimates of the growth parameter μ calculated from fluorescence curve data. The accuracy of measurement can be improved by reducing this

uncertainty factor, which applies when the difference between the specific growth rate μ_{OD} (estimated from optical density) and the specific growth rate μ_{fl} (estimated from the fluorescence) of a plasmid bearing strain is statistically non-significant, or at least as small as possible. This is particularly important to consider when planning experiments with co-cultures, as the interrogation of growth dynamics can result in incorrect conclusions on interspecies interactions, as has been observed with some of the tested co-cultures (see 4.3.2.2). The best plasmid-species combination must be experimentally determined for each species in monoculture under the intended experimental conditions, which adds an extra characterization step to the experimental design but is only required once for each species. From another perspective, the strain-specific growth parameters are also needed to infer interspecies interactions in co-cultures from changes in their growth behaviour (see 3.9.3 and 4.3.2.4).

While fluorescence curve data can be used to quantitatively estimate the specific growth rate μ , it is not possible to derive valid quantitative estimates for the carrying capacity. The specific growth rate is a rate constant that indicates the increase of biomass per unit time relative to the initial biomass. Any response variable, *e.g.*, optical density or fluorescence, that is considered to be proportional to biomass can thus, in theory, be assumed to experience an identical increase per unit time. With both approaches, *i.e.*, the extrapolation of the parameter K from a logistic growth model and determination of the highest fluorescence value measured, used to estimate the carrying capacity from fluorescence curve data in this work, the carrying capacity is given as a fluorescence emission intensity in units of RFU, but not biomass, and can therefore not be quantitatively related to the actual ecological carrying capacity. However, the comparison of the relative relationship of K_{OD} and K_{fl} , and OD_{max} and F_{max} estimates showed that both approaches can be used as a tool to assess the qualitative relationship between the carrying capacities of species (see 4.2.2.2), which is advantageous for the investigation of population dynamics in ecological settings and the observation of synthetic co-cultures. If a quantitatively valid estimate of carrying capacity is required, the workflow could be extended by an additional analytical step including a measurement of total cell number at the end of co-culture growth, *e.g.*, using flow cytometry, but at the expense of scalability, time, and workload. Flow cytometry is a common method that is often used in combination with dyes or fluorescent probes to quantify individual bacterial species in mixed cultures (Midani & David, 2022; Ogundero et al., 2022; Wallner et al., 1993), but can also be used for the quantification of fluorescent protein-expressing cells (Duncan et al., 2018), such as the plasmid bearing strains from this toolkit.

Another uncertainty factor in the methodology is introduced by fitting the logistic growth model (Equation 6) to experimental OD600 and fluorescence curve data to extrapolate the parameter K as surrogate measure for the carrying capacity. As the growth model is fitted to optical density and fluorescence measurements, K estimates represent maximum measures of OD600 (K_{OD}) and fluorescence (K_{fl}). To assess the accuracy of model fits and derived K estimates, a different measure of fitness was used, where carrying capacity is interpreted as maximum optical density (OD_{max}) or fluorescence (F_{max}) measured with the plate reader. The comparison of the two surrogate measures

estimated from fluorescence measurements (K_{fl} and F_{max}) during cultivation of mono- and co-cultures occasionally revealed inconsistencies in the similarity of their values (Figure 16 and Figure 20). Furthermore, the decoupling of bacterial population growth dynamics in co-cultures was found to be biased depending on which surrogate measure is used to interpret the carrying capacity (see 4.3.2.4), indicating uncertainty and some degree of error associated with the nonlinear regression of the logistic growth model to the experimental data. This was more frequently observed for *H. oceanii* compared to the other species. This could indicate that the uncertainty associated with this approach may vary between species, especially if their growth traces differ significantly from the standard growth curve, such as the growth trajectory of *H. oceanii*, which is characterized by diauxic growth. In general, this observed uncertainty can likely be ascribed to poor model fitting (Archontoulis & Miguez, 2015). For the methodology to remain compatible with high throughput and automation, the logistic growth model must be fitted across large datasets using one set of initial starting values. The simplest and most scalable way to implement this comes at the expense of the accuracy of the model fitting and parameter K estimates. Moreover, the partially large observed standard deviations (Figure 16 and Figure 20) can be another indicator of poor model fitting (Archontoulis & Miguez, 2015). One way to reduce the uncertainty caused by nonlinear regression could be to exclude artifacts that represent values outside a meaningful range. This could be accomplished by introducing thresholds in the data processing pipeline that counter-select for these replicates and exclude them from further analysis. On the other hand, it would be simpler and conceivable to dispense with the logistic growth model approach and simply use the maximum measured response value of the plate reader as a surrogate measure for the carrying capacity, thereby completely avoiding the uncertainty associated with nonlinear regression analysis. The estimation of species-specific growth parameters during combinatorial growth has further revealed that outliers can have a noteworthy influence on the F_{max} estimates (see 4.3.2.1). To obtain more accurate F_{max} values, thresholds could be used in the data processing pipeline to exclude outliers, *e.g.*, replicates with maximum measured response value exceeding a specific threshold value. An additional uncertainty factor in the estimation of the carrying capacity could result from the varying fluorescence emission intensities at the beginning of the growth experiments, which can be seen from some fluorescence curves in Figure 20. These, like the fitting of growth models across large datasets, must be accepted without individual optimization in relatively high throughput approaches.

Another important factor to consider in experimental design is the impact of batch effects on reproducibility (Figure 8). One way to keep the reproducibility of results within and between laboratories as high as possible could be to set a fixed number of replicates to be included in the data analysis, *e.g.*, two experimental replicates with seven biological replicates each. This would increase the total number of replicates required and double the number of experiments to be performed. Considering the simplicity and cost-effectiveness of the workflow, the possibility to grow many cultures in parallel in 96-well plates, and the computational scalability of data processing, analysis, and determination of growth parameters, it would be feasible to increase the number of biological and

experimental replicates depending on the application. In general, the use of biological replicates is strongly recommended to improve the validity and reliability of the experimental results.

Overall, there are several factors that should be considered in the experimental design, such as the use of proxy measures for species-specific biomass and derived growth parameters, uncertainties associated with inverse modelling of growth, the influence of batch effects on reproducibility, and the correct choice of fluorescent reporter tools for each species. However, they are all tolerated in a 96-well approach due to their advantageous properties that allow inferences to be made about ecologically relevant growth parameters and interactions between species in a practical, cost-effective, scalable, and high throughput manner.

5.3 Advancing Broad-Host-Range Synthetic Biology

Broad-host-range synthetic biology is an emerging field in synthetic biology that aims to expand the range of microbial hosts for biodesign applications by developing engineered device circuits that are functional across a broad range of host organisms. While the number of well characterized modular genetic bioparts such as promoters and reporter proteins, as well as the functional complexity of programmed biological behaviors, is rapidly increasing, advances in synthetic biology are largely limited to the use of a small group of common model organisms (Chan et al., 2023). These traditional hosts can have limited metabolic potentials, are often not adapted to the environments relevant for synthetic biology applications and are therefore often not suitable as an optimal chassis for genetic circuits (Khan et al., 2020). Exploring new chassis beyond the traditional hosts of synthetic biology for engineered circuits will allow the leveraging of the natural phenotypic diversity and the unique characteristics and metabolic capabilities of microorganisms, thereby promoting new biotechnological applications, such as event detection within diverse environments (Khan et al., 2020), the biomanufacturing of unusual fatty acids (K. Wang et al., 2022) and the production of natural products (Gao et al., 2021). With the toolkit developed in this work, a set of six broad-host-range reporter plasmids with different fluorescent outputs are provided for the use in a wide range of potential host organisms considered non-traditional bacterial hosts.

One of the major challenges of broad-host-range synthetic biology is the chassis-effect, which describes the influence of a chassis on the performance of an engineered device circuit (Chan et al., 2023). In this study, chassis-effects on the performance of all six broad-host-range genetic tools were identified in most of the six different bacterial hosts (Figure 18). Moreover, differences in the performance levels of the genetic tools were observed during the characterization of all plasmid bearing strains, indicated through different specific growth rates (Figure 9 - Figure 14) and carrying capacities (Figure 16) derived from fluorescence measurements. This suggests that the fluorescent output of the genetic tools depends significantly on the host in which they are operating in. Thus, the

chassis-effect is an important factor to consider when designing broad-host-range toolkits such as this one.

The success of an engineered device within a microbial chassis can be influenced by several factors coupled to different physiological metrics such as growth rate, gene copy number and codon usage bias, which can be used to study the functional phenotype of expression plasmids within a chassis (Chan et al., 2023). Here, metabolic burden was used to quantify the chassis-effect (Chan et al., 2023), which was calculated from the specific growth rates of plasmid bearing and corresponding wild-type strains. The overall fitness of most plasmid bearing strains in this toolkit was reduced by up to 20 % upon transformation, in some cases even more (Figure 17). This can be explained by the redistribution of cellular resources for plasmid propagation and expression of recombinant proteins that would otherwise be allocated to growth (G. Wu et al., 2016). In contrast, an increase in overall fitness was observed for some plasmid bearing strains, particularly of the species *H. oceanii*, compared to their wild-type counterparts (Figure 17). Interestingly, such an increase in growth rate and thus overall fitness of *H. oceanii* was also observed in the study of Chan et al., (2023) after the bacterium had been transformed with a genetic toggle switch built onto a pSEVA231-derived vector. Furthermore, that study reported that *P. deceptionensis* and *P. fluorescens* carrying the same plasmid experienced the most severe growth reduction (Chan et al., 2023), which is partly consistent with the results of this study. In this work, the most severe metabolic burden was also observed in strains belonging to these two species, with exception of *Pd* pCPkate and *Pf* pCPcer, which showed a distinct increase in growth of more than 10 % compared to their wild-type controls (Figure 17E and F). This could indicate a potentially interesting pattern with respect to broad-host-range synthetic biology, where *P. deceptionensis* and *P. fluorescens* tend to experience comparatively strong metabolic burdens upon transformation, while *H. aestusnigri* and *H. oceanii* are only marginally impaired or even enhanced in their overall fitness, corresponding to a lower or higher performance level of the broad-host-range genetic tools, as measured by fluorescence. These observed differences in the metabolic burden displayed by different hosts in response to the same plasmid could be explained by the plasmid copy number. It is known that plasmid copy number affects host growth - in general, maintaining a higher number of plasmids requires more cellular resources, which places a greater metabolic burden on the host cell, which can lead to a reduction in growth (Rouches et al., 2022). Since plasmid copy number is subject to the chassis-effect (Chan et al., 2023), this could be one possible reason why identical plasmids have different effects on the growth of different host organisms.

5.4 Measures of Ecological Fitness

The tools and methods developed in this work aim to interrogate population dynamics with respect to fitness in relation to two ecologically important growth outputs, the specific growth rate and carrying capacity. The importance of these two growth phenotypes is based on the ecological concept of r- and

K-selection, which was initially defined for macroorganisms (MacArthur & Wilson, 1967), but also applies to bacteria and microbial communities (Andrews & Harris, 1986). It postulates two life strategies for organisms to maximize their fitness for survival, based on rapid growth and competitive superiority. This theory of r- and K-selection is based on the logistic differential equation (Equation 6) provided by Alfred J. Lotka (Lotka, 1925, 1956), where N is the population size, the parameter μ describes the specific growth rate, *i.e.*, r , and the parameter K describes the carrying capacity, *i.e.*, K (Green, 1980). Opportunistic r-strategists, also referred to as generalists, are characterized by fast growth, *i.e.*, high specific growth rates, and can react quickly and use resources as they become available. In contrast, K-strategists, also considered as specialists, grow slowly and have high substrate affinity as well as substrate utilization efficiency, which gives them a competitive advantage in crowded and resource-limited environments and enables them to reach high carrying capacities. Therefore, K-strategists outcompete r-strategists in nutrient limited conditions and at higher population densities, while r-strategists outperform K-strategists under nutrient replete conditions (Andrews & Harris, 1986; Yin et al., 2022).

Experimental co-culture platforms built from the toolkit could be used as an ecological model framework for the transition from r-conditions with initially high nutrient availability and low population densities to K-conditions with population densities close to carrying capacity and limited nutrients. Based on the growth preferences of species derived from estimates of their specific growth rates and carrying capacities, the applied methodology could potentially be used to determine if bacterial species are r- or K-strategists. The identification of r- and K-strategists and understanding their underlying ecological strategies can be an important tool for the design and construction of synthetic microbial co-cultures with optimized community function and structure. To this end, K-selection has been used, for example, to reduce the incidence of pathogens in aquaculture (De Schryver & Vadstein, 2014), to increase the viability of marine larvae to improve sustainability and performance (Vadstein et al., 2018), for bioaugmentation (Brzeszcz et al., 2016), and for wastewater treatment (Yin et al., 2022).

5.5 Standardized Model Systems

Much of our current understanding of biological processes and ecological principles is based on the intensive study of biological model systems. Among the most significant and well-known model systems is *Escherichia coli*, a model organism for molecular biology and bacterial metabolism (Bengtsson-Palme, 2020). Model systems provide simplified and controlled experimental platforms to study complex processes through reproducible observations and targeted manipulations, allowing for advances in many scientific fields with applications in biotechnology, ecology, and medicine (Zengler et al., 2019).

The standardization of methods and model systems is an essential key to reproducibility and comparability of results between researchers and across laboratories, as well as facilitating collaboration that enables the sharing of resources and data (McCoy et al., 2017; Müller & Arndt, 2012; Zengler et al., 2019). The toolkit described in this thesis is based on a set of standardized reporter devices with measurable fluorescent outputs built onto broad-host-range vector scaffolds derived from a pSEVA231 plasmid in the BASIC environment (see 4.1.1) and a set of well-established and non-traditional hosts of biotechnological interest (Bitzenhofer et al., 2021; Bollinger, Thies, Katzke, et al., 2020; Isnansetyo & Kamei, 2009) that can be genetically engineered allowing targeted modifications, testing of novel phenotypes, and validation of engineering approaches. In conjunction with the toolkit, a methodology was developed that enables the simple measurement and observation of growth in modular mono- and co-cultures using fluorescence. These fluorescence measurements can be used to estimate species-specific fitness measures as well as changes in their fitness due to combinatorial growth in co-cultures, which allows to infer interactions between species. The compatibility with high throughput assays was further demonstrated by growth experiments in 96-well approaches using a plate reader allowing for relatively high numbers of replicates. In addition, this methodology involves simple, low-cost workflows, convenient cultivation conditions with standard LB culture medium, and common computational tools for the modelling of bacterial growth and estimation of growth parameters by fitting a first order growth model representing exponential growth (Equation 4) and a logistic growth model (Equation 6) to experimental data using the package `growthrates` in R (Petzoldt, 2022). Thus it has essential characteristics that are considered important for model systems (Bengtsson-Palme, 2020; Zengler et al., 2019), demonstrating the potential as an ecology or biotechnology platform for synthetic model co-cultures that could be built upon, addressing the need for standardized and reproducible model microbial communities required for the advancement of microbial community and microbiome research.

5.6 Future Directions

The modular tools provided as part of this work serve as the base level of this toolkit and were used for its characterization and validation as a platform for the interrogation of population dynamics and inference of interspecies interactions in synthetic co-cultures. A major focus in the design of the genetic tools was on its ability to be expanded upon. Hence, the “base” toolkit described here can easily be reproduced and adapted to the needs of a wide range of researchers from different disciplines of microbial ecology, synthetic biology, and biotechnology. This was accomplished by combining other scalable standards in synthetic biology – *i.e.*, SEVA and BASIC. Reconfiguration or expansion of the toolkit can be reached by adding new species, which is facilitated by broad-host-range plasmids onto which the genetic devices are built, by adding new fluorescent proteins, *i.e.*, by expanding the number of reporter plasmids with different fluorescent outputs, and by modifying constitutive parts of the reporter plasmids, *e.g.*, by changing the resistance markers and promoters.

The “base” toolkit, as provided with this work, can be used for the simultaneous tracking of species-specific biomasses of up to three fluorescently labelled species in co-culture using the Biotek Synergy H1 plate reader. This can be attributed to the different degrees of spectral overlap of the sfGFP, mRFP, mKate, mEYFP, mCitrine and mCerulean fluorescent proteins, which only allow for the unambiguous detection of three fluorescence emission signals, *i.e.*, red fluorescence (mRFP or mKate), blue fluorescence (mCerulean) and green/yellow fluorescence (sfGFP, mEYFP or mCitrine), with the methodology developed (see 4.2.2.1.1). For applications that require the construction and parallel observation of communities composed of four bacterial populations it could be considered to expand the toolkit by mCarmine (Fabritius et al., 2018), a far-red emitting fluorescent protein. It has an emission peak at 675 nm and is therefore within the detection range of the Biotek Synergy H1 plate reader (BioTek, 2016). However, this monomer has a lower quantum yield and brightness compared to the other fluorescent proteins used, so that its suitability for monitoring species-specific biomass requires experimental validation. Significant spectral overlaps with the mKate protein further suggest that mCarmine fluorescence can only be unambiguously distinguished from the mRFP protein with an emission peak further towards the ultraviolet radiation of the electromagnetic spectrum compared to the emission peak of mKate. This would require additional characterization of the pCPkate plasmid across species, which was not performed as part of this study due to the high redundancy of the mKate and mRFP proteins. The suitability of the mKate protein for assessing bacterial growth was however limited across species, additionally increasing the interest to investigate the suitability of the mRFP protein. This was demonstrated by often considerably high specific growth rates estimated from Kate fluorescence compared to the specific growth rates as given by OD600, especially observed for the slow growing species *H. aestusnigri* (Figure 11) and *H. oceani* (Figure 12), but also for *P. putida* (Figure 10) and *P. deceptionensis* (Figure 13). One possible reason for this observation could be that the fluorescence of the mKate protein was measured at a gain more than 1.5 times higher than that of the other fluorescent proteins to compensate for the lower brightness of the mKate protein, potentially contributing to the deviations between the estimates of specific growth rate obtained from fluorescence and OD600 measurements. In addition, the estimates of both surrogate measures for the carrying capacity, K_{fl} and F_{max} , for the pCPkate bearing strains of *H. aestusnigri*, *H. oceani* and *P. deceptionensis* have considerably higher values than the estimates of the other plasmid bearing strains of the same species (Figure 16). As both values represent measures of the maximum fluorescence, this is indicative for high Kate fluorescence signals. Apart from the specific example of mCarmine, the toolkit can certainly be extended to include any desired fluorescent proteins within the detection range of the Biotek Synergy H1 by assembling three BASIC integrated bioparts – the promoter-cassette, the fluorescent reporter, and a SEVA vector-derived backbone with an origin of replication and an antibiotic selection marker.

The toolkit can further be expanded by adding new species, facilitated by the reporter devices being built onto broad-host-range vectors. This base level kit includes a group of six Gammaproteobacteria consisting of model and non-traditional hosts of six bacterial species belonging to three different genera (*i.e.*, *Escherichia*, *Halopseudomonas* and *Pseudomonas*) that were all successfully transformed

with each of the reporter tools (Table 2). Along with other successfully reported transformations of *Pseudomonas* species using SEVA vector backbones, such as *Pseudomonas aeruginosa* (Lammens et al., 2021), *Pseudomonas entomophila* (Sun et al., 2020), *Pseudomonas sp.* UYIF39 and *Pseudomonas sp.* UYIF41 (Amarelle et al., 2019, 2023), this suggests that the toolkit can be readily expanded to include new hosts, particularly species of the genus *Pseudomonas*, and possibly others. This would allow the combinatorial construction and observation of diverse microbial co-cultures and associated growth phenotypes and inferable interactions.

Another possibility to customize and expand the toolkit is by modifying or changing constitutive modular parts of the genetic tools, *e.g.*, promoters, ribosome binding sites, and resistance markers. The interchangeable modules of SEVA plasmids enable the easy exchange of the antibiotic resistance marker of the SEVA vector scaffolds that the genetic devices are built onto. By cloning the promoter-reporter-cassettes into backbones carrying different antibiotic resistance markers, facilitated by the modularity and idempotency of the BASIC DNA assembly method, the toolkit can be expanded by modified broad-host-range plasmids, *e.g.*, allowing the inclusion of kanamycin-resistant species. Further, the existence of SEVA plasmids with dual antibiotic resistance markers and their integration into the toolkit would enable the interrogation of population dynamics of co-cultured bacteria sensitive to different antibiotics. In addition, it is conceivable to extend the application range to Gram-positive bacteria if this is of application-specific interest, by building promoter-reporter-cassettes onto SEVA vector backbones developed for the establishment of synthetic constructs in Gram-positive bacteria (Martínez-García et al., 2022).

In summary, the modularity and standardized concept of SEVA and BASIC can allow researchers around the world to easily, quickly, and reproducibly modify the components of the genetic tools to adapt this base level toolkit for different applications. Moreover, the use of broad-host-range plasmids enables their transformation across additional species, which expands the design space for the construction of synthetic microbial co-cultures. This work further demonstrated the compatibility with their observation in a relatively high throughput manner in 96-well approaches. The next conceivable step for the future development of this platform would therefore be automation, which would allow the monitoring and interrogation of many different permutations of engineered microbial co-cultures. By coupling this methodology, for example, with the DNA-BOT platform developed for the automated BASIC DNA assembly and cloning with Opentrons liquid handling robots (Storch et al., 2020), it could be possible to automate the assembly and observation of growth dynamics of engineered microbial communities, which would represent a significant advance in screening larger design spaces with respect to synthetic microbial co-cultures. In addition to the experimental observation and interrogation of population dynamics, another area of application for this device platform could be the data-driven modelling of microbial growth interactions. This could be achieved by using context-specific growth rates obtained during co-cultivation experiments to parameterize a generalized Lotka-Volterra model capable of predicting how each species affects the growth of each potential partner.

The study of microbial communities is essential to understand the role of microorganisms in ecological processes and to identify their potential applications in biotechnology. However, the lack of practical tools to study population dynamics and interspecies interactions, which play an important role in community stability and function, is an ongoing challenge and limits the ability to fully harness their potential. This thesis work contributes to the evolving field of microbial community science by providing a toolkit and methodology for reproducible, standardized, and high throughput interrogation of population dynamics and interactions based on bacterial fitness – with potential applications within relevant ecological, biotechnological, and synthetic biology frameworks owing to its high flexibility.

6 Conclusion

This thesis introduces a synthetic biology toolkit based on a set of broad-host-range fluorescent reporter plasmids that can be used to fluorescently label a wide range of bacterial species. Using 96-well plate assays, it was successfully demonstrated that these genetic tools can be used to decouple population dynamics and infer binary interactions in relation to two measures of ecological fitness – specific growth rate and carrying capacity – based on scalable measurements of strain-specific fluorescence as proxy for species-specific biomass in mono- and co-cultures. However, the results have also shown that the experimental design is coupled to some challenges that need to be considered when using or adopting this toolkit. The main findings of this work include:

- Each of the broad-host-range genetic tools can be transformed across all six bacterial hosts of the genera *Escherichia*, *Halopseudomonas* and *Pseudomonas*.
- The reporter plasmids are functional across all hosts, but chassis-effects have been observed. Both the measurable fluorescence outputs of the genetic tools and the fitness of the bacterial hosts depend on the plasmid-species combination.
- The suitability of fluorescence as a proxy for biomass is strongly dependent on the combination of host species and fluorescent reporter protein.
- The pCPgfp, pCPeyfp and pCPcit plasmids should not be used together for the fluorescent labelling of bacterial populations for co-cultivation, as their fluorescence emission cannot be clearly separated using the methodology developed in this study.
- Comparative proxy measures for the ecological carrying capacity have shown that fitting the logistic growth model across large datasets comes at the expense of model accuracy, leading to uncertainty and occasional errors in the K estimates.
- The maximum fluorescence F_{max} measured by the plate reader is arguably the better surrogate measure for the carrying capacity as it is not susceptible to uncertainties arising from nonlinear regression modelling of bacterial growth.
- Constitutive expression of fluorescent reporter proteins allows the interrogation of population dynamics in co-cultures by estimating growth parameters from strain-specific fluorescence data.
- The choice of genetic tools has a significant impact on the prediction and decoupling of growth dynamics in co-cultures. For significant results and the correct inference of interspecies interactions, only strains with close or matching specific growth rates estimated from OD600 (μ_{OD}) and fluorescence (μ_{fl}) should be used.
- The inference of interspecies interactions and determination of the more fit species is biased towards the approach used to interpret the carrying capacity.
- Batch effects on the reproducibility are likely and should therefore be considered in the experimental design.
- *Pseudomonas putida* has the highest overall fitness of all species studied, both in terms of specific growth rate and carrying capacity.

This toolkit builds on the emerging and cross-disciplinary movement of standardized systems and scalable standards such as SEVA, BASIC, and EcoFABs that promote collaboration, reproducibility, and scientific progress. Designed for scalability and reproducibility, the tools and methods can be easily adopted and customized and offer potential applications for decoupling growth dynamics and inferring ecological interactions between species, the emerging field of broad-host-range synthetic biology, or as a platform for mixing and screening synthetic microbial communities that contribute to different disciplines of microbial ecology, synthetic biology, and biotechnology.

The results of this thesis additionally give reason to generally caution the use of constitutively expressed fluorescent proteins to approximate bacterial growth. The quantitative investigation of fluorescence as a proxy for bacterial biomass has shown that fluorescence can be a useful and practical tool. However, the accuracy of growth parameters estimated from fluorescence curve data can vary greatly depending on fluorescent protein and species. Therefore, the considered and appropriate use of fluorescence as a tool is essential to ensure the retention of meaningful data.

7 References

- Adams, B. L. (2016). The Next Generation of Synthetic Biology Chassis: Moving Synthetic Biology from the Laboratory to the Field. *ACS Synthetic Biology*, 5(12), 1328–1330. <https://doi.org/10.1021/acssynbio.6b00256>
- Allocati, N., Masulli, M., Alexeyev, M. F., & Di Ilio, C. (2013). Escherichia coli in Europe: An Overview. *International Journal of Environmental Research and Public Health*, 10(12), 6235–6254. <https://doi.org/10.3390/ijerph10126235>
- Amarelle, V., Roldán, D. M., Fabiano, E., & Guazzaroni, M.-E. (2023). Synthetic Biology Toolbox for Antarctic Pseudomonas sp. Strains: Toward a Psychrophilic Nonmodel Chassis for Function-Driven Metagenomics. *ACS Synthetic Biology*, 12(3), 722–734. <https://doi.org/10.1021/acssynbio.2c00543>
- Amarelle, V., Sanches-Medeiros, A., Silva-Rocha, R., & Guazzaroni, M.-E. (2019). Expanding the Toolbox of Broad Host-Range Transcriptional Terminators for Proteobacteria through Metagenomics. *ACS Synthetic Biology*, 8(4), 647–654. <https://doi.org/10.1021/acssynbio.8b00507>
- Andrews, J. H., & Harris, R. F. (1986). R- and K-Selection and Microbial Ecology. In K. C. Marshall (Ed.), *Advances in Microbial Ecology* (pp. 99–147). Springer US. https://doi.org/10.1007/978-1-4757-0611-6_3
- Ankenbauer, A., Schäfer, R. A., Viegas, S. C., Pobre, V., Voß, B., Arraiano, C. M., & Takors, R. (2020). Pseudomonas putida KT2440 is naturally endowed to withstand industrial-scale stress conditions. *Microbial Biotechnology*, 13(4), 1145–1161. <https://doi.org/10.1111/1751-7915.13571>
- Anton, B. P., & Raleigh, E. A. (2016). Complete Genome Sequence of NEB 5-alpha, a Derivative of Escherichia coli K-12 DH5a. *Genome Announcements*, 4(6), e01245-16. <https://doi.org/10.1128/genomeA.01245-16>
- Archontoulis, S. V., & Miguez, F. E. (2015). Nonlinear Regression Models and Applications in Agricultural Research. *Agronomy Journal*, 107(2), 786–798. <https://doi.org/10.2134/agronj2012.0506>
- Bailey, M. J., Lilley, A. K., Thompson, I. P., Rainey, P. B., & Ellis, R. J. (1995). Site directed chromosomal marking of a fluorescent pseudomonad isolated from the phytosphere of sugar beet; stability and potential for marker gene transfer. *Molecular Ecology*, 4(6), 755–764. <https://doi.org/10.1111/j.1365-294X.1995.tb00276.x>
- Baranyi, J., Roberts, T. A., & McClure, P. (1993). A non-autonomous differential equation to model bacterial growth. *Food Microbiology*, 10(1), 43–59. <https://doi.org/10.1006/fmic.1993.1005>
- Baty, F., & Delignette-Muller, M.-L. (2004). Estimating the bacterial lag time: Which model, which precision? *International Journal of Food Microbiology*, 91(3), 261–277. <https://doi.org/10.1016/j.ijfoodmicro.2003.07.002>
- Beal, J., Farny, N. G., Haddock-Angelli, T., Selvarajah, V., Baldwin, G. S., Buckley-Taylor, R., Gershater, M., Kiga, D., Marken, J., Sanchania, V., Sison, A., & Workman, C. T. (2020). Robust estimation of bacterial cell count from optical density. *Communications Biology*, 3(1), Article 1. <https://doi.org/10.1038/s42003-020-01127-5>
- Beck, A. E., Hunt, K. A., Bernstein, H. C., & Carlson, R. P. (2016). Chapter 15—Interpreting and Designing Microbial Communities for Bioprocess Applications, from Components to Interactions to Emergent Properties. In C. A. Eckert & C. T. Trinh (Eds.), *Biotechnology for Biofuel Production and Optimization* (pp. 407–432). Elsevier. <https://doi.org/10.1016/B978-0-444-63475-7.00015-7>
- Beliaev, A. S., Romine, M. F., Serres, M., Bernstein, H. C., Linggi, B. E., Markillie, L. M., Isern, N. G., Chrisler, W. B., Kucek, L. A., Hill, E. A., Pinchuk, G. E., Bryant, D. A., Steven Wiley, H., Fredrickson, J. K., & Konopka, A. (2014). Inference of interactions in cyanobacterial–heterotrophic co-cultures via transcriptome sequencing. *The ISME Journal*, 8(11), Article 11. <https://doi.org/10.1038/ismej.2014.69>
- Bengtsson-Palme, J. (2020). Microbial model communities: To understand complexity, harness the power of simplicity. *Computational and Structural Biotechnology Journal*, 18, 3987–4001. <https://doi.org/10.1016/j.csbj.2020.11.043>
- Benner, S. A., & Sismour, A. M. (2005). Synthetic biology. *Nature Reviews Genetics*, 6(7), Article 7. <https://doi.org/10.1038/nrg1637>
- Bernstein, H. C. (2019). Reconciling Ecological and Engineering Design Principles for Building Microbiomes. *MSystems*, 4(3), e00106-19. <https://doi.org/10.1128/mSystems.00106-19>
- Bernstein, H. C., & Carlson, R. P. (2012). MICROBIAL CONSORTIA ENGINEERING FOR CELLULAR FACTORIES: IN VITRO TO IN SILICO SYSTEMS. *Computational and Structural Biotechnology Journal*, 3(4), e201210017. <https://doi.org/10.5936/csbj.201210017>

- Bernstein, H. C., Paulson, S. D., & Carlson, R. P. (2012). Synthetic *Escherichia coli* consortia engineered for syntrophy demonstrate enhanced biomass productivity. *Journal of Biotechnology*, *157*(1), 159–166. <https://doi.org/10.1016/j.jbiotec.2011.10.001>
- BioTek. (2016). *Hybrid Multi-Mode Microplate Reader—Synergy H1 (Operator’s Manual)*. BioTek Instruments, Inc. [chrome-extension://efaidnbmnnnibpcajpcgclefindmkaj/https://www2.fcfa.unesp.br/Home/Instituicao/Departamentos/cienciasbiologicasnovo/laboratoriomultiusuariosfinep/biotek-synergy-h1-manual.pdf](https://www2.fcfa.unesp.br/Home/Instituicao/Departamentos/cienciasbiologicasnovo/laboratoriomultiusuariosfinep/biotek-synergy-h1-manual.pdf)
- Bitzenhofer, N. L., Kruse, L., Thies, S., Wynands, B., Lechtenberg, T., Rönitz, J., Kozaeva, E., Wirth, N. T., Eberlein, C., Jaeger, K.-E., Nickel, P. I., Heipieper, H. J., Wierckx, N., & Loeschcke, A. (2021). Towards robust *Pseudomonas* cell factories to harbour novel biosynthetic pathways. *Essays in Biochemistry*, *65*(2), 319–336. <https://doi.org/10.1042/EBC20200173>
- Bollinger, A., Molitor, R., Thies, S., Koch, R., Coscolín, C., Ferrer, M., & Jaeger, K.-E. (2020). Organic-Solvent-Tolerant Carboxylic Ester Hydrolases for Organic Synthesis. *Applied and Environmental Microbiology*, *86*(9), e00106-20. <https://doi.org/10.1128/AEM.00106-20>
- Bollinger, A., Thies, S., Katzke, N., & Jaeger, K. (2018). The biotechnological potential of marine bacteria in the novel lineage of *Pseudomonas pertucinogena*. *Microbial Biotechnology*, *13*(1), 19–31. <https://doi.org/10.1111/1751-7915.13288>
- Bollinger, A., Thies, S., Katzke, N., & Jaeger, K.-E. (2020). The biotechnological potential of marine bacteria in the novel lineage of *Pseudomonas pertucinogena*. *Microbial Biotechnology*, *13*(1), 19–31. <https://doi.org/10.1111/1751-7915.13288>
- Bollinger, A., Thies, S., Knieps-Grünhagen, E., Gertzen, C., Kobus, S., Höppner, A., Ferrer, M., Gohlke, H., Smits, S. H. J., & Jaeger, K.-E. (2020). A Novel Polyester Hydrolase From the Marine Bacterium *Pseudomonas aestusnigri* – Structural and Functional Insights. *Frontiers in Microbiology*, *11*. <https://doi.org/10.3389/fmicb.2020.00114>
- Bosdriesz, E., Molenaar, D., Teusink, B., & Bruggeman, F. J. (2015). How fast-growing bacteria robustly tune their ribosome concentration to approximate growth-rate maximization. *The Febs Journal*, *282*(10), 2029–2044. <https://doi.org/10.1111/febs.13258>
- Brzeszcz, J., Steliga, T., Kapusta, P., Turkiewicz, A., & Kaszycki, P. (2016). R-strategist versus K-strategist for the application in bioremediation of hydrocarbon-contaminated soils. *International Biodeterioration & Biodegradation*, *106*, 41–52. <https://doi.org/10.1016/j.ibiod.2015.10.001>
- Cameron, D. E., Bashor, C. J., & Collins, J. J. (2014). A brief history of synthetic biology. *Nature Reviews Microbiology*, *12*(5), Article 5. <https://doi.org/10.1038/nrmicro3239>
- Cardinale, S., & Arkin, A. P. (2012). Contextualizing context for synthetic biology – identifying causes of failure of synthetic biological systems. *Biotechnology Journal*, *7*(7), 856–866. <https://doi.org/10.1002/biot.201200085>
- Carrara, F., Giometto, A., Seymour, M., Rinaldo, A., & Altermatt, F. (2015). Inferring species interactions in ecological communities: A comparison of methods at different levels of complexity. *Methods in Ecology and Evolution*, *6*(8), 895–906. <https://doi.org/10.1111/2041-210X.12363>
- Carrión, O., Curson, A. R. J., Kumaresan, D., Fu, Y., Lang, A. S., Mercadé, E., & Todd, J. D. (2015). A novel pathway producing dimethylsulphide in bacteria is widespread in soil environments. *Nature Communications*, *6*(1), Article 1. <https://doi.org/10.1038/ncomms7579>
- Carrión, O., Miñana-Galbis, D., Montes, M. J., & Mercadé, E. (2011). *Pseudomonas deceptionensis* sp. Nov., a psychrotolerant bacterium from the Antarctic. *International Journal of Systematic and Evolutionary Microbiology*, *61*(10), 2401–2405. <https://doi.org/10.1099/ijs.0.024919-0>
- Casini, A., Storch, M., Baldwin, G. S., & Ellis, T. (2015). Bricks and blueprints: Methods and standards for DNA assembly. *Nature Reviews Molecular Cell Biology*, *16*(9), Article 9. <https://doi.org/10.1038/nrm4014>
- Chan, D. T. C., Baldwin, G. S., & Bernstein, H. C. (2023). *Revealing the chassis-effect on a broad-host-range genetic switch and its concordance with interspecies bacterial physiologies* (p. 2023.02.27.529268). [bioRxiv. https://doi.org/10.1101/2023.02.27.529268](https://doi.org/10.1101/2023.02.27.529268)
- Cornell, J. A., & Berger, R. D. (1987). Factors that Influence the Value of the Coefficient of Determination in Simple Linear and Nonlinear Regression Models. *The American Phytopathological Society*, *77*. <https://www.semanticscholar.org/paper/Factors-that-Influence-the-Value-of-the-Coefficient-A.-D./a410ec58bd5ff80a4e7978955ab11d096af6d138>
- Cotto, A., Looper, J. K., Mota, L. C., & Son, A. (2015). Quantitative Polymerase Chain Reaction for Microbial Growth Kinetics of Mixed Culture System. *Journal of Microbiology and Biotechnology*, *25*(11), 1928–1935. <https://doi.org/10.4014/jmb.1503.03090>

- Cox, R. S., Madsen, C., McLaughlin, J., Nguyen, T., Roehner, N., Bartley, B., Bhatia, S., Bissell, M., Clancy, K., Gorochowski, T., Grünberg, R., Luna, A., Le Novère, N., Pocock, M., Sauro, H., Sexton, J. T., Stan, G.-B., Tabor, J. J., Voigt, C. A., ... Wipat, A. (2018). Synthetic Biology Open Language Visual (SBOL Visual) Version 2.0. *Journal of Integrative Bioinformatics*, 15(1), 20170074. <https://doi.org/10.1515/jib-2017-0074>
- De Roy, K., Marzorati, M., Van den Abbeele, P., Van de Wiele, T., & Boon, N. (2014). Synthetic microbial ecosystems: An exciting tool to understand and apply microbial communities. *Environmental Microbiology*, 16(6), 1472–1481. <https://doi.org/10.1111/1462-2920.12343>
- De Schryver, P., & Vadstein, O. (2014). Ecological theory as a foundation to control pathogenic invasion in aquaculture. *The ISME Journal*, 8(12), 2360–2368. <https://doi.org/10.1038/ismej.2014.84>
- Dolinšek, J., Goldschmidt, F., & Johnson, D. R. (2016). Synthetic microbial ecology and the dynamic interplay between microbial genotypes. *FEMS Microbiology Reviews*, 40(6), 961–979. <https://doi.org/10.1093/femsre/fuw024>
- D'Souza, G., Shitut, S., Preussger, D., Yousif, G., Waschina, S., & Kost, C. (2018). Ecology and evolution of metabolic cross-feeding interactions in bacteria. *Natural Product Reports*, 35(5), 455–488. <https://doi.org/10.1039/C8NP00009C>
- Duncan, M. C., Forbes, J. C., Nguyen, Y., Shull, L. M., Gillette, R. K., Lazinski, D. W., Ali, A., Shanks, R. M. Q., Kadouri, D. E., & Camilli, A. (2018). *Vibrio cholerae* motility exerts drag force to impede attack by the bacterial predator *Bdellovibrio bacteriovorus*. *Nature Communications*, 9(1), Article 1. <https://doi.org/10.1038/s41467-018-07245-3>
- Elena, S. F., & Lenski, R. E. (2003). Evolution experiments with microorganisms: The dynamics and genetic bases of adaptation. *Nature Reviews Genetics*, 4(6), Article 6. <https://doi.org/10.1038/nrg1088>
- Ellis, T., Adie, T., & Baldwin, G. (2011). DNA assembly for synthetic biology: From parts to pathways and beyond. *Integrative Biology: Quantitative Biosciences from Nano to Macro*, 3, 109–118. <https://doi.org/10.1039/c0ib00070a>
- Espinosa-Urgel, M., Salido, A., & Ramos, J.-L. (2000). Genetic Analysis of Functions Involved in Adhesion of *Pseudomonas putida* to Seeds. *Journal of Bacteriology*, 182(9), 2363–2369. <https://doi.org/10.1128/JB.182.9.2363-2369.2000>
- Fabritius, A., Ng, D., Kist, A. M., Erdogan, M., Portugues, R., & Griesbeck, O. (2018). Imaging-Based Screening Platform Assists Protein Engineering. *Cell Chemical Biology*, 25(12), 1554-1561.e8. <https://doi.org/10.1016/j.chembiol.2018.08.008>
- Faust, K., & Raes, J. (2012). Microbial interactions: From networks to models. *Nature Reviews Microbiology*, 10(8), Article 8. <https://doi.org/10.1038/nrmicro2832>
- Foster, E. D., & Deardorff, A. (2017). Open Science Framework (OSF). *Journal of the Medical Library Association: JMLA*, 105(2), 203–206. <https://doi.org/10.5195/jmla.2017.88>
- Fredrickson, J. K. (2015). Ecological communities by design. *Science*, 348(6242), 1425–1427. <https://doi.org/10.1126/science.aab0946>
- Galdzicki, M., Clancy, K. P., Oberortner, E., Pocock, M., Quinn, J. Y., Rodriguez, C. A., Roehner, N., Wilson, M. L., Adam, L., Anderson, J. C., Bartley, B. A., Beal, J., Chandran, D., Chen, J., Densmore, D., Endy, D., Grünberg, R., Hallinan, J., Hillson, N. J., ... Sauro, H. M. (2014). The Synthetic Biology Open Language (SBOL) provides a community standard for communicating designs in synthetic biology. *Nature Biotechnology*, 32(6), Article 6. <https://doi.org/10.1038/nbt.2891>
- Gao, J., Jiang, L., & Lian, J. (2021). Development of synthetic biology tools to engineer *Pichia pastoris* as a chassis for the production of natural products. *Synthetic and Systems Biotechnology*, 6(2), 110–119. <https://doi.org/10.1016/j.synbio.2021.04.005>
- García-Jiménez, B., Torres-Bacete, J., & Nogales, J. (2021). Metabolic modelling approaches for describing and engineering microbial communities. *Computational and Structural Biotechnology Journal*, 19, 226–246. <https://doi.org/10.1016/j.csbj.2020.12.003>
- Goers, L., Freemont, P., & Polizzi, K. M. (2014). Co-culture systems and technologies: Taking synthetic biology to the next level. *Journal of the Royal Society Interface*, 11(96), 20140065. <https://doi.org/10.1098/rsif.2014.0065>
- Green, R. F. (1980). A Note on K-Selection. *The American Naturalist*, 116(2), 291–296. <https://doi.org/10.1086/283627>
- Haines, M. C., Carling, B., Marshall, J., Shenshin, V. A., Baldwin, G. S., Freemont, P., & Storch, M. (2022). basicsynbio and the BASIC SEVA collection: Software and vectors for an established DNA assembly method. *Synthetic Biology*, 7(1), ysac023. <https://doi.org/10.1093/synbio/ysac023>

- Hall, A. R., Iles, J. C., & MacLean, R. C. (2011). The Fitness Cost of Rifampicin Resistance in *Pseudomonas aeruginosa* Depends on Demand for RNA Polymerase. *Genetics*, *187*(3), 817–822. <https://doi.org/10.1534/genetics.110.124628>
- Hall, B. G., Acar, H., Nandipati, A., & Barlow, M. (2014). Growth Rates Made Easy. *Molecular Biology and Evolution*, *31*(1), 232–238. <https://doi.org/10.1093/molbev/mst187>
- Hothorn, T., Bretz, F., & Westfall, P. (2008). Simultaneous inference in general parametric models. *Biometrical Journal*, *50*(3), 346–363. <https://doi.org/10.1002/bimj.200810425>
- Ibrahim, M., Raajaraam, L., & Raman, K. (2021). Modelling microbial communities: Harnessing consortia for biotechnological applications. *Computational and Structural Biotechnology Journal*, *19*, 3892–3907. <https://doi.org/10.1016/j.csbj.2021.06.048>
- Isnansetyo, A., & Kamei, Y. (2009). Bioactive substances produced by marine isolates of *Pseudomonas*. *Journal of Industrial Microbiology & Biotechnology*, *36*(10), 1239–1248. <https://doi.org/10.1007/s10295-009-0611-2>
- Jiru, T. M., Groenewald, M., Pohl, C., Steyn, L., Kiggundu, N., & Abate, D. (2017). Optimization of cultivation conditions for biotechnological production of lipid by *Rhodotorula kratochvilovae* (syn, *Rhodospiridium kratochvilovae*) SY89 for biodiesel preparation. *3 Biotech*, *7*(2), 145. <https://doi.org/10.1007/s13205-017-0769-7>
- Junicke, H., Abbas, B., Oentoro, J., van Loosdrecht, M., & Kleerebezem, R. (2014). Absolute Quantification of Individual Biomass Concentrations in a Methanogenic Coculture. *AMB Express*, *4*, 35. <https://doi.org/10.1186/s13568-014-0035-x>
- Kampers, L. F. C., Volkens, R. J. M., & Martins dos Santos, V. A. P. (2019). *Pseudomonas putida* KT2440 is HV1 certified, not GRAS. *Microbial Biotechnology*, *12*(5), 845–848. <https://doi.org/10.1111/1751-7915.13443>
- Kehe, J., Kulesa, A., Ortiz, A., Ackerman, C. M., Thakku, S. G., Sellers, D., Kuehn, S., Gore, J., Friedman, J., & Blainey, P. C. (2019). Massively parallel screening of synthetic microbial communities. *Proceedings of the National Academy of Sciences of the United States of America*, *116*(26), 12804–12809. <https://doi.org/10.1073/pnas.1900102116>
- Kehe, J., Ortiz, A., Kulesa, A., Gore, J., Blainey, P. C., & Friedman, J. (2021). Positive interactions are common among culturable bacteria. *Science Advances*, *7*(45). <https://doi.org/10.1126/sciadv.abi7159>
- Khan, N., Maezato, Y., McClure, R. S., Brislawn, C. J., Mobberley, J. M., Isern, N., Chrisler, W. B., Markillie, L. M., Barney, B. M., Song, H.-S., Nelson, W. C., & Bernstein, H. C. (2018). Phenotypic responses to interspecies competition and commensalism in a naturally-derived microbial co-culture. *Scientific Reports*, *8*(1), Article 1. <https://doi.org/10.1038/s41598-017-18630-1>
- Khan, N., Yeung, E., Farris, Y., Fansler, S., & Bernstein, H. (2020). A broad-host-range event detector: Expanding and quantifying performance between *Escherichia coli* and *Pseudomonas* species. *Synthetic Biology*, *5*. <https://doi.org/10.1093/synbio/ysaa002>
- Kim, J., Salvador, M., Saunders, E., González, J., Avignone-Rossa, C., & Jiménez, J. I. (2016). Properties of alternative microbial hosts used in synthetic biology: Towards the design of a modular chassis. *Essays in Biochemistry*, *60*(4), 303–313. <https://doi.org/10.1042/EBC20160015>
- Kvålseth, T. O. (1985). Cautionary Note about R 2. *The American Statistician*, *39*(4), 279–285. <https://doi.org/10.1080/00031305.1985.10479448>
- Lammens, E., Boon, M., Grimon, D., Briens, Y., & Lavigne, R. (2021). SEVAtile: A standardised DNA assembly method optimised for *Pseudomonas*. *Microbial Biotechnology*, *15*(1), 370–386. <https://doi.org/10.1111/1751-7915.13922>
- Lawson, C. E., Harcombe, W. R., Hatzepichler, R., Lindemann, S. R., Löffler, F. E., O'Malley, M. A., García-Martin, H., Pflieger, B. F., Raskin, L., Venturelli, O. S., Weissbrodt, D. G., Noguera, D. R., & McMahon, K. D. (2019). Common principles and best practices for engineering microbiomes. *Nature Reviews. Microbiology*, *17*(12), 725–741. <https://doi.org/10.1038/s41579-019-0255-9>
- Liang, Y., Ma, A., & Zhuang, G. (2022). Construction of Environmental Synthetic Microbial Consortia: Based on Engineering and Ecological Principles. *Frontiers in Microbiology*, *13*. <https://www.frontiersin.org/articles/10.3389/fmicb.2022.829717>
- Liao, J. C., Mi, L., Pontrelli, S., & Luo, S. (2016). Fuelling the future: Microbial engineering for the production of sustainable biofuels. *Nature Reviews Microbiology*, *14*(5), Article 5. <https://doi.org/10.1038/nrmicro.2016.32>
- Lindemann, S. R., Bernstein, H. C., Song, H.-S., Fredrickson, J. K., Fields, M. W., Shou, W., Johnson, D. R., & Beliaev, A. S. (2016). Engineering microbial consortia for controllable outputs. *The ISME Journal*, *10*(9), Article 9. <https://doi.org/10.1038/ismej.2016.26>

- Liu, X., Xiang, L., Yin, Y., Li, H., Ma, D., & Qu, Y. (2021). Pneumonia caused by *Pseudomonas fluorescens*: A case report. *BMC Pulmonary Medicine*, 21(1), 212. <https://doi.org/10.1186/s12890-021-01573-9>
- Lotka, A. J. (1925). Elements of Physical Biology. *Nature*, 116(2917), Article 2917. <https://doi.org/10.1038/116461b0>
- Lotka, A. J. (1956). *Elements of Mathematical Biology*. Dover Publications.
- MacArthur, R. H., & Wilson, E. O. (1967). *The Theory of Island Biogeography*. Princeton University Press.
- Madsen, C., Goñi Moreno, A., P, U., Palchick, Z., Roehner, N., Atallah, C., Bartley, B., Choi, K., Cox, R. S., Gorochowski, T., Grünberg, R., Macklin, C., McLaughlin, J., Meng, X., Nguyen, T., Pocock, M., Samineni, M., Scott-Brown, J., Tarter, Y., ... Wipat, A. (2019). Synthetic Biology Open Language (SBOL) Version 2.3. *Journal of Integrative Bioinformatics*, 16(2), 20190025. <https://doi.org/10.1515/jib-2019-0025>
- Martínez-García, E., Fraile, S., Algar, E., Aparicio, T., Velázquez, E., Calles, B., Tas, H., Blázquez, B., Martín, B., Prieto, C., Sánchez-Sampedro, L., Nørholm, M. H. H., Volke, D. C., Wirth, N. T., Dvořák, P., Alejaldre, L., Grozinger, L., Crowther, M., Goñi-Moreno, A., ... de Lorenzo, V. (2022). SEVA 4.0: An update of the Standard European Vector Architecture database for advanced analysis and programming of bacterial phenotypes. *Nucleic Acids Research*, 51(D1), D1558–D1567. <https://doi.org/10.1093/nar/gkac1059>
- Martínez-García, E., Goñi-Moreno, A., Bartley, B., McLaughlin, J., Sánchez-Sampedro, L., Pascual del Pozo, H., Prieto Hernández, C., Marletta, A. S., De Lucrezia, D., Sánchez-Fernández, G., Fraile, S., & de Lorenzo, V. (2020). SEVA 3.0: An update of the Standard European Vector Architecture for enabling portability of genetic constructs among diverse bacterial hosts. *Nucleic Acids Research*, 48(D1), D1164–D1170. <https://doi.org/10.1093/nar/gkz1024>
- McCarty, N. S., & Ledesma-Amaro, R. (2019). Synthetic Biology Tools to Engineer Microbial Communities for Biotechnology. *Trends in Biotechnology*, 37(2), 181–197. <https://doi.org/10.1016/j.tibtech.2018.11.002>
- McClure, R. S., Overall, C. C., Hill, E. A., Song, H.-S., Charania, M., Bernstein, H. C., McDermott, J. E., & Beliaev, A. S. (2018). Species-specific transcriptomic network inference of interspecies interactions. *The ISME Journal*, 12(8), Article 8. <https://doi.org/10.1038/s41396-018-0145-6>
- McCoy, K. D., Geuking, M. B., & Ronchi, F. (2017). Gut Microbiome Standardization in Control and Experimental Mice. *Current Protocols in Immunology*, 117(1), 23.1.1–23.1.13. <https://doi.org/10.1002/cpim.25>
- Medlock, G. L., Carey, M. A., McDuffie, D. G., Mundy, M. B., Giallourou, N., Swann, J. R., Kolling, G. L., & Papin, J. A. (2018). Inferring Metabolic Mechanisms of Interaction within a Defined Gut Microbiota. *Cell Systems*, 7(3), 245–257.e7. <https://doi.org/10.1016/j.cels.2018.08.003>
- Midani, F. S., & David, L. A. (2022). Tracking defined microbial communities by multicolor flow cytometry reveals tradeoffs between productivity and diversity. *Frontiers in Microbiology*, 13, 910390. <https://doi.org/10.3389/fmicb.2022.910390>
- Migula, W. (1894). *Über ein neues System der Bakterien. Arbeiten aus dem Bakteriologischen Institut der Technischen Hochschule zu Karlsruhe*. Verlag von Otto Nernich.
- Molitor, R., Bollinger, A., Kubicki, S., Loeschcke, A., Jaeger, K.-E., & Thies, S. (2020). Agar plate-based screening methods for the identification of polyester hydrolysis by *Pseudomonas* species. *Microbial Biotechnology*, 13(1), 274–284. <https://doi.org/10.1111/1751-7915.13418>
- Monod, J., & Jacob, F. (1961). Teleonomic mechanisms in cellular metabolism, growth, and differentiation. *Cold Spring Harbor Symposia on Quantitative Biology*, 26, 389–401. <https://doi.org/10.1101/sqb.1961.026.01.048>
- Mougi, A. (2016). The roles of amensalistic and commensalistic interactions in large ecological network stability. *Scientific Reports*, 6(1), Article 1. <https://doi.org/10.1038/srep29929>
- Müller, K. M., & Arndt, K. M. (2012). Standardization in Synthetic Biology. In W. Weber & M. Fussenegger (Eds.), *Synthetic Gene Networks: Methods and Protocols* (pp. 23–43). Humana Press. https://doi.org/10.1007/978-1-61779-412-4_2
- Nakazawa, T. (2002). Travels of a *Pseudomonas*, from Japan around the world. *Environmental Microbiology*, 4(12), 782–786. <https://doi.org/10.1046/j.1462-2920.2002.00310.x>
- Nelson, K. E., Weinel, C., Paulsen, I. T., Dodson, R. J., Hilbert, H., Martins dos Santos, V. a. P., Fouts, D. E., Gill, S. R., Pop, M., Holmes, M., Brinkac, L., Beanan, M., DeBoy, R. T., Daugherty, S., Kolonay, J., Madupu, R., Nelson, W., White, O., Peterson, J., ... Fraser, C. M. (2002). Complete genome sequence and comparative analysis of the metabolically versatile *Pseudomonas putida* KT2440. *Environmental Microbiology*, 4(12), 799–808. <https://doi.org/10.1046/j.1462-2920.2002.00366.x>
- Nestor, E., Toledano, G., & Friedman, J. (2023). Interactions between Culturable Bacteria Are Predicted by Individual Species' Growth. *ASM Journals, MSystems*, e00836-22. <https://doi.org/10.1128/msystems.00836-22>

- Nikel, P. I., Chavarría, M., Danchin, A., & de Lorenzo, V. (2016). From dirt to industrial applications: *Pseudomonas putida* as a Synthetic Biology chassis for hosting harsh biochemical reactions. *Current Opinion in Chemical Biology*, 34, 20–29. <https://doi.org/10.1016/j.cbpa.2016.05.011>
- Nikel, P. I., Martínez-García, E., & de Lorenzo, V. (2014). Biotechnological domestication of pseudomonads using synthetic biology. *Nature Reviews Microbiology*, 12(5), Article 5. <https://doi.org/10.1038/nrmicro3253>
- Ogundero, A., Vignola, M., Connelly, S., & Sloan, W. T. (2022). Validating Flow Cytometry as a Method for Quantifying *Bdellovibrio* Predatory Bacteria and Its Prey for Microbial Ecology. *Microbiology Spectrum*, 10(1), e0103321. <https://doi.org/10.1128/spectrum.01033-21>
- Ou, B., Garcia, C., Wang, Y., Zhang, W., & Zhu, G. (2018). Techniques for chromosomal integration and expression optimization in *Escherichia coli*. *Biotechnology and Bioengineering*, 115(10), 2467–2478. <https://doi.org/10.1002/bit.26790>
- Pacheco, A. R., Moel, M., & Segrè, D. (2019). Costless metabolic secretions as drivers of interspecies interactions in microbial ecosystems. *Nature Communications*, 10(1), 103. <https://doi.org/10.1038/s41467-018-07946-9>
- Panikov, N. S. (2019). 1.18—Microbial Growth Dynamics. In M. Moo-Young (Ed.), *Comprehensive Biotechnology* (3rd ed., Vol. 1, pp. 231–273). Pergamon. <https://doi.org/10.1016/B978-0-444-64046-8.00019-7>
- Paulander, W., Maisnier-Patin, S., & Andersson, D. I. (2009). The fitness cost of streptomycin resistance depends on rpsL mutation, carbon source and RpoS (σ^S). *Genetics*, 183(2), 539–546, 1S1-2S1. <https://doi.org/10.1534/genetics.109.106104>
- Pawelczyk, S., Abraham, W.-R., Harms, H., & Müller, S. (2008). Community-based degradation of 4-chlorosalicylate tracked on the single cell level. *Journal of Microbiological Methods*, 75(1), 117–126. <https://doi.org/10.1016/j.mimet.2008.05.018>
- Peix, A., Ramírez-Bahena, M.-H., & Velázquez, E. (2018). The current status on the taxonomy of *Pseudomonas* revisited: An update. *Infection, Genetics and Evolution*, 57, 106–116. <https://doi.org/10.1016/j.meegid.2017.10.026>
- Perni, S., Andrew, P. W., & Shama, G. (2005). Estimating the maximum growth rate from microbial growth curves: Definition is everything. *Food Microbiology*, 22(6), 491–495. <https://doi.org/10.1016/j.fm.2004.11.014>
- Petrof, E. O., Gloor, G. B., Vanner, S. J., Weese, S. J., Carter, D., Daigneault, M. C., Brown, E. M., Schroeter, K., & Allen-Vercoe, E. (2013). Stool substitute transplant therapy for the eradication of *Clostridium difficile* infection: ‘RePOOPulating’ the gut. *Microbiome*, 1(1), 3. <https://doi.org/10.1186/2049-2618-1-3>
- Petzoldt, T. (2022). *growthrates: Estimate Growth Rates from Experimental Data* (0.8.4). <https://cran.r-project.org/web/packages/growthrates/index.html>
- Phalak, P., Bernstein, H. C., Lindemann, S. R., Renslow, R. S., Thomas, D. G., Henson, M. A., & Song, H.-S. (2022). Spatiotemporal Metabolic Network Models Reveal Complex Autotroph-Heterotroph Biofilm Interactions Governed by Photon Incidences. *IFAC-PapersOnLine*, 55(7), 112–118. <https://doi.org/10.1016/j.ifacol.2022.07.430>
- Preston, G., Spiers, A., Zhang, X. X., Jackson, R., Gal, M., Knight, C., Gehrig, S., Malone, J., Moon, C., Godfrey, S., Robinson, Z., Bertrand, N., Dawn, F., & Rainey, P. B. (2003). *Pseudomonas* in the underworld: The secret life of *Pseudomonas fluorescens* SBW25. In *Pseudomonas syringae and related pathogens: Biology and genetic* (1st ed., pp. 347–353). Kluwer Academic Publishers. https://doi.org/10.1007/978-94-017-0133-4_37
- R Core Team. (2022). *R: A Language and Environment for Statistical Computing*. R Foundation for Statistical Computing. <https://www.R-project.org/>
- Ratkowsky, D. A. (1993). Principles of nonlinear regression modeling. *Journal of Industrial Microbiology*, 12(3), 195–199. <https://doi.org/10.1007/BF01584190>
- Robinson, J. A. (1985). Determining Microbial Kinetic Parameters Using Nonlinear Regression Analysis. In K. C. Marshall (Ed.), *Advances in Microbial Ecology: Volume 8* (pp. 61–114). Springer US. https://doi.org/10.1007/978-1-4615-9412-3_2
- Roller, B. R., & Schmidt, T. M. (2015). The physiology and ecological implications of efficient growth. *The ISME Journal*, 9(7), Article 7. <https://doi.org/10.1038/ismej.2014.235>
- Rouches, M. V., Xu, Y., Cortes, L. B. G., & Lambert, G. (2022). A plasmid system with tunable copy number. *Nature Communications*, 13, 3908. <https://doi.org/10.1038/s41467-022-31422-0>
- Rudra, B., & Gupta, R. S. (2021). Phylogenomic and comparative genomic analyses of species of the family Pseudomonadaceae: Proposals for the genera *Halopseudomonas* gen. nov. and *Atopomonas* gen. nov., merger of the genus *Oblitimonas* with the genus *Thiopseudomonas*, and transfer of some misclassified species of the genus *Pseudomonas* into other genera. *International Journal of Systematic and Evolutionary Microbiology*, 71(9), 005011. <https://doi.org/10.1099/ijsem.0.005011>

- Sánchez, D., Mulet, M., Rodríguez, A. C., David, Z., Lalucat, J., & García-Valdés, E. (2014). *Pseudomonas aestusnigri* sp. Nov., isolated from crude oil-contaminated intertidal sand samples after the Prestige oil spill. *Systematic and Applied Microbiology*, 37(2), 89–94. <https://doi.org/10.1016/j.syapm.2013.09.004>
- Sanjana, N. E. (2021). Voices of the new generation: Open science is good for science (and for you). *Nature Reviews Molecular Cell Biology*, 22(11), Article 11. <https://doi.org/10.1038/s41580-021-00414-1>
- Sbarciog, M., Loccufier, M., & Noldus, E. (2011). Optimization of microorganisms growth processes. *Computer Methods and Programs in Biomedicine*, 104(2), 112–119. <https://doi.org/10.1016/j.cmpb.2010.05.009>
- Scales, B. S., Dickson, R. P., LiPuma, J. J., & Huffnagle, G. B. (2014). Microbiology, Genomics, and Clinical Significance of the *Pseudomonas fluorescens* Species Complex, an Unappreciated Colonizer of Humans. *Clinical Microbiology Reviews*, 27(4), 927–948. <https://doi.org/10.1128/CMR.00044-14>
- Schlechter, R. O., Jun, H., Bernach, M., Oso, S., Boyd, E., Muñoz-Lintz, D. A., Dobson, R. C. J., Remus, D. M., & Remus-Emsermann, M. N. P. (2018). Chromatic Bacteria—A Broad Host-Range Plasmid and Chromosomal Insertion Toolbox for Fluorescent Protein Expression in Bacteria. *Frontiers in Microbiology*, 9, 3052. <https://doi.org/10.3389/fmicb.2018.03052>
- Schlechter, R. O., Kear, E. J., Remus, D. M., & Remus-Emsermann, M. N. P. (2021). Fluorescent Protein Expression as a Proxy for Bacterial Fitness in a High-Throughput Assay. *Applied and Environmental Microbiology*, 87(18), e00982-21. <https://doi.org/10.1128/AEM.00982-21>
- Schuster, L. A., & Reisch, C. R. (2021). A plasmid toolbox for controlled gene expression across the Proteobacteria. *Nucleic Acids Research*, 49(12), 7189–7202. <https://doi.org/10.1093/nar/gkab496>
- Shahinas, D., Silverman, M., Sittler, T., Chiu, C., Kim, P., Allen-Vercocoe, E., Weese, S., Wong, A., Low, D. E., & Pillai, D. R. (2012). Toward an understanding of changes in diversity associated with fecal microbiome transplantation based on 16S rRNA gene deep sequencing. *MBio*, 3(5), e00338-12. <https://doi.org/10.1128/mBio.00338-12>
- Shoemaker, W. R., Jones, S. E., Muscarella, M. E., Behringer, M. G., Lehmkuhl, B. K., & Lennon, J. T. (2021). Microbial population dynamics and evolutionary outcomes under extreme energy limitation. *Proceedings of the National Academy of Sciences*, 118(33), e2101691118. <https://doi.org/10.1073/pnas.2101691118>
- Silva-Rocha, R., Martínez-García, E., Calles, B., Chavarría, M., Arce-Rodríguez, A., de las Heras, A., Páez-Espino, A. D., Durante-Rodríguez, G., Kim, J., Nikel, P. I., Platero, R., & de Lorenzo, V. (2013). The Standard European Vector Architecture (SEVA): A coherent platform for the analysis and deployment of complex prokaryotic phenotypes. *Nucleic Acids Research*, 41(Database issue), D666–D675. <https://doi.org/10.1093/nar/gks1119>
- Smyth, G. K. (2002). Nonlinear regression. In *Encyclopedia of Environmetrics* (Vol. 3, pp. 1405–1411). John Wiley & Sons.
- Soetaert, K., & Petzoldt, T. (2010). Inverse Modelling, Sensitivity and Monte Carlo Analysis in R Using Package FME. *Journal of Statistical Software*, 33, 1–28. <https://doi.org/10.18637/jss.v033.i03>
- Song, H.-S., Lee, J.-Y., Haruta, S., Nelson, W. C., Lee, D.-Y., Lindemann, S. R., Fredrickson, J. K., & Bernstein, H. C. (2019). Minimal Interspecies Interaction Adjustment (MIIA): Inference of Neighbor-Dependent Interactions in Microbial Communities. *Frontiers in Microbiology*, 10. <https://doi.org/10.3389/fmicb.2019.01264>
- Song, Y., Lee, B.-R., Cho, S., Cho, Y.-B., Kim, S.-W., Kang, T. J., Kim, S. C., & Cho, B.-K. (2015). Determination of single nucleotide variants in *Escherichia coli* DH5 α by using short-read sequencing. *FEMS Microbiology Letters*, 362(11), fnv073. <https://doi.org/10.1093/femsle/fnv073>
- Stevenson, K., McVey, A. F., Clark, I. B. N., Swain, P. S., & Pilizota, T. (2016). General calibration of microbial growth in microplate readers. *Scientific Reports*, 6(1), Article 1. <https://doi.org/10.1038/srep38828>
- Storch, M., Casini, A., Mackrow, B., Ellis, T., & Baldwin, G. S. (2017). BASIC: A Simple and Accurate Modular DNA Assembly Method. In R. A. Hughes (Ed.), *Synthetic DNA: Methods and Protocols* (pp. 79–91). Springer. https://doi.org/10.1007/978-1-4939-6343-0_6
- Storch, M., Casini, A., Mackrow, B., Fleming, T., Trewhitt, H., Ellis, T., & Baldwin, G. S. (2015). BASIC: A New Biopart Assembly Standard for Idempotent Cloning Provides Accurate, Single-Tier DNA Assembly for Synthetic Biology. *ACS Synthetic Biology*, 4(7), 781–787. <https://doi.org/10.1021/sb500356d>
- Storch, M., Haines, M. C., & Baldwin, G. S. (2020). DNA-BOT: A low-cost, automated DNA assembly platform for synthetic biology. *Synthetic Biology*, 5(1), ysaa010. <https://doi.org/10.1093/synbio/ysaa010>
- Sullivan, I., DeHaven, A., & Mellor, D. (2019). Open and Reproducible Research on Open Science Framework. *Current Protocols Essential Laboratory Techniques*, 18(1), e32. <https://doi.org/10.1002/cpet.32>

- Sun, Lu, L.-B., Liang, T.-X., Yang, L.-R., & Wu, J.-P. (2020). CRISPR-Assisted Multiplex Base Editing System in *Pseudomonas putida* KT2440. *Frontiers in Bioengineering and Biotechnology*, 8. <https://doi.org/10.3389/fbioe.2020.00905>
- Sun, Y.-Y., Chi, H., & Sun, L. (2016). *Pseudomonas fluorescens* Filamentous Hemagglutinin, an Iron-Regulated Protein, Is an Important Virulence Factor that Modulates Bacterial Pathogenicity. *Frontiers in Microbiology*, 7. <https://doi.org/10.3389/fmicb.2016.01320>
- Tas, H., Amara, A., Cueva, M. E., Bongaerts, N., Calvo-Villamañán, A., Hamadache, S., & Vavitsas, K. (2020). Are synthetic biology standards applicable in everyday research practice? *Microbial Biotechnology*, 13(5), 1304–1308. <https://doi.org/10.1111/1751-7915.13612>
- Tauer, C., Heinel, S., Egger, E., Heiss, S., & Grabherr, R. (2014). Tuning constitutive recombinant gene expression in *Lactobacillus plantarum*. *Microbial Cell Factories*, 13(1), 150. <https://doi.org/10.1186/s12934-014-0150-z>
- Trippe, K., McPhail, K., Armstrong, D., Azevedo, M., & Banowetz, G. (2013). *Pseudomonas fluorescens* SBW25 produces furanomycin, a non-proteinogenic amino acid with selective antimicrobial properties. *BMC Microbiology*, 13(1), 111. <https://doi.org/10.1186/1471-2180-13-111>
- Tshikantwa, T. S., Ullah, M. W., He, F., & Yang, G. (2018). Current Trends and Potential Applications of Microbial Interactions for Human Welfare. *Frontiers in Microbiology*, 9. <https://www.frontiersin.org/articles/10.3389/fmicb.2018.01156>
- Tsoi, R., Dai, Z., & You, L. (2019). Emerging strategies for engineering microbial communities. *Biotechnology Advances*, 37(6), 107372. <https://doi.org/10.1016/j.biotechadv.2019.03.011>
- Vadstein, O., Attramadal, K. J. K., Bakke, I., & Olsen, Y. (2018). K-Selection as Microbial Community Management Strategy: A Method for Improved Viability of Larvae in Aquaculture. *Frontiers in Microbiology*, 9. <https://www.frontiersin.org/articles/10.3389/fmicb.2018.02730>
- Venturelli, O. S., Carr, A. V., Fisher, G., Hsu, R. H., Lau, R., Bowen, B. P., Hromada, S., Northen, T., & Arkin, A. P. (2018). Deciphering microbial interactions in synthetic human gut microbiome communities. *Molecular Systems Biology*, 14(6), e8157. <https://doi.org/10.15252/msb.20178157>
- Verusevski, V. (2022). *Modeling the “microbial chassis effect” on the performance of a genetic switch* [Master thesis, UiT The Arctic University of Norway]. <https://munin.uit.no/handle/10037/25258>
- Vicente-Saez, R., & Martinez-Fuentes, C. (2018). Open Science now: A systematic literature review for an integrated definition. *Journal of Business Research*, 88, 428–436. <https://doi.org/10.1016/j.jbusres.2017.12.043>
- Wallner, G., Amann, R., & Beisker, W. (1993). Optimizing fluorescent in situ hybridization with rRNA-targeted oligonucleotide probes for flow cytometric identification of microorganisms. *Cytometry*, 14(2), 136–143. <https://doi.org/10.1002/cyto.990140205>
- Wang, K., Shi, T.-Q., Lin, L., Wei, P., Ledesma-Amaro, R., Ji, X.-J., & Huang, H. (2022). Advances in synthetic biology tools paving the way for the biomanufacturing of unusual fatty acids using the *Yarrowia lipolytica* chassis. *Biotechnology Advances*, 59, 107984. <https://doi.org/10.1016/j.biotechadv.2022.107984>
- Wang, M., & Sun, L. (2016). *Pseudomonas oceani* sp. Nov., isolated from deep seawater. *International Journal of Systematic and Evolutionary Microbiology*, 66(10), 4250–4255. <https://doi.org/10.1099/ijsem.0.001343>
- Weimer, A., Kohlstedt, M., Volke, D. C., Nickel, P. I., & Wittmann, C. (2020). Industrial biotechnology of *Pseudomonas putida*: Advances and prospects. *Applied Microbiology and Biotechnology*, 104(18), 7745–7766. <https://doi.org/10.1007/s00253-020-10811-9>
- Wilson, E., Okuom, M., Kyes, N., Mayfield, D., Wilson, C., Sabatka, D., Sandoval, J., Foote, J. R., Kangas, M. J., Holmes, A. E., & Sutlief, A. L. (2018). Using Fluorescence Intensity of Enhanced Green Fluorescent Protein to Quantify *Pseudomonas aeruginosa*. *Chemosensors (Basel, Switzerland)*, 6(2), 21. <https://doi.org/10.3390/chemosensors6020021>
- Worthan, S. B., McCarthy, R. D. P., & Behringer, M. G. (2023). Case Studies in the Assessment of Microbial Fitness: Seemingly Subtle Changes Can Have Major Effects on Phenotypic Outcomes. *Journal of Molecular Evolution*. <https://doi.org/10.1007/s00239-022-10087-9>
- Wu, G., Yan, Q., Jones, J. A., Tang, Y. J., Fong, S. S., & Koffas, M. A. G. (2016). Metabolic Burden: Cornerstones in Synthetic Biology and Metabolic Engineering Applications. *Trends in Biotechnology*, 34(8), 652–664. <https://doi.org/10.1016/j.tibtech.2016.02.010>
- Wu, L., & Qiu, J. (2021). Chapter 8 Linear and Nonlinear Regression Models. In *Applied Multivariate Statistical Analysis and Related Topics with R* (pp. 111–130). EDP Sciences. <https://doi.org/10.1051/978-2-7598-2602-5.c009>

- Xiao, X., White, E. P., Hooten, M. B., & Durham, S. L. (2011). On the use of log-transformation vs. Nonlinear regression for analyzing biological power laws. *Ecology*, *92*(10), 1887–1894. <https://doi.org/10.1890/11-0538.1>
- Yin, Q., Sun, Y., Li, B., Feng, Z., & Wu, G. (2022). The r/K selection theory and its application in biological wastewater treatment processes. *Science of The Total Environment*, *824*, 153836. <https://doi.org/10.1016/j.scitotenv.2022.153836>
- Yu, D., Banting, G., & Neumann, N. F. (2021). A review of the taxonomy, genetics, and biology of the genus *Escherichia* and the type species *Escherichia coli*. *Canadian Journal of Microbiology*, *67*(8), 553–571. <https://doi.org/10.1139/cjm-2020-0508>
- Zengler, K., Hofmockel, K., Baliga, N. S., Behie, S. W., Bernstein, H. C., Brown, J. B., Dinneny, J. R., Floge, S. A., Forry, S. P., Hess, M., Jackson, S. A., Jansson, C., Lindemann, S. R., Pett-Ridge, J., Maranas, C., Venturelli, O. S., Wallenstein, M. D., Shank, E. A., & Northen, T. R. (2019). EcoFABs: Advancing microbiome science through standardized fabricated ecosystems. *Nature Methods*, *16*(7), Article 7. <https://doi.org/10.1038/s41592-019-0465-0>
- Zwietering, M. H., Jongenburger, I., Rombouts, F. M., & van 't Riet, K. (1990). Modeling of the Bacterial Growth Curve. *Applied and Environmental Microbiology*, *56*(6), 1875–1881.

8 Appendix

8.1 Appendix A

The correct assembly of the constructed broad-host-range reporter plasmids was verified in two steps by colony-PCR and streaking of LB agar plates supplemented with different antibiotics. The presence of the J23104-reporter cassettes was confirmed by screening four colonies of each plasmid bearing *E. coli* strain by cPCR (Figure 24). To verify the correct integration of the promoter-reporter cassettes into the pSEVA231-derived backbone, *i.e.*, the presence of the backbone, *E. coli* strains carrying the newly assembled reporter plasmids with kanamycin selection markers and *E. coli* strains with the promoter-reporter cassettes stored in vectors with a chloramphenicol selection marker (starting material) were streaked on LB agar plates (Figure 25 and Figure 26).

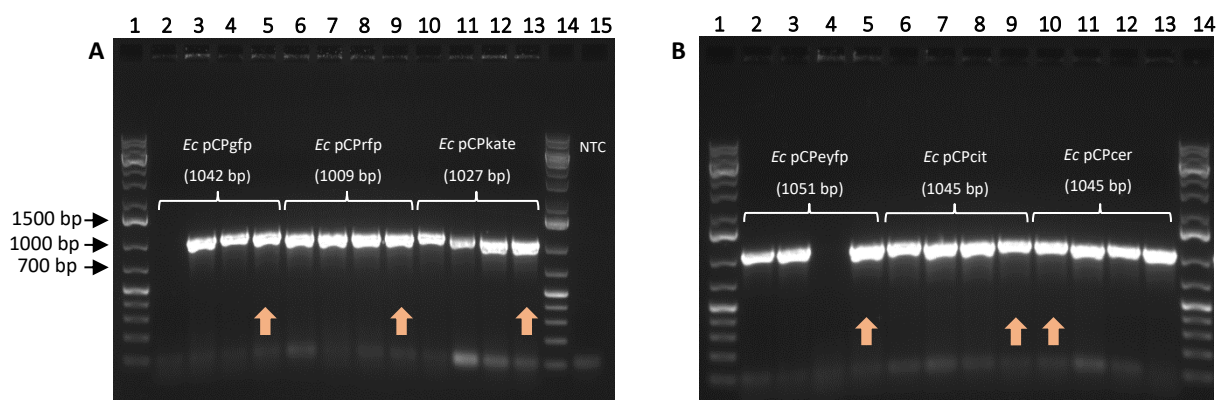


Figure 24: Confirmation of the presence of the promoter-reporter cassettes in the newly assembled broad-host-range reporter plasmids by cPCR.

Colony-PCR was performed with the L1-F forward and L2-R reverse PCR primers. Four colonies were screened for the presence of the respective promoter-reporter cassettes for each of the six strains. No DNA was added to the PCR-negative control (NTC). The DNA size standard used is the GeneRuler 1 kb Plus DNA Ladder (**A**: lane 1 and 14; **B**: lane 1 and 14). The orange arrows indicate the colonies used to inoculate clonal populations of the respective plasmid bearing strains to make glycerol stocks.

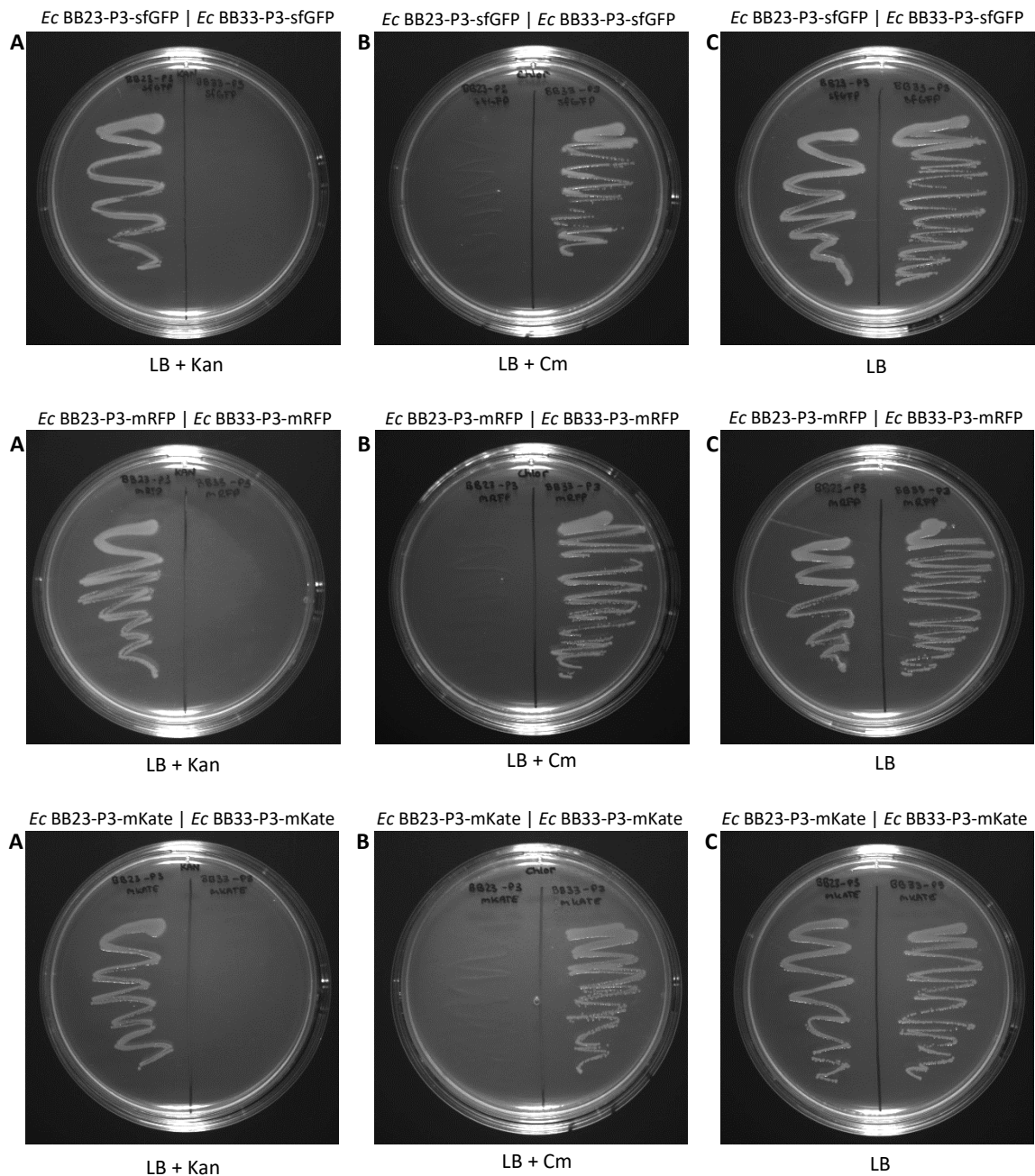


Figure 25: Confirmation of successful integration of the BB23-backbone into the pCPgfp, pCPrfp, and pCPkate plasmid.

E. coli DH5 α strains carrying the pCPgfp (*Ec* BB23-P3-sfGFP), pCPrfp (*Ec* BB23-P3-mRFP), and pCPkate (*Ec* BB23-P3-mKate) plasmid, as well as *E. coli* DH5 α strains carrying the J23104-sfGFP cassette (*Ec* BB33-P3-sfGFP), J23104-mRFP cassette (*Ec* BB33-P3-mRFP), and J23104-mKate (*Ec* BB33-P3-mKate) cassette stored in BASIC integrated pSEVA331 vectors were streaked on LB agar plates with kanamycin (A), with chloramphenicol (B) and without antibiotics (C), respectively. While strains carrying plasmids with a kanamycin resistance marker (*Ec* BB23-P3-sfGFP, *Ec* BB23-P3-mRFP, *Ec* BB23-P3-mKate) are sensitive to chloramphenicol, strains carrying plasmids with a chloramphenicol selection marker (*Ec* BB33-P3-sfGFP, *Ec* BB33-P3-mRFP, *Ec* BB33-P3-mKate) only show sensitivity towards kanamycin.

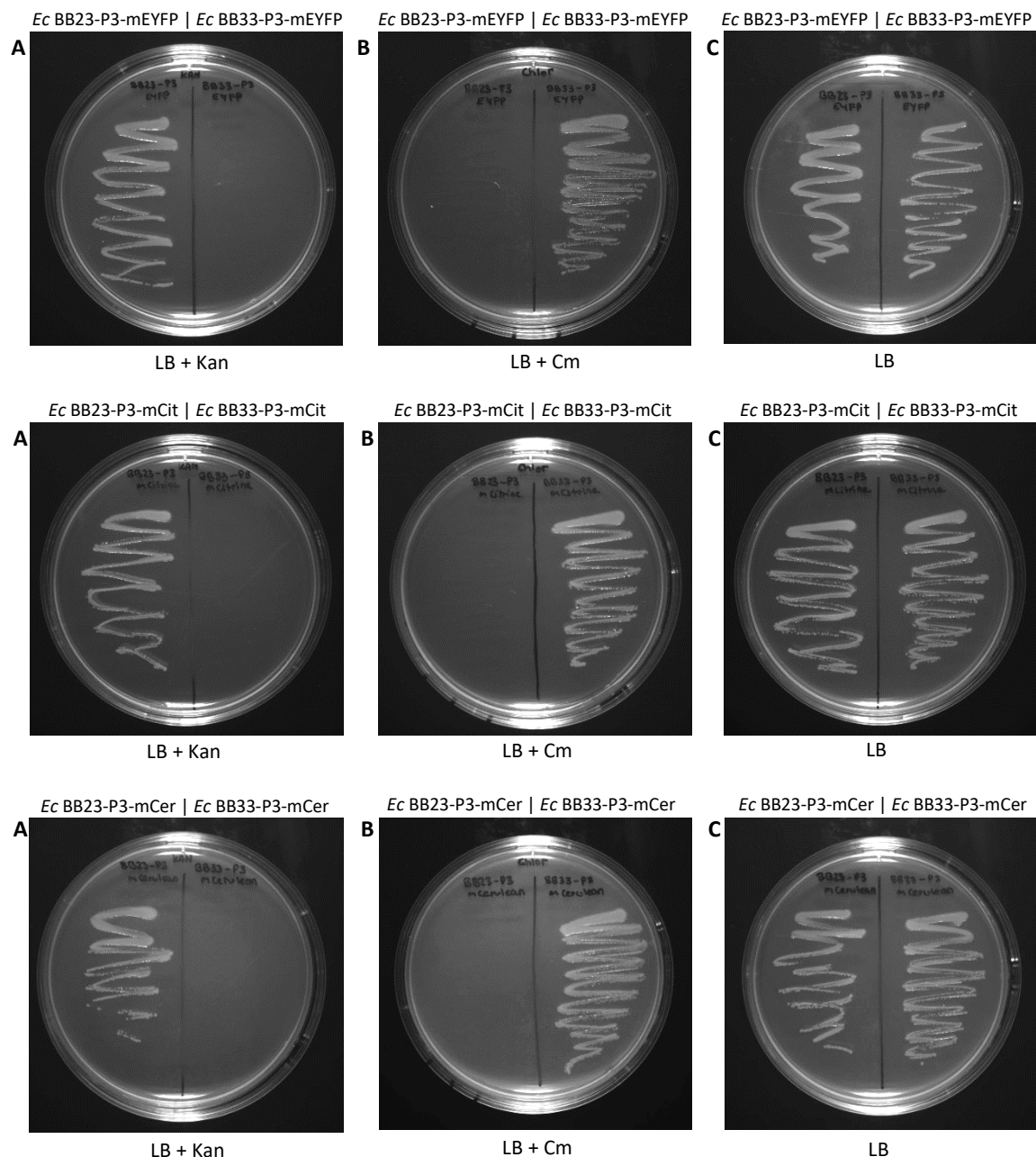


Figure 26: Confirmation of successful integration of the BB23-backbone into the pCPgfp, pCPrfp, and pCPkate plasmid. *E. coli* DH5 α strains carrying the pCPeyfp (*Ec* BB23-P3-mEYFP), pCPrfp (*Ec* BB23-P3-mCit), and pCPkate (*Ec* BB23-P3-mCer) plasmid, as well as *E. coli* DH5 α strains carrying the J23104-mEYFP cassette (*Ec* BB33-P3-mEYFP), J23104-mCitrine cassette (*Ec* BB33-P3-mCit), and J23104-mCerulean (*Ec* BB33-P3-mCer) cassette stored in BASIC integrated pEVA331 vectors were streaked on LB agar plates with kanamycin (A), with chloramphenicol (B) and without antibiotics (C), respectively. While strains carrying plasmids with a kanamycin resistance marker (*Ec* BB23-P3-mEYFP, *Ec* BB23-P3-mCit, *Ec* BB23-P3-mCer) are sensitive to chloramphenicol, strains carrying plasmids with a chloramphenicol selection marker (*Ec* BB33-P3-mEYFP, *Ec* BB33-P3-mCit, *Ec* BB33-P3-mCer) only show sensitivity towards kanamycin.

8.2 Appendix B

After transforming *P. putida* with each of the broad-host-range reporter plasmids, four colonies of each plasmid bearing strain were picked and screened by cPCR for the presence of the respective promoter-reporter cassettes (Figure 27 and Figure 28).

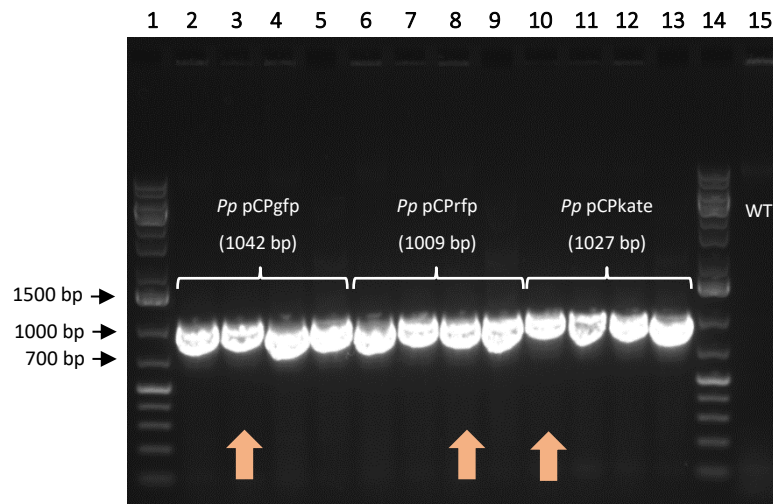


Figure 27: Confirmation of the successful transformation of *P. putida* with the plasmids pCPgfp, pCPrfp and pCPkate by verifying the presence of the respective promoter-reporter cassettes.

Colony-PCR was performed with the L1-F forward and L2-R reverse PCR primers. The sample applied in lane 15 is the negative control to which a colony of strain *Pp* wild-type was added. The DNA size standard used is the GeneRuler 1 kb Plus DNA Ladder (lane 1 and 14). The orange arrows indicate the colonies used to inoculate clonal populations of the respective plasmid bearing strains to make glycerol stocks.

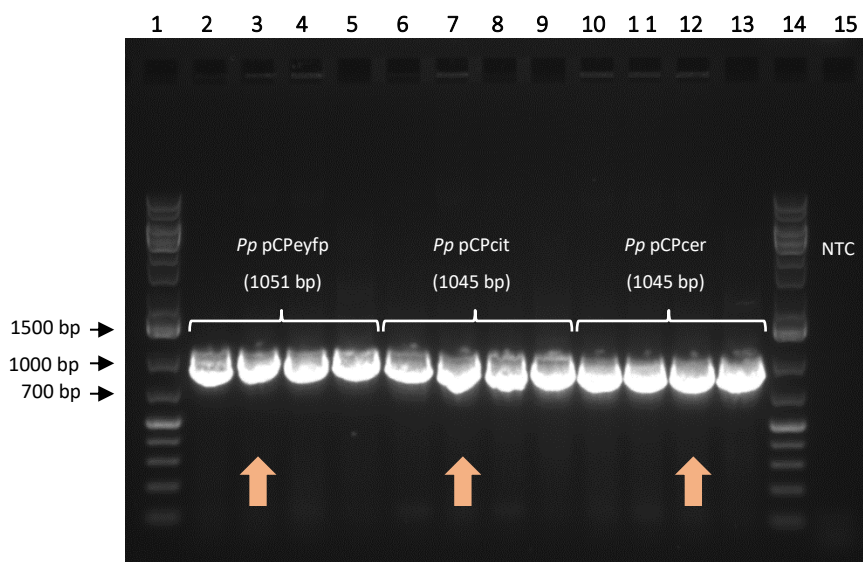


Figure 28: Confirmation of the successful transformation of *P. putida* with the plasmids pCPeyfp, pCPcit and pCPcer by verifying the presence of the respective promoter-reporter cassettes.

Colony-PCR was performed with the L1-F forward and L2-R reverse PCR primers. No DNA was added to the PCR-negative control (NTC). The DNA size standard used is the GeneRuler 1 kb Plus DNA Ladder (lane 1 and 14). The orange arrows indicate the colonies used to inoculate clonal populations of the respective plasmid bearing strains to make glycerol stocks.

8.3 Appendix C

After transforming *H. aestusnigri* with each of the broad-host-range reporter plasmids, four to eight colonies of each plasmid bearing strain were picked and screened by cPCR for the presence of the respective promoter-reporter cassettes (Figure 29 and Figure 30).

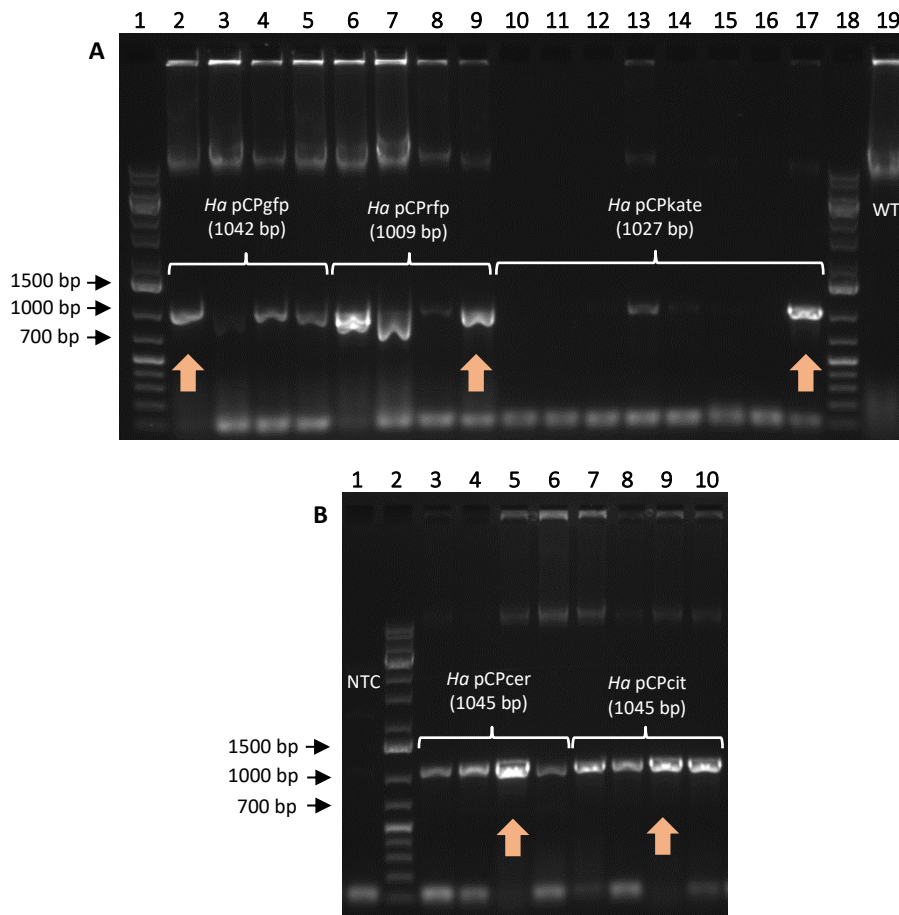


Figure 29: Confirmation of the successful transformation of *H. aestusnigri* with the plasmids pCPgfp, pCPrfp, pCPkate, pCPcit and pCPcer by verifying the presence of the respective promoter-reporter cassettes.

Colony-PCR was performed with the L1-F forward and L2-R reverse PCR primers. The sample applied in lane 19 (A) is the negative control to which a colony of the strain *Ha* wild-type was added. No DNA was added to the PCR-negative control (NTC) in lane 1 (B). The DNA size standard used is the GeneRuler 1 kb Plus DNA Ladder (A: lane 1 and 18; B: lane 2). The orange arrows indicate the colonies used to inoculate clonal populations of the respective plasmid bearing strains to make glycerol stocks.

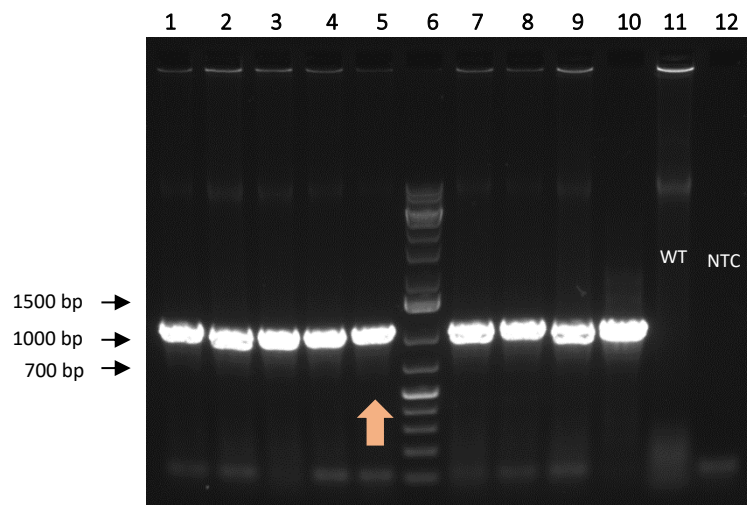


Figure 30: Confirmation of the successful transformation of *H. aestusnigri* with the plasmid pCPeyfp by verifying the presence of the respective promoter-reporter cassette.

Colony-PCR was performed with the L1-F forward and L2-R reverse PCR primers. The part of interest, *i.e.*, promoter-reporter cassette, has a size of 1051 bp. The sample applied in lane 11 is the negative control to which a colony of the strain *Ha* wild-type was added. No DNA was added to the PCR-negative control (NTC, lane 12). The DNA size standard used is the GeneRuler 1 kb Plus DNA Ladder (lane 6). The orange arrow indicates the colony used to inoculate a clonal population of the respective plasmid bearing strain to make glycerol stocks.

8.4 Appendix D

After transforming *H. oceanii* with each of the broad-host-range reporter plasmids, eight colonies of each plasmid bearing strain were picked and screened by cPCR for the presence of the respective promoter-reporter cassettes (Figure 31 - Figure 36).

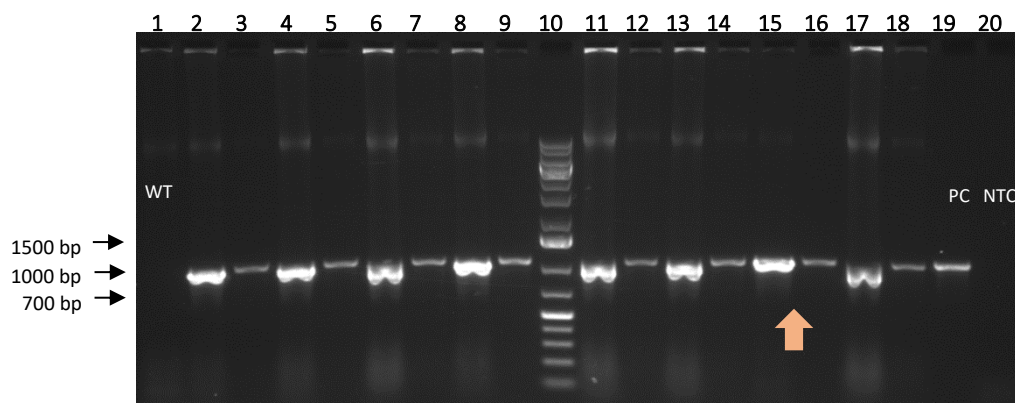


Figure 31: Confirmation of the successful transformation of *H. oceanii* with the plasmid pCPgfp by verifying the presence of the respective promoter-reporter cassette.

Colony-PCR was performed with the L1-F forward and L2-R reverse PCR primers. The part of interest, *i.e.*, promoter-reporter cassette, has a size of 1042 bp. The PCR reaction products of each colony screened for the respective promoter-reporter cassette were applied undiluted and in a 1:5 dilution to adjacent lanes on the gel. For example, in lane 2 the amplification products of the first colony examined were applied and in lane 3 the corresponding sample was applied in a 1:5 dilution. The sample applied in lane 1 is the negative control to which a colony of the strain *Ho* wild-type was added. No DNA was added to the PCR-negative control (NTC, lane 20). Lane 19 shows the positive control (PC) to which only pCPgfp plasmid DNA was added before the amplification reaction. The DNA size standard used is the GeneRuler 1 kb Plus DNA Ladder (lane 10). The orange arrow indicates the colony used to inoculate a clonal population of the respective plasmid bearing strain to make glycerol stocks.

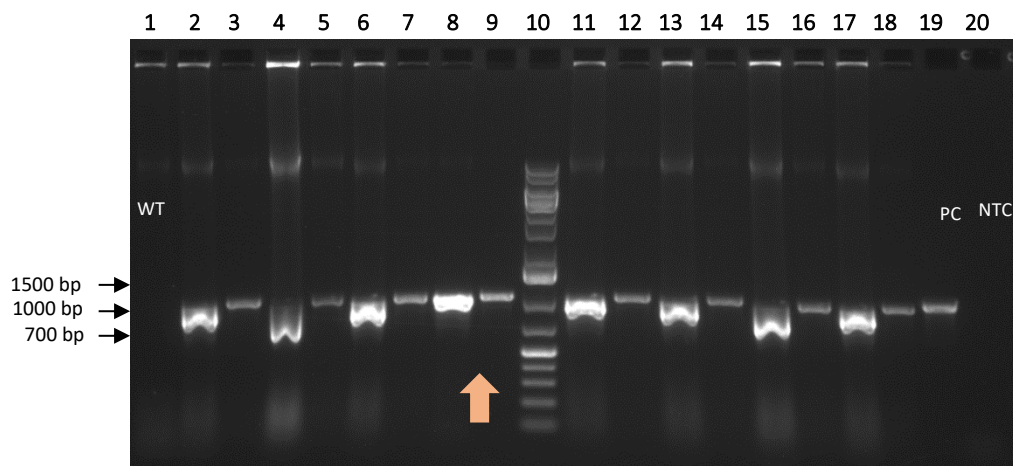


Figure 32: Confirmation of the successful transformation of *H. oceanii* with the plasmid pCPrfp by verifying the presence of the respective promoter-reporter cassette.

Colony-PCR was performed with the L1-F forward and L2-R reverse PCR primers. The part of interest, *i.e.*, promoter-reporter cassette, has a size of 1009 bp. The PCR reaction products of each colony screened for the respective promoter-reporter cassette were applied undiluted and in a 1:5 dilution to adjacent lanes on the gel. For example, in lane 2 the amplification products of the first colony examined were applied and in lane 3 the corresponding sample was applied in a 1:5 dilution. The sample applied in lane 1 is the negative control to which a colony of the strain *Ho* wild-type was added. No DNA was added to the PCR-negative control (NTC, lane 20). Lane 19 shows the positive control (PC) to which only pCPrfp plasmid DNA was added before the amplification reaction. The DNA size standard used is the GeneRuler 1 kb Plus DNA Ladder (lane 10). The orange arrow indicates the colony used to inoculate a clonal population of the respective plasmid bearing strain to make glycerol stocks.

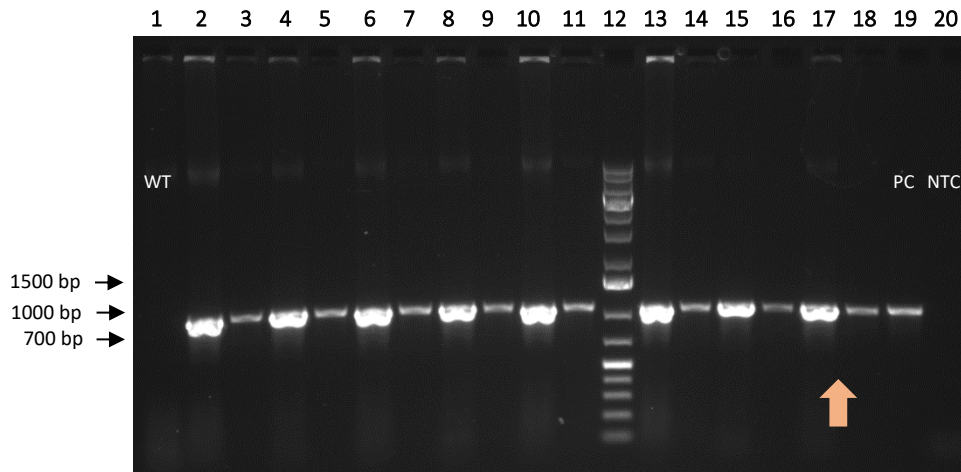


Figure 33: Confirmation of the successful transformation of *H. oceanii* with the plasmid pCPkate by verifying the presence of the respective promoter-reporter cassette.

Colony-PCR was performed with the L1-F forward and L2-R reverse PCR primers. The part of interest, *i.e.*, promoter-reporter cassette, has a size of 1027 bp. The PCR reaction products of each colony screened for the respective promoter-reporter cassette were applied undiluted and in a 1:5 dilution to adjacent lanes on the gel. For example, in lane 2 the amplification products of the first colony examined were applied and in lane 3 the corresponding sample was applied in a 1:5 dilution. The sample applied in lane 1 is the negative control to which a colony of the strain *Ho* wild-type was added. No DNA was added to the PCR-negative control (NTC, lane 20). Lane 19 shows the positive control (PC) to which only pCPkate plasmid DNA was added before the amplification reaction. The DNA size standard used is the GeneRuler 1 kb Plus DNA Ladder (lane 12). The orange arrow indicates the colony used to inoculate a clonal population of the respective plasmid bearing strain to make glycerol stocks.

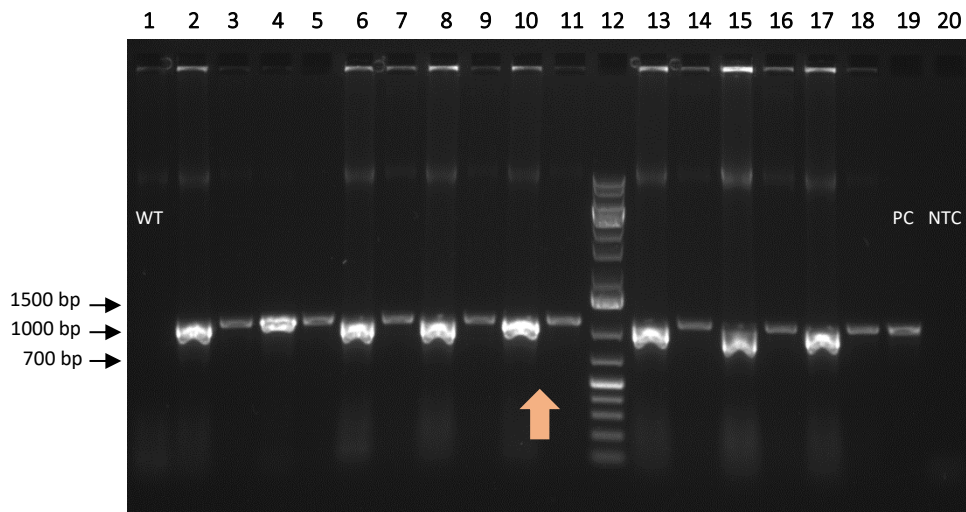


Figure 34: Confirmation of the successful transformation of *H. oceanii* with the plasmid pCPeyfp by verifying the presence of the respective promoter-reporter cassette.

Colony-PCR was performed with the L1-F forward and L2-R reverse PCR primers. The part of interest, *i.e.*, promoter-reporter cassette, has a size of 1051 bp. The PCR reaction products of each colony screened for the respective promoter-reporter cassette were applied undiluted and in a 1:5 dilution to adjacent lanes on the gel. For example, in lane 2 the amplification products of the first colony examined were applied and in lane 3 the corresponding sample was applied in a 1:5 dilution. The sample applied in lane 1 is the negative control to which a colony of the strain *Ho* wild-type was added. No DNA was added to the PCR-negative control (NTC, lane 20). Lane 19 shows the positive control (PC) to which only pCPeyfp plasmid DNA was added before the amplification reaction. The DNA size standard used is the GeneRuler 1 kb Plus DNA Ladder (lane 12). The orange arrow indicates the colony used to inoculate a clonal population of the respective plasmid bearing strain to make glycerol stocks.

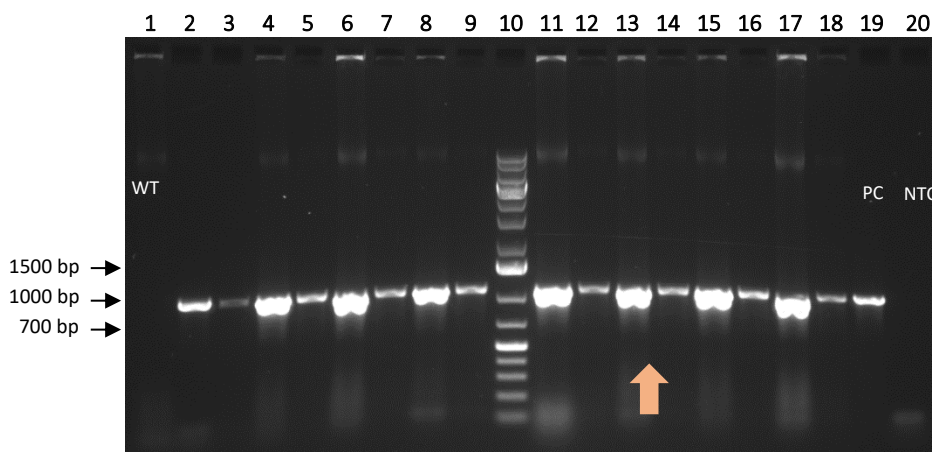


Figure 35: Confirmation of the successful transformation of *H. oceanii* with the plasmid pCPcit by verifying the presence of the respective promoter-reporter cassette.

Colony-PCR was performed with the L1-F forward and L2-R reverse PCR primers. The part of interest, *i.e.*, promoter-reporter cassette, has a size of 1045 bp. The PCR reaction products of each colony screened for the respective promoter-reporter cassette were applied undiluted and in a 1:5 dilution to adjacent lanes on the gel. For example, in lane 2 the amplification products of the first colony examined were applied and in lane 3 the corresponding sample was applied in a 1:5 dilution. The sample applied in lane 1 is the negative control to which a colony of the strain *Ho* wild-type was added. No DNA was added to the PCR-negative control (NTC, lane 20). Lane 19 shows the positive control (PC) to which only pCPcit plasmid DNA was added before the amplification reaction. The DNA size standard used is the GeneRuler 1 kb Plus DNA Ladder (lane 10). The orange arrow indicates the colony used to inoculate a clonal population of the respective plasmid bearing strain to make glycerol stocks.

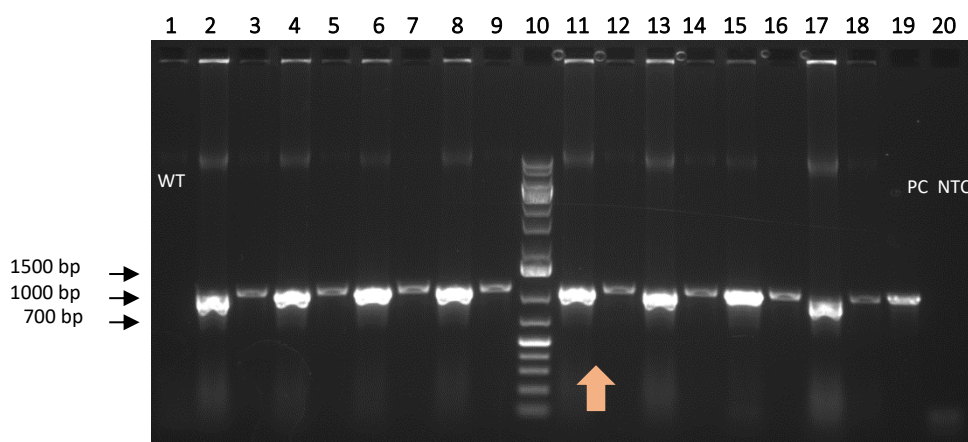


Figure 36: Confirmation of the successful transformation of *H. oceanii* with the plasmid pCPcer by verifying the presence of the respective promoter-reporter cassette.

Colony-PCR was performed with the L1-F forward and L2-R reverse PCR primers. The part of interest, *i.e.*, promoter-reporter cassette, has a size of 1045 bp. The PCR reaction products of each colony screened for the respective promoter-reporter cassette were applied undiluted and in a 1:5 dilution to adjacent lanes on the gel. For example, in lane 2 the amplification products of the first colony examined were applied and in lane 3 the corresponding sample was applied in a 1:5 dilution. The sample applied in lane 1 is the negative control to which a colony of the strain *Ho* wild-type was added. No DNA was added to the PCR-negative control (NTC, lane 20). Lane 19 shows the positive control (PC) to which only pCPcer plasmid DNA was added before the amplification reaction. The DNA size standard used is the GeneRuler 1 kb Plus DNA Ladder (lane 10). The orange arrow indicates the colony used to inoculate a clonal population of the respective plasmid bearing strain to make glycerol stocks.

8.5 Appendix E

After transforming *P. deceptionensis* with each of the broad-host-range reporter plasmids, four colonies of each plasmid bearing strain were picked and screened by cPCR for the presence of the respective promoter-reporter cassettes (Figure 37, Figure 38 and Figure 39).

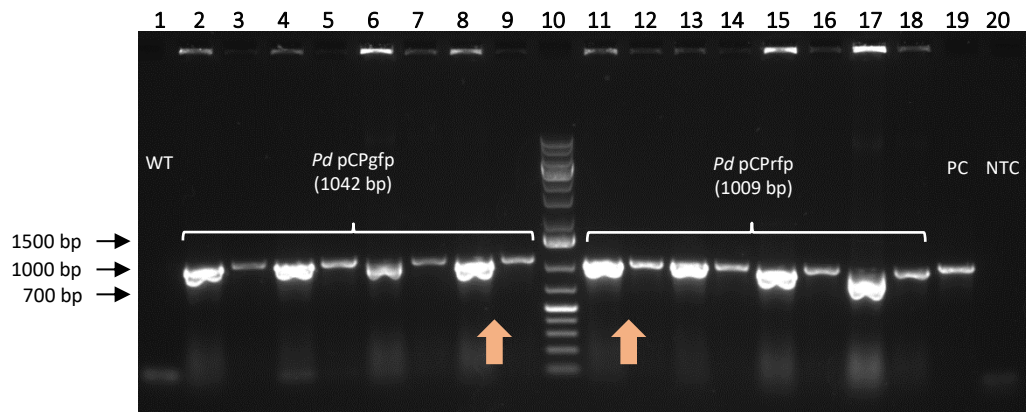


Figure 37: Confirmation of the successful transformation of *P. deceptionensis* with the plasmids pCPgfp and pCPrfp by verifying the presence of the respective promoter-reporter cassettes.

Colony-PCR was performed with the L1-F forward and L2-R reverse PCR primers. The amplification products of each colony screened were applied undiluted and in a 1:5 dilution to adjacent lanes on the gel. For example, in lane 2 the amplification products of the first colony examined were applied and in lane 3 the corresponding sample was applied in a 1:5 dilution. The sample applied in lane 1 is the negative control to which a colony of the strain *Pd* wild-type was added. No DNA was added to the PCR-negative control (NTC, lane 20). Lane 19 shows the positive control (PC) to which only pCPgfp plasmid DNA was added before the amplification reaction. The DNA size standard used is the GeneRuler 1 kb Plus DNA Ladder (lane 10). The orange arrows indicate the colonies used to inoculate clonal populations of the respective plasmid bearing strains to make glycerol stocks.

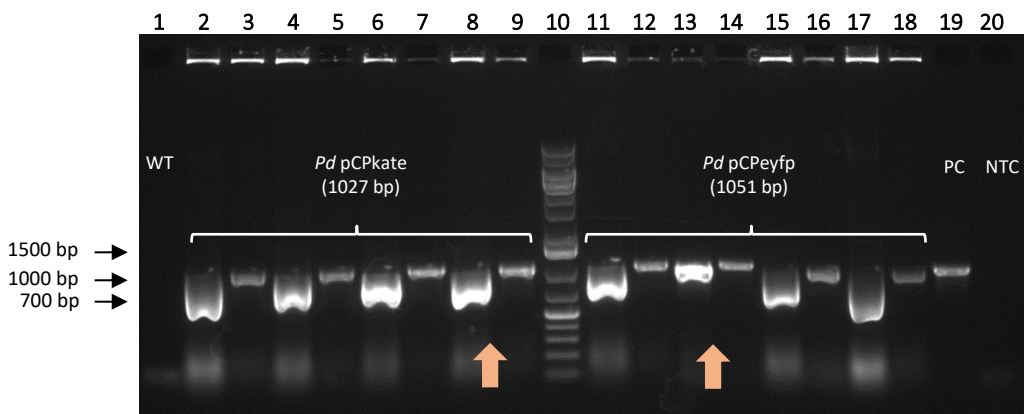


Figure 38: Confirmation of the successful transformation of *P. deceptionensis* with the plasmids pCPkate and pCPeyfp by verifying the presence of the respective promoter-reporter cassettes.

Colony-PCR was performed with the L1-F forward and L2-R reverse PCR primers. The amplification products of each colony screened were applied undiluted and in a 1:5 dilution to adjacent lanes on the gel. For example, in lane 2 the amplification products of the first colony examined were applied and in lane 3 the corresponding sample was applied in a 1:5 dilution. The sample applied in lane 1 is the negative control to which a colony of the strain *Pd* wild-type was added. No DNA was added to the PCR-negative control (NTC, lane 20). Lane 19 shows the positive control (PC) to which only pCPeyfp plasmid DNA was added before the amplification reaction. The DNA size standard used is the GeneRuler 1 kb Plus DNA Ladder (lane 10). The orange arrows indicate the colonies used to inoculate clonal populations of the respective plasmid bearing strains to make glycerol stocks.

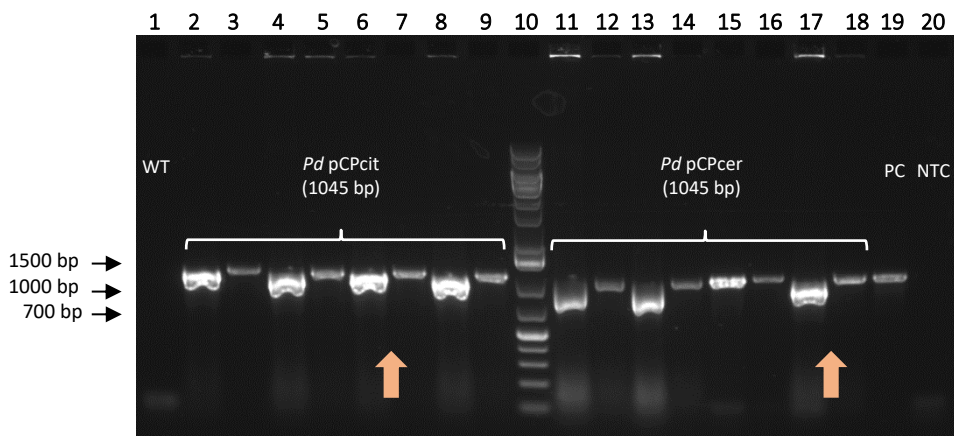


Figure 39: Confirmation of the successful transformation of *P. deceptionensis* with the plasmids pCPcit and pCPcer by verifying the presence of the respective promoter-reporter cassettes.

Colony-PCR was performed with the L1-F forward and L2-R reverse PCR primers. The amplification products of each colony screened were applied undiluted and in a 1:5 dilution to adjacent lanes on the gel. For example, in lane 2 the amplification products of the first colony examined were applied and in lane 3 the corresponding sample was applied in a 1:5 dilution. The sample applied in lane 1 is the negative control to which a colony of the strain *Pd* wild-type was added. No DNA was added to the PCR-negative control (NTC, lane 20). Lane 19 shows the positive control (PC) to which only pCPcer plasmid DNA was added before the amplification reaction. The DNA size standard used is the GeneRuler 1 kb Plus DNA Ladder (lane 10). The orange arrows indicate the colonies used to inoculate clonal populations of the respective plasmid bearing strains to make glycerol stocks.

8.6 Appendix F

After transforming *P. fluorescens* with each of the broad-host-range reporter plasmids, four colonies of each plasmid bearing strain were picked and screened by cPCR for the presence of the respective promoter-reporter cassettes (Figure 40, Figure 41 and Figure 42).

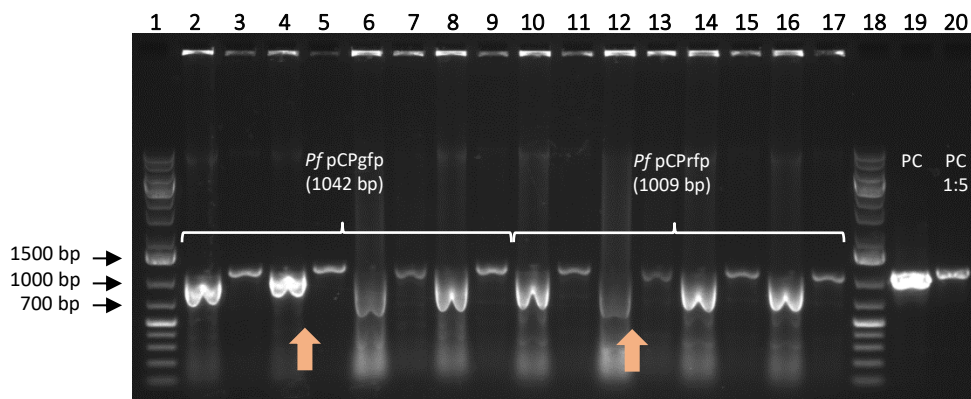


Figure 40: Confirmation of the successful transformation of *P. fluorescens* with the plasmids pCPgfp and pCPrfp by verifying the presence of the respective promoter-reporter cassettes.

Colony-PCR was performed with the L1-F forward and L2-R reverse PCR primers. The amplification products of each colony screened were applied undiluted and in a 1:5 dilution to adjacent lanes on the gel. For example, in lane 2 the amplification products of the first colony examined were applied and in lane 3 the corresponding sample was applied in a 1:5 dilution. Lanes 19 and 20 show the undiluted and 1:5 diluted positive control (PC) to which only pCPgfp plasmid DNA was added before the amplification reaction. The DNA size standard used is the GeneRuler 1 kb Plus DNA Ladder (lane 1 and 18). The orange arrows indicate the colonies used to inoculate clonal populations of the respective plasmid bearing strains to make glycerol stocks.

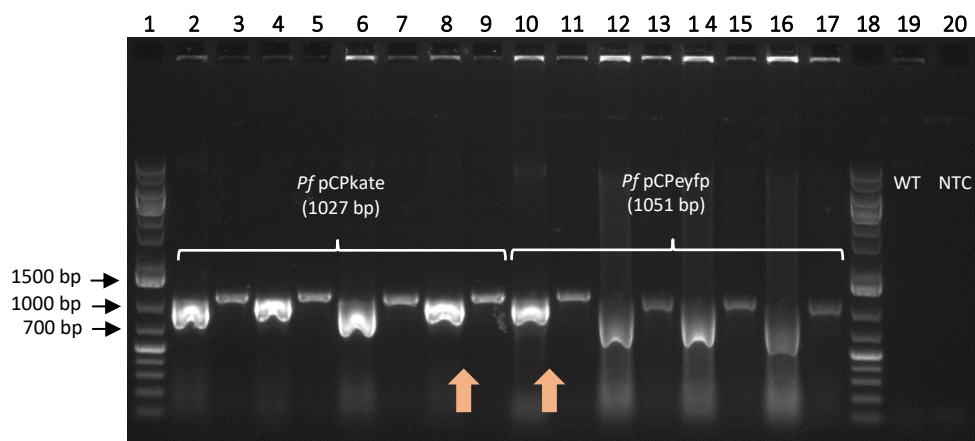


Figure 41: Confirmation of the successful transformation of *P. fluorescens* with the plasmids pCPkate and pCPeyfp by verifying the presence of the respective promoter-reporter cassettes.

Colony-PCR was performed with the L1-F forward and L2-R reverse PCR primers. The amplification products of each colony screened were applied undiluted and in a 1:5 dilution to adjacent lanes on the gel. For example, in lane 2 the amplification products of the first colony examined were applied and in lane 3 the corresponding sample was applied in a 1:5 dilution. The sample applied in lane 19 is the negative control to which a colony of the strain *Pf* wild-type was added. No DNA was added to the PCR-negative control (NTC, lane 20). The DNA size standard used is the GeneRuler 1 kb Plus DNA Ladder (lane 1 and 18). The orange arrows indicate the colonies used to inoculate clonal populations of the respective plasmid bearing strains to make glycerol stocks.

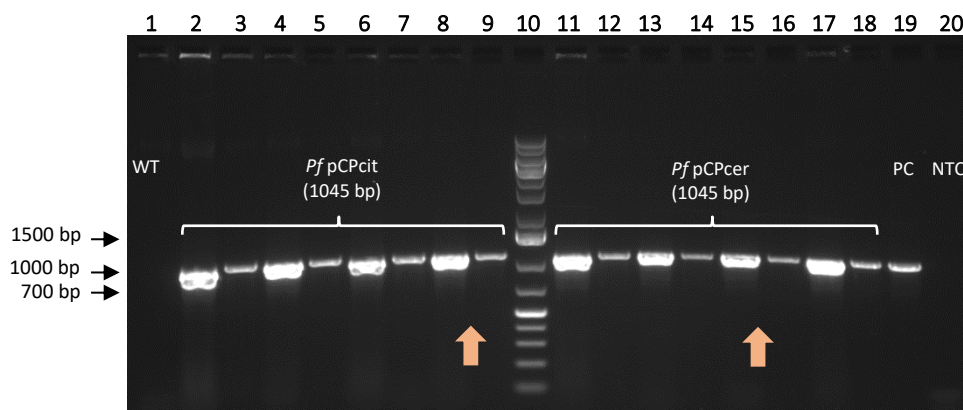


Figure 42: Confirmation of the successful transformation of *P. fluorescens* with the plasmids pCPcit and pCPcer by verifying the presence of the respective promoter-reporter cassettes.

Colony-PCR was performed with the L1-F forward and L2-R reverse PCR primers. The amplification products of each colony screened were applied undiluted and in a 1:5 dilution to adjacent lanes on the gel. For example, in lane 2 the amplification products of the first colony examined were applied and in lane 3 the corresponding sample was applied in a 1:5 dilution. The sample applied in lane 1 is the negative control to which a colony of the strain *Pf* wild-type was added. No DNA was added to the PCR-negative control (NTC, lane 20). Lane 19 shows the positive control (PC) to which only pCPcer plasmid DNA was added before the amplification reaction. The DNA size standard used is the GeneRuler 1 kb Plus DNA Ladder (lane 10). The orange arrows indicate the colonies used to inoculate clonal populations of the respective plasmid bearing strains to make glycerol stocks.

